9-1-2012

Risk Quantification of Maple Trees Subjected to Wind Loading

Cihan Ciftci
University of Massachusetts - Amherst, cihanc58@gmail.com

RISK QUANTIFICATION OF MAPLE TREES SUBJECTED TO WIND LOADING

A Dissertation Presented

by

CIHAN CIFTCI

Submitted to the Graduate School of the
University of Massachusetts Amherst in partial fulfillment
of the requirements for the degree of

DOCTOR OF PHILOSOPHY

September 2012

Civil and Environmental Engineering

RISK QUANTIFICATION OF MAPLE TREES SUBJECTED TO WIND LOADING

A Dissertation Presented

by

CIHAN CIFTCI

Approved as to style and content by:

_____

Sergio F. Brena, Co-chair

_____

Brian Kane, Co-chair

_____

Sanjay R. Arwade, Member

_____

Richard N. Palmer, Department Head
Civil and Environmental Engineering

DEDICATION

To Earth…

ABSTRACT

RISK QUANTIFICATION OF MAPLE TREES SUBJECTED TO WIND LOADING

SEPTEMBER 2012

CIHAN CIFTCI. B.Sc., BOGAZICI UNIVERSITY

M.Sc., BOGAZICI UNIVERSITY

Ph.D., UNIVERSITY OF MASSACHUSETTS AMHERST

Directed by: Professor Sergio F. Brena and Professor Brian Kane

Because of property damage and people injuries in, almost, every year in different locations of the earth, unfortunately the topic of understanding trees and their risk assessments under wind forces has not lost its importance since approximately a half of the last century. In contrast to loss its importance, the number of researchers or studies increases with time thanks to inter-disciplinary studies on that topic. In this Thesis, tree dynamics and their risk assessments subjected to wind forces were addressed by two different disciplines (civil engineering and environmental conservation).

To mention includes of this inter-disciplinary study, first, a finite element modeling was developed for a real tree in Belchertown, MA. Then this modeling was compared with the experimental tests. After comparing the model and the tests of the real tree, same methodology of the modeling was, again, applied to a different tree in Amherst, MA. Second, a number of wind samples were generated randomly in order to apply to the models of the trees. Then, by comparing the moments at the stem of the trees and calculated maximum moments of the stems, the fragility curves of the failures of these trees was obtained with respect to mean wind-speed of the random wind samples. Third, the decay effects on the fragility curves were investigated by considering

decreasing moment capacity of tree cross-sections due to decays. Finally, crown structure effects on tree dynamics were examined by several parametric studies which were applied to the tree in Belchertown, MA. These parametric studies refer to separately changes in several physical (such as stem diameter, branch slenderness ratio etc.) and material property (MOE) of the tree. Thus, thanks to these parametric studies, tree dynamics were understood better and the complex relationship between the stem and branches of the tree was explained better. Those better understandings, off course, produced several important practical outcomes for the life of the trees and as well as human-being.

TABLE OF CONTENTS

Page

LIST OF TABLES

Table Page

LIST OF FIGURES

Figure Page

CHAPTER 1

INTRODUCTION

1.1 Motivation

Trees have some important roles for human lives due to their environmental and sociological benefits (Nowak and Dwyer 2000). However, tree failure due to uprooting or breakage-failures of stems or branches may offset these benefits because of the consequences of damage including death, personal injury, cold-sickness due to power outage, traffic jams and economic losses (Kerzenmacher and Gardiner 1998, Gardiner and Quine 2000, Kane and Ryan 2004, James et al. 2006). Litigation associated with tree failures (Mortimer and Kane 2004) increases the economic cost of tree damage to higher levels than simply the cost of removing the tree and repairing the damages. To minimize the impact of tree damage and to understand the response of trees under wind forces, three main goals were chosen for this dissertation, as discussed in Section 1.2. The research is limited to wind-induced tree damage since several studies have identified this environmental factor as the main source of uprooting or breakage failures (Ancelin et al. 2004, Gardiner et al. 2008).

Most of the tree risk assessment studies found in the literature based on mechanical models mainly focus on studying trees within forests subjected to wind forces. In contrast, no work has been done on open grown trees. Thus, the current work focuses on risk quantification of open grown maple trees subjected to wind loading to fill the gap in knowledge in this field.

1.2 Overall Goals of Research

The overall goals of the current study are achieved by focusing on answering the following three main questions: (1) What is the likelihood of tree failures subjected to wind forces, quantified by construction of wind failure cumulative distribution functions (CDFs)? ; (2) What effect do tree decays have on the probability of tree failures?; and (3) How can we evaluate the probability of tree failures through a better understanding of dynamic response of trees and the dynamic response relationship between the stem and the branches of the trees.

The different chapters in this dissertation present the methodology that was designed to answer these important questions. Section 1.3 provides more details of the methodology and content within each chapter.

1.3 Scope of Work and Organization of Thesis

The dissertation is organized primarily to answer the questions posed in Section 1.2. Chapter 2 contains a summary of the work past research groups have done in topics that are relevant to the goals of this research. The literature survey contained in this chapter highlights information that helped identify gaps in the knowledge of wind-induced tree failures where better understanding was needed.

Chapter 3 focuses on the description of the finite element modeling needed to achieve the first goal as indicated Section 1.2. Before conducting the Monte Carlo simulations, a detailed calibrated model of a tree prototype is needed. The basic assumptions in the model creation as well as the analysis techniques are presented in this chapter. A prototype finite element (FE) model was created from a tree located in

Belchertown, MA, USA that has been the subject of previous studies by Kane et al. (In preparation). The FE model and analysis was conducted using a general purpose FE analysis program, ADINA 8.5. The FE model was validated by comparing the modal frequency results with experimental values, which had been measured by Kane et al. (In preparation). Additional model validation is conducted by comparing the computed results with several empirical and numerical formulae.

In Chapter 4 Monte-Carlo (MC) simulation techniques were applied to the FE tree model created in Chapter 3 to directly investigate the risk assessment of tree failures under random wind excitation forces occurring during different seasons (winter and summer seasons). For the application of MC simulations, a total of 1000 random wind samples (for each mean wind-speed value) were deemed appropriate. Wind spectral density of these wind samples was first generated assuming exposure conditions of continental areas. Ochi-Shin's equation, which was developed for the wind spectral density in offshore regions, was modified by using time-history data and spectral densities of several experimental wind measurements for a selected land region in Amherst, MA. Using this new modified Ochi-Shin's equation, wind samples were generated under the assumption that winds can be modeled using log-normal distributions (Luna and Church 1974, Kiss and Jánosi 2008, Carta et al. 2009, Morgan et al. 2011). The generated wind samples were applied to the loading scenarios of two different tree models of trees in Belchertown and Amherst, MA creating 3D-FE models using the assumptions described in Chapter 3. Therefore, randomness was assumed to only apply to loading wind scenarios, and the trees themselves were considered deterministic. However, tree models were developed to capture the response during two seasons: winter

season and summer, because tree behavior may change drastically in each of these seasons. Two modeling parameters were specifically varied for each season: wind drag-forces and damping effects of leaves. These two parameters capture the differences in canopy architecture of the trees in the two seasons that were selected for this research. The maximum moments at breast height (1.4 m form the base) of each model as a result of the dynamic analysis of each model were compared. These moments are considered to be the governing actions that may cause tree failure. Finally, cumulative distribution function (CDF) curves were obtained for these two trees with respect to each season and the various wind scenarios.

The FE modeling and Monte-Carlo simulations in Chapters 3 and 4 assume that trees have not experienced any decays or defects in their cross-sections. By using this assumption, it is known that all the probabilistic assessments on tree failures will overestimate the critical wind forces for tree failures. For this reason, the effect of decays on the risk assessment of tree failures (the second question posed in Section 1.2) was investigated in Chapter 5. The methodology of this investigation is based on determining the moment capacity loss of cross-sections of tree stems with varying decay sizes and decay cross-sectional position. Bending moment capacity of trunk cross-sections in trees was calculated using an algorithm created in Matlab and computed with respect to size and location of any circular decays in these sections. Moment capacity loss was calculated by using the ratio of the bending moment capacity of a section with decay to the moment capacity of the same section without decay. For these computations, three important assumptions were used: (1) bending failure of trees is governed by compression failure; (2) axial load effects in cross-sectional flexural strength is

negligible; and (3) wood is a composite material so tension and compression behaviors parallel to the grain are not same (elastic moduli differ). The differences in behavior are captured using a linear model of a composite section, that is, the ratio of the modulus of elasticity in tension and compression was initially assumed to be 2.0 ($n = E_t/E_c$). Because tree moduli may differ substantially depending on species and tree age other ratios were investigated. The modular ratio was varied to 1.5 and 2.5 to determine the effect of this parameter on moment capacity loss. The decay model was further improved by considering the possibility of other shapes of decay (noncircular). In this way the methodology developed in Chapter 5 would be more generally applicable. The methodology developed in this chapter was used to compare the results of moment strength with experimental data. The methodology developed in this chapter can be used to estimate the moment capacity of decayed sections given that the decay geometry can be identified through any method (e.g. visual approaches (Fink 2009), tomography (Gilbert and Smiley 2004, Wang and Allison 2008), radar (Butnor et al. 2009), and strain gauges and inclinometers (Sinn and Wessolly 1989)). Once the moment capacity loss is estimated, cumulative distribution functions of decayed tree failures are determined as several examples show in graphs contained in Chapter 4.

As several past studies have indicated (Milne 1991, Moore and Maguire 2004, Sellier and Fourcaud 2005, Sellier et al. 2006, Castro-García et al. 2008, Rodriguez et al. 2008, Moore and Maguire 2008, Sellier and Fourcaud 2009, Kane and James 2011), the dynamic response of trees is highly affected by the tree geometry and characteristics of stems and branches. A widespread reduction of risk of failure requires that the dynamic response of trees be well understood. In Chapter 6 the relationship between stem and

complex design of branches when the trees are subjected to wind forces is studied in detail. A parametric study conducted to identify critical geometric properties that affect the dynamic response of trees, with reference to the base model used in Chapter 3, M100, was conducted as described in Chapter 6. Different tree models were created by varying selected properties of M100 using ADINA-8.5. Eight different parameters (stem diameter, slenderness ratio of branches, number of branches, damping ratio, branch attachment heights, branch attachment angles, branch azimuth angles, and the distribution of the modulus of elasticity in the members of trees) were varied to compare the sway motion of Maple trees in this research.

To conclude with the final chapter in the current research, three main opportunities were identified for future works: (1) Decay effect on tree dynamic response; (2) Effects of all the pruning types in literature on tree dynamic response; (3) Likelihood of random tree failures subjected to random wind forces.

CHAPTER 2

LITERATURE REVIEW

2.1 Introduction

For, especially, arborists and urban foresters, it is important to understand the behavior of trees under a variety of forces, especially wind forces (Ancelin et al. 2004, Gardiner et al. 2008), in order to reduce the risk of tree failures. Thus many experimental and theoretical research studies have focused on investigating tree response and tree failures under wind forces. For instance, the first study on trees subjected to wind forces began with Metzger in 1893 and continued respectively with (Tiren 1929), Fritzsche (1933), and Ylinen (1952). Then, the importance of these studies has been progressively increased up to now thanks to the encouragements of several countries (e.g. lastly, the countries in G20 have decided on encouragements on green growth 2012 in Mexico City), and forestry agencies within governments that are interested in determining how to minimize the loss of timber value due to storms.

The studies on tree response for wind forces can be divided into three main groups such as (1) experimental, (2) theoretical and (3) computational or numeric studies. This thesis is a computational study, thus only the literature of the third group will be focused and presented in detail (Section 2.2). However, it is possible to see some information from experimental and theoretical studies as be separated into whole part of this chapter, because the results of these studies are inevitable to use as the inputs for the computational studies. After mentioning the computational studies, two important topics (tree dynamic response under wind induced excitation, and tree mechanics and tree

failures) will be addressed in sections 2.3 and 2.4, respectively. Finally, this chapter will include a conclusion section at the end.

2.2 Computational Studies on Tree Response Subjected to Wind Forces

Computational studies on tree response subjected to wind forces will be presented by concerning two different approaches (static and dynamic methods). Using static approach stands to an earlier time than the dynamic approach. Metzger (1893), Tiren (1929), Fritzsche (1933), and Ylinen (1952) are examples for the oldest studies by using the static approach. Subsequently, by considering the possibility of underestimation on the response of trees, several researchers Papesch (1974), Forsching (1974), Holbo et al. (1980), and Amtmann (1982) started investigating tree response subjected to wind forces by using dynamic analysis approach. As these researchers, dynamic approach was chosen for this thesis as the type of the analysis approach, so this chapter will address this approach in much more detail than the static one.

2.2.1 Static Approach

This method is based on the static formula of $ku = F$, which is commonly used by engineers. According to this equation, stiffness [N/m] and displacement [m] of the members of trees can be represented by k and u, respectively. F [N] corresponds to the wind force on trees as in the research of Mattheck and Bethge (2004). Stiffness in this static formula and the other properties (e.g. density, damping) of trees also exist in the formula which is used for the dynamic approach (section 2.2.2), thus the stiffness property of trees will be mentioned later, in detail, as the other properties. Additionally,

one of the most important differences between the static and the dynamic approaches is that static one does not depend on time. Thus, every symbol in the static formula is not represented as a function of time, thus static approach may not really simulate the sway motion of trees with time (Oliver and Mayhead 1974, Gardiner et al. 1997), and moreover static approach cannot consider the interaction of branches on this sway motion (James 2003). On the other hand, the advantage of the static approach is to have less cost and less time on which it is supposed to be spent. That is why, several studies (Peltola et al. 1999, Gardiner and Quine 2000, Ancelin et al. 2004, Schelhaas et al. 2007, Kane and Clouston 2008) use the static approach for risk assessment of trees subjected to wind forces.

2.2.2 Dynamic Approach

Dynamic approach on the tree response subjected to wind forces has been caught on by, especially, recent studies (James 2003, Moore and Maguire 2004, Sellier et al. 2006, Moore and Maguire 2008, Sellier et al. 2008, Rodriguez et al. 2008, Sellier and Fourcaud 2009). This approach is based on a formula (Eq. 1) which is commonly used in engineering. To apply this equation for trees, one of the easiest ways is to use finite element methods (FEM) in a computer based package program. Thus, several recent studies (Moore and Maguire 2008, Sellier et al. 2008, Sellier and Fourcaud 2009) on dynamic tree response used FE methods.

$$m\ddot{u} + c\dot{u} + ku = F \tag{2.1}$$

where m is the mass [kg], $\ddot{u}$ is the acceleration [m/s^2], c is the damping coefficient [kg/s], and $\dot{u}$ is the velocity [m/s]. As mentioned in section 2.2.1, ku is the stiffness part of Eq. 1. Finally, F is the external force of this equation. The variables (acceleration, velocity, displacement, and force) in Eq. 1 should be considered as functions of time. It means that after each timing case (Δt, which is determined by researchers), the new position and the new velocity depend on the previous case (the previous position, velocity, and acceleration (Chopra 2007). To apply this dynamic approach successfully, all the computational studies on tree response need to know mass, damping and stiffness of the trees with the external forces, together. All these properties of the trees will be mentioned in the next sections, in detail.

2.2.2.1 Mass Property of Tree Dynamics

Mass can be represented by using density and geometry in 3-Dimension (volume) of tree elements (such as branches and stem). That is why the computational studies encoded the geometric properties (e.g. stem diameter, branch diameters, tree height, crown width and height) of trees from field measurements and their density values (depend on specific gravity).

According to Niklas (1997), density changes within not only tree specious but also the cross-section of stems or branches, thus to determine the density of trees may be quite complex. As depicted in Figure 2.1, for example, Niklas found that a sudden decrease of the density occurred within the tree trunk near the center of the heartwood. Another drop also occurred in the boundary region between the heartwood and the sapwood of trees. Thus it can be accepted that the variance of the specific density with

respect to the cross-section is not so high except the places at which sudden decreases of the specific gravity exist.

The density of trees can depend not only on formed layers of heartwood or sapwood in the stems but can be also related to the tree-age, because there may be a relation between the forming of layers and the age of trees. For instance, Niklas (1997) observed from his research that density of wood in black locust trees varied parabolically with tree-age (Figure 2.2). Density was high in young trees and then decreased to a minimum at an age of approximately 12 years. Then, this density increases again in older trees to values similar to those found in young trees (see Figure 2.2). But, increasing density of older trees may not continue up to the density value of young trees for all the species, as an example in Table 2.1 that the density (1100 kg/m^3) of the 4 years old maritime is significantly higher than the density (850 kg/m^3) of the 35 years old maritime pine.

Although density is varying within the age of trees and the cross-section of trees, several studies in general have used one value to model the trees in their research. Table 2.1 has several examples for the density values of the trees which were used in these studies.

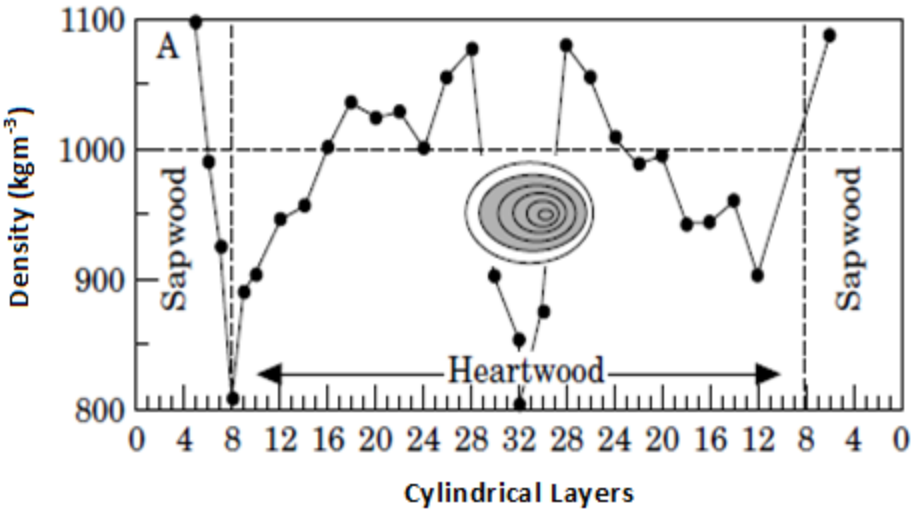

Figure 2.1: Wood density layers with respect to the approximate age of samples isolated from the tree major trunks (Niklas 1997).

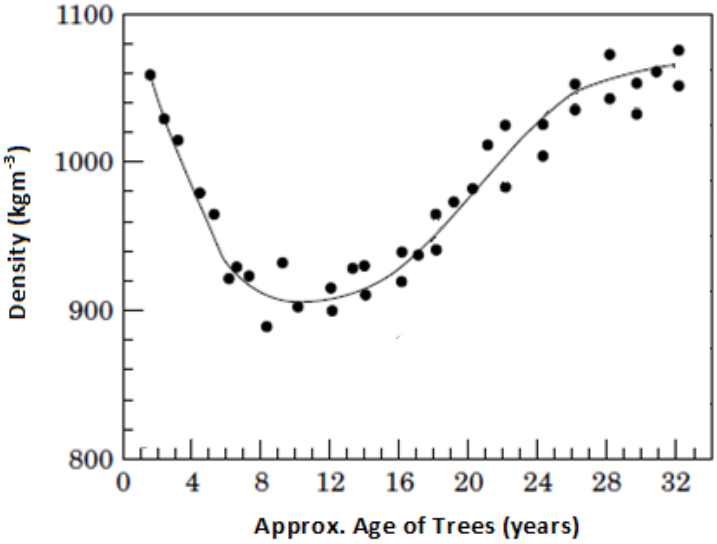

Figure 2.2: Mean wood density plotted as a function of approximate age of trunk sections in Locust black trees (Niklas 1997).

Table 2.1: Density in tree models which were selected from several studies.

Citation	Tree Species	Tree Age	Density (kg/m^3)
Sellier et al. 2006	Maritime Pine	4	1100
Rodriguez et al. 2008	Walnut Tree, Maritime Pine	20, 4	805, 1300
Moore & Maguire 2008	Douglas-fir (Stem, branches)	20	1000, 1160
Sellier & Fourcaud 2009	Maritime Pine	35	850

2.2.2.2 Damping Property of Tree Dynamics

Tree damping is an inherent mechanism that dissipates energy from the total mechanical energy of trees. If a tree is deformed from its at-rest condition and released, the tree will oscillate with decreasing amplitude until finally coming to rest. Damping is responsible for generate a reduction in the amplitude of the dynamic response of trees. Some researches (Milne 1991, James 2003, Castro-García et al. 2008, Spatz et al. 2007) generally focus on three types of damping on the dynamic behavior of trees. These are (1) damping due to collision of branches with those of neighbors, (2) aerodynamic drag forces due to foliage area of the branches and leaves, and (3) viscous damping in trees. Milne conducted experiments to study damping differences between the cases of (a) selected trees with branch interference of neighbors, (b) same trees without branch interference (removed by pruning the neighbors), and (c) only stems of the same trees. When he compared these cases of the trees, he found that the ratios of the damping of each case to the overall damping are respectively 0.5, 0.4, and 0.1 (can be seen in Figure 2.3). According to him, the first damping is not related only to the distance to neighbors,

but also to the sizes of the chosen trees and their neighbors. The second one in general depends on the canopy areas and the drag coefficient for the existing canopy. Furthermore, the direction of the oscillation of trees is important, because canopy areas depend on the varying of azimuth angles of the branches. For instance, Sellier and Fourcaud (2005) defined two perpendicular directions (x and y) in which the stem of trees was initially bent for their research. According to the definition of these directions, they stated that whereas the removal of the foliage area in the x direction causes to decrease the aerodynamic damping ratio from 12 % to 4 %, the removal of the foliage area in the y direction leads to decrease this damping ratio type from 8 % to 4 %. Thus it can be investigated that for the deciduous trees the aerodynamic damping ratio would be different in winter terms than in the summer terms (Kane and James 2011). For the viscous damping, however Moore and Maguire (2004) stated that there is no relation between the internal damping and tree diameter, it is related to stem diameter and the varying of water content in living trees, because it is about the self-friction at the medium, tree stem (Spatz et al. 2004).

As another damping type in trees, James (2003) and Spatz et al. (2007) also introduced tuned mass damping in trees due to the vibration of additional masses (branches and leaves) to the main stem. According to James (2003), tuned mass damping reduces the overall swaying energy of the trees with the drag forces of the canopy (branches, or leaves masses) so that trees can be more stable against high wind forces.

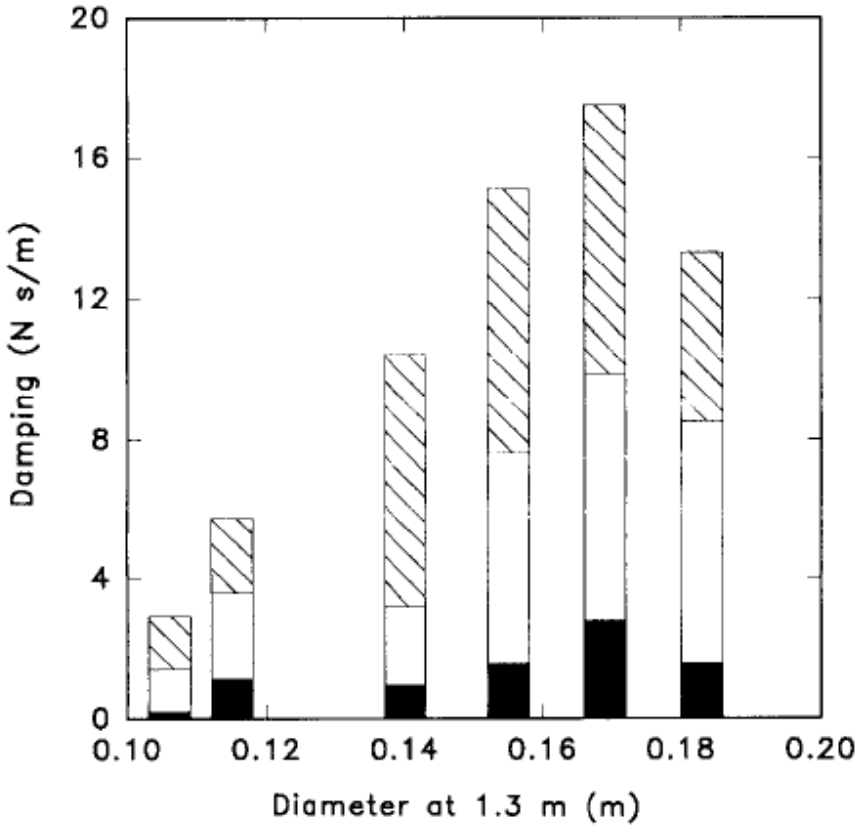

Figure 2.3: Components of damping (due to branch interference, cross-hatched; aerodynamic drag, open; and stem damping, solid) in Sitka spruce expressed as a function of stem diameter at breast height (Milne 1991).

The summation value of all damping types in trees is different for each mode, because the frequency of each mode-shape changes. Mayer (1987) and Peltola (1996) state that it is more useful to focus on the first mode damping. Their ideas can be explained by two reasons. The first reason is that the mode of dynamic behavior whose frequency value is the lowest one can dissipate the highest portion of the total kinetic energy. The second reason is that the second mode frequencies of the members in trees are higher than the first mode frequency of trees with respect to the dominant ones in the frequency distribution of wind spectra (as an example to wind spectra graph, see in Chapter 4).

To apply varying damping to the computational models of trees for each mode frequency of these trees, the resultant modal damping can be converted into an equivalent Rayleigh damping coefficients (α, and β) (Chowdhury and Dasgupta 2003). This method is a good effective way to approximate real damping in systems with a large number of degrees of freedom. According to the definition of Rayleigh damping, the resultant damping is broken down into two damping components such as α and β as in Eq. 2.2.

$$[C] = \alpha[M] + \beta[K] \tag{2.2}$$

where the damping matrix [C] is linearly related to the mass [M] and stiffness [K] matrices in terms of the Rayleigh damping coefficients. To find these coefficients, the formula of Thomson (1993) can be used as below (Eq. 2.3). The coefficient (α) is basically proportional to the energy dissipation by aerodynamic friction. It is about the resonance phenomena for trees, because aerodynamic friction is related to the maximum speed of materials at the rest position of the dynamic behavior, thus to increase the maximum speed is about the resonance or greatest displacement or greatest potential energy when the speed is zero. For the other coefficient (β), it represents the damping component related to the stiffness matrix, thus it is proportional to the dissipation of energy by the hysteresis (nonlinear behavior) of materials. Moreover this coefficient, β has less importance for the first few modes of the dynamic behaviors of trees (Mayer 1987), because the expectation is that trees will stay within the linear range. Some researchers have used a high value for the first coefficient (α) and a small value for the second coefficient (β), when response is dominated by the first few modes. Moreover, Castro-García et al. (2008) state that these first few modes comprise the first two modes, because according to them the participation of these two modes makes up nearly 80 % of

the total response of trees. To give several examples for the values of the coefficients α and β, Castro-García et al. (2008) used α = 10.68 and β = 0.00045; Sellier et al. (2006) proposed using α = 6.72 and β = 0.001 rather than a null value to minimize numeric noise at the first few mode frequencies. Additionally, there is a relation between the coefficients α and β and the mode frequencies of dynamic systems. Thus the values of the coefficients α and β in the previous research studies (Sellier et al. 2006, Castro-García et al. 2008) are consistent with Eq. 2.3 and the mode frequencies in their studies.

$$\alpha + \beta\omega_k^2 = 2\omega_k\zeta_k \tag{2.3}$$

where w_k is the frequency of the k^{th} mode and ζ_k is the damping ratio for this mode. Due to this formula (Rayleigh damping coefficients), the different damping ratios can be participated into the finite element programs for many significant mode-shapes.

2.2.2.3 Stiffness Property of Tree Dynamics

Stiffness is related to the geometric and material properties of trees. That is why, the geometric and material property information are important. In computational studies, geometric properties of trees in general are defined by introducing some parameters such as, especially, crown structure, height of trees, stem diameter and so on. These parameters may be so various in trees for even a specific species.

Modulus of elasticity (MOE) of trees is the important parameter to define the material properties of trees. This parameter in general changes through branches (Dahle and Grabosky 2010) and stems (Spatz et al. 2007) of trees, or this parameter can be also associated with the age of trees (Mencuccini et al. 1997). To mention about the varying

of the young modulus (or MOE) through the length of members of trees, in general MOE is lower at the tip of branches or stems than the base point of these elements (Yoshida et al. 1992, Spatz et al. 2007, Dahle and Grabosky 2010). In contrast to this inference, rarely MOE may be higher near the tip parts than the base for particular trees like Eucalyptus-Rubida (Yoshida et al. 1992). Changing of MOE (or E, elasticity) through the length of branches can be seen in Figure 2.4.

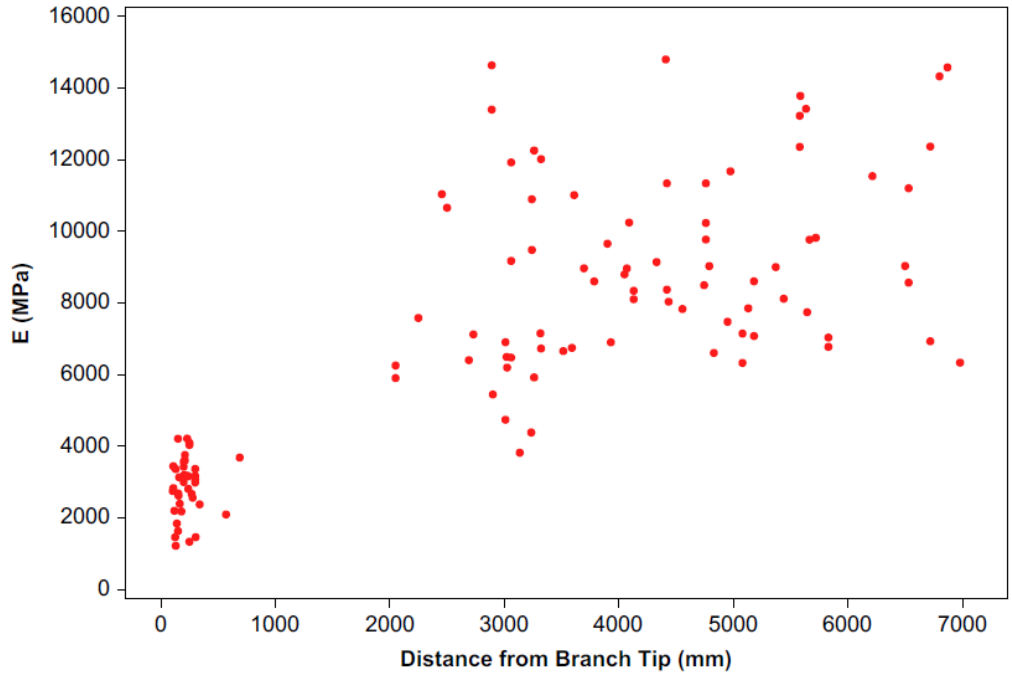

Figure 2.4: A scatter plot of modulus of elasticity (MPa) by the distance (mm) from the branch terminal bud for Acer-Platanoides branches (Dahle and Grabosky 2010).

Mencuccini et al. (1997) determined values of modulus of elasticity of Scots Pine trees by concerning the age and location of trees. According to the investigators, the modulus of elasticity increases with tree age from 1.7 GN/m^2 to 7.8 GN/m^2 up to 25 years. After 25 years old, it remains approximately constant as can be seen in Figure 2.5. Moreover the effect of cambial age of trees on the young modulus was also investigated

by some researchers (Lindström et al. 1998, Lichtenegger et al. 1999, Reiterer et al. 1999, Bruchert et al. 2000, Spatz and Bruechert 2000).

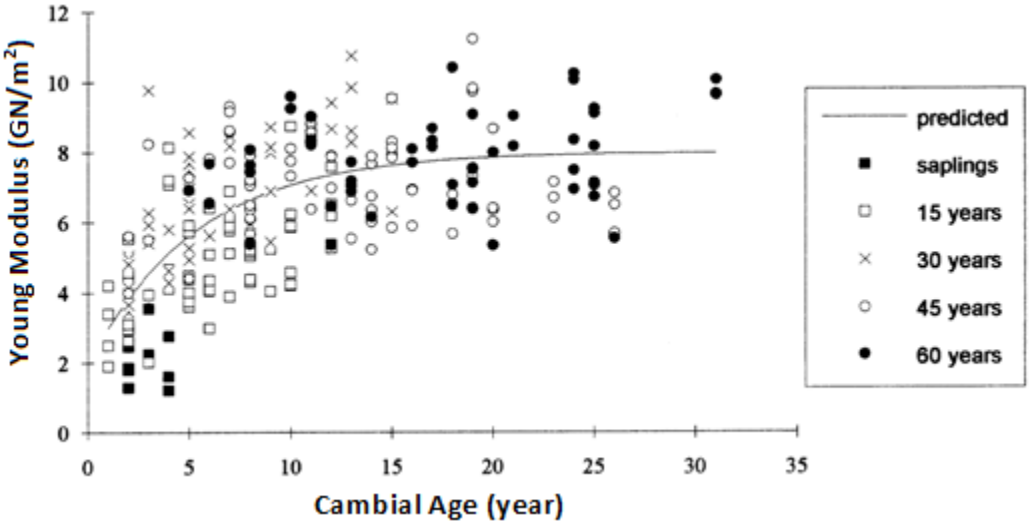

Figure 2.5: Variation in Young's modulus, MOE (GN/m^2) with cambial age of single specimens (Mencuccini et al. 1997).

The rising of the modulus of elasticity in Figure 2.5 causes that younger wood or tree is more flexible than old one (James 2003). Furthermore, sapling trees have a lower MOE than mature trees as in many research studies (Panshin et al. 1980, Plomion et al. 2001, Woodrum et al. 2003, Chauhan and Walker 2006, Read and Stokes 2006). In addition, it can be expected that MOE may depend on the diameter of tree members such as branch elements in trees (Spatz et al. 2007) as in Figure 2.6, because the number of rings (or diameter) of tree cross-sections is related to tree age.

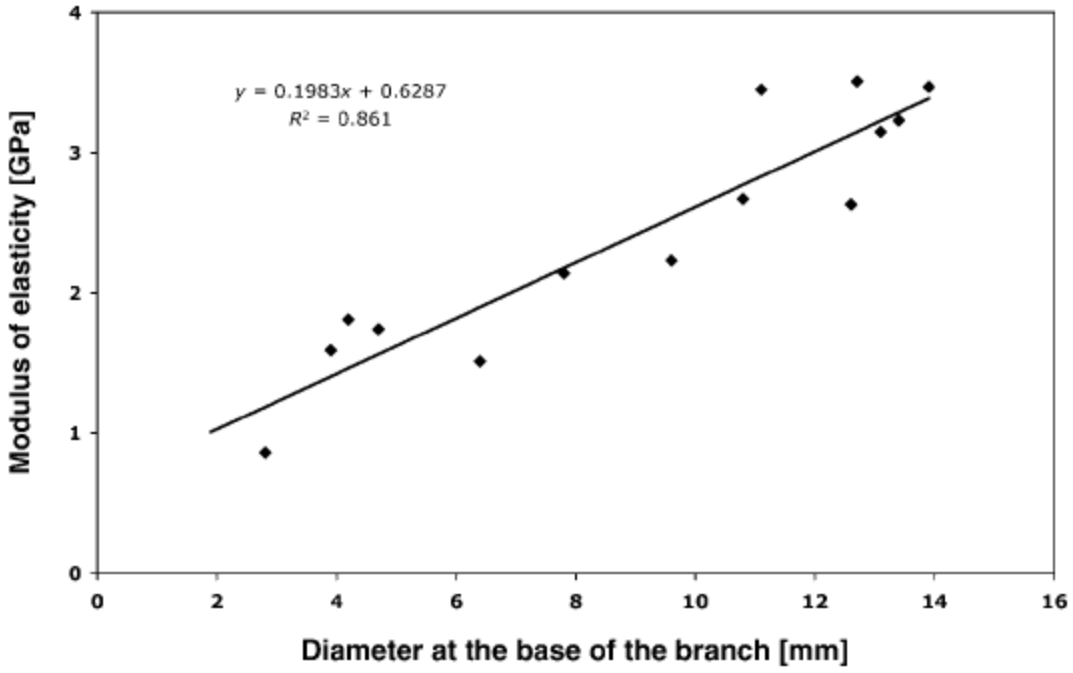

Figure 2.6: MOE of primary branches for a Douglas fir tree with respect to diameter of these branches (Spatz et al. 2007).

Modulus of elasticity may also vary within the cross-section of the wood material because of the adaptive mechanism which is defined in section 2.2.2.4. The research of Mencuccini et al. (1997) indicates that the effect of the sapwood of trees does not contribute much more on the modulus of elasticity than heartwood part of trees. According to Alméras et al. (2005), MOE is usually lower in compression part of the cross-section than in the tension part. Langum et al. (2009) supports Alméras et al. (2005) by finding that MOE tension parallel to grain is approximately equal to 1.10 times of MOE compression parallel to grain for two different species, douglas-fir and western hemlock. Furthermore, Niklas (1997) had also a research about the variety of MOE within cross-section of trees, and Figure 2.7 explains his research, briefly:

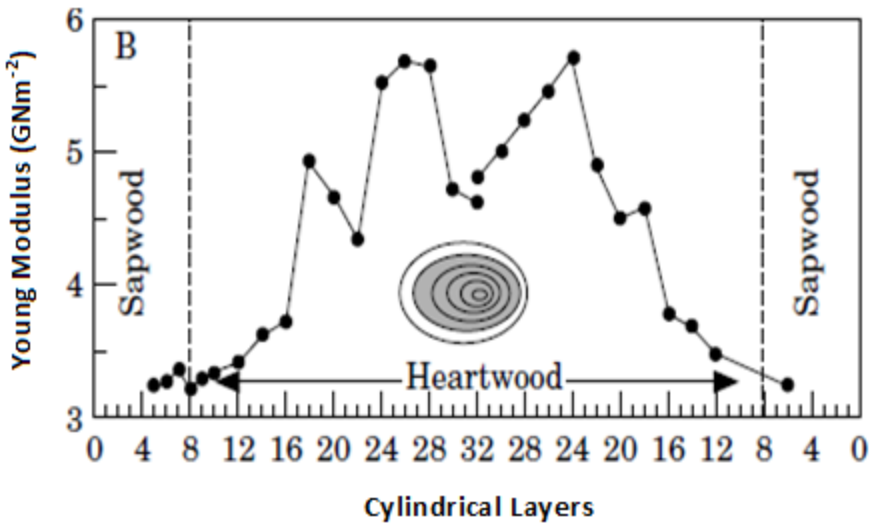

Figure 2.7: Young's modulus (E) of wood layers with respect to the approximate age of samples isolated from the tree major trunks (Niklas 1997).

2.2.2.4 External Force for Tree Dynamics

Some of the most important loads are in general dead load and wind load for trees. The first one is typically vertical and static load. This load type is not so detrimental and harmful for trees, because of the adaptive mechanism (James 2003, Rowe and Speck 2005, Telewski 2006, Moulia et al. 2006, Brüchert and Gardiner 2006, Sellier and Fourcaud 2009). According to adaptive mechanism, if a tree has an internal or external load, it will try to enlarge some areas at its critical tissue-points on which the stresses are larger than the initial stresses in order to adapt the changes of loading and to decrease the stress values on these points. In other words, unless trees had this mechanism, the increasing of internal stresses due to increasing of dead loads in time would cause to some stem or branch breakage. As for the wind load, it is a kind of spatially, and temporally changeable and suddenly exposed dynamic load (Ennos 1999).

Therefore, the adaptive mechanism cannot immediately prevent the failure due to wind force. Because of this reason, the second load type (wind forces) is really important for tree lives. To calculate this load type on trees, many studies (e.g. Peltola and Kellomäki 1993, Gardiner and Quine 2000, Ancelin et al. 2004, Cullen 2005, and Sellier and Fourcaud 2009) used the formula of the drag-force, which is defined by Eq. 2.4, from fluid mechanics.

$$F_D = \frac{1}{2}\rho U^2 A C_D \tag{2.4}$$

in which F_D is the drag force, ρ is the air density, A is the frontal area on which the wind forces is exposed, U is the wind speed, and C_D is the drag coefficient.

2.2.2.4.1 Air Density for Wind Drag Forces on Trees

Air density is one of the variables of calculating drag forces (Eq. 2.4) on trees. This variable changes approximately from 1.16 kg/m^3 to 1.42 kg/m^3 with regarding to the temperature of the air. When the weather is cold, the air density increases as seen in Table 2.2. As an example, air density is selected as ρ=1.226 kg/m^3 in the research of Kane and Smiley (2006). Moreover, varying of air density with respect to temperature can be calculated by using Eq. 2.5 (ideal gas law).

$$\rho = \frac{P}{RT} \tag{2.5}$$

in which P is the absolute pressure, R is the specific gas constant for dry air like 287.05 J/K^o in SI units, and T is the temperature in K^o.

Table 2.2: Air density with respect to temperature.

	Temperature (°C)											
	30	25	20	15	10	5	0	-5	-10	-15	-20	-25
Air Density (kgm^{-3})	1.16	1.18	1.20	1.22	1.25	1.27	1.29	1.32	1.34	1.37	1.39	1.42

2.2.2.4.2 Wind Speed for Wind Drag Forces on Trees

As Zhu et al. (2000) mentioned that the wind profile or the variation of wind speed with height is important, and this relation depends on the height (z) along stem and branches. Thus Kerzenmacher and Gardiner (1998) used the following formula (Eq. 2.6) as in several researches (Oliver and Mayhead 1974, Cionco 1978) to represent the wind profile in stands simulated in their mathematical models.

$$u(z) = u_h exp\left(6\left(\frac{z}{h} - 1\right)\right) \tag{2.6}$$

where u_h is the wind speed at the top (z=h) of the beam elements in models.

In addition to Eq. 2.6, wind profile was also determined by Eq. 2.7 (Panofsky and Dutton 1984), which is commonly used in engineering texts for land based and for the neutral stability of the atmosphere:

$$u(z) = u_h(z/h)^{1/7} \tag{2.7}$$

where u_h is the same within Eq. 2.7. Furthermore, this formula can be comparable with the codes in ASCE-7 about the changing of wind speed with height.

Moreover, wind speed is a kind of spatially, and temporally changeable and suddenly exposed dynamic speed (Ennos 1999). Thus, it contains many different frequencies for each direction in a wind time history. This kind of speed causes the drag forces on trees to be the fluctuating excitation loads, and these drag forces have also many frequencies. In general, some engineering or mathematical techniques can be used in order to see the participation of the dominant frequencies in all frequency values of wind forces by drawing the PSD (power spectral density) functions of these forces which describes how the power of these forces is distributed with frequency. There are some significant studies (such as Harris 1971, Davenport 1961, Ochi and Shin 1988) which formulated these PSD functions in terms of average wind speed. Moreover, the application of the formula in the research of Ochi and Shin (1988) can be seen in Chapter 4.

2.2.2.4.3 Frontal Area for Wind Drag Forces on Trees

According to the studies of Rudnicki et al. (2004) and Vollsinger et al. (2005), frontal areas decrease when wind speed increases. Because all the materials in trees like branches and leaves bend away from the wind and they reconfigure into more aerodynamic shapes. The varying of frontal areas with respect to wind speed can be shown in Figure 2.8. Thus, if the frontal area is considered as a function of wind speed, Eq. 2.4 can change. Kane and Smiley (2006) considered this changing in Eq. 2.4. According to them, drag force is proportional to wind speed raised to an exponent of 1.4, instead of 2.0 in Eq. 2.4. But for the other red maples whose foliage is stripped, drag force is proportional to wind speed raised to an exponent of 1.9.

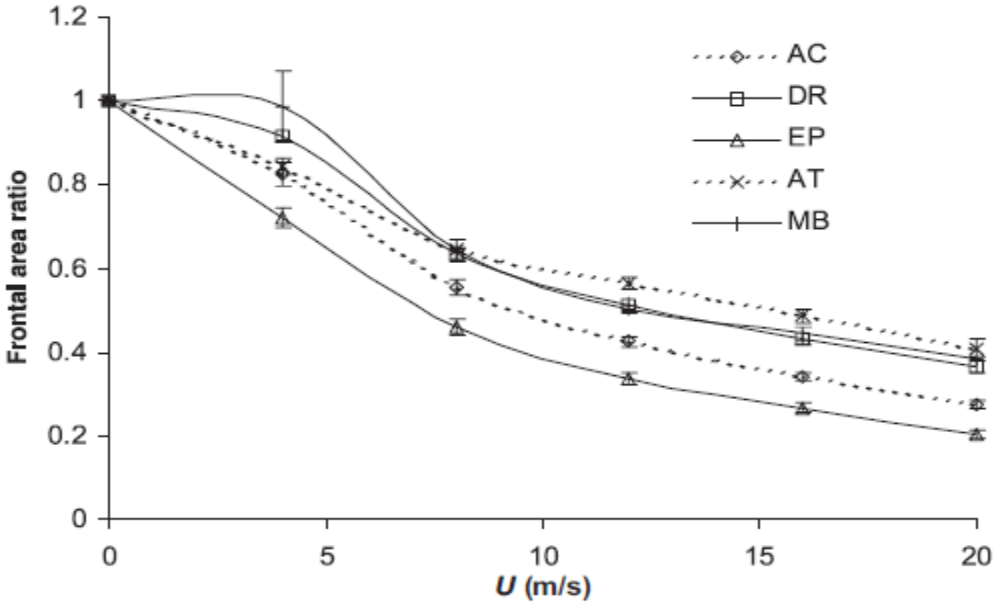

Figure 2.8: Frontal area ratio of crowns in selected species digitized from video image at wind speeds (U) from 0 to 20 m/s (Vollsinger et al. 2005).

2.2.2.4.4 Drag Coefficient (C_D) for Wind Drag Forces on Trees

Drag coefficient, C_D varies as a function of wind speed, flow direction, object shape, object size, fluid density and fluid viscosity. Speed, dynamic viscosity, density, and the traveled-length of fluids (for instance, the fluid is represented by wind for this Thesis) are incorporated into a dimensionless quantity which is called the Reynolds number or *Re* in fluid mechanics.

According to Figure 2.9, C_D values depend on the object shape and Reynolds number. Moreover, it can be accepted that drag coefficient decreases due to increasing of wind speed, because when wind speed increases, Reynolds number increases. At some wind speed, however, C_D likely reaches an asymptote. The relationship between C_D and wind speed is investigated by using 60 different trees in the research of Kane and Smiley

(2006) as can be seen within Figure 2.10. To choose of the object shape, if the crown area of the selected red maple trees is assumed as an ellipse or a rectangle shape in order to calculate the drag coefficient by using the chart (Figure 2.9) with Reynolds number, they obtained nearly underestimated the drag coefficient by 29% and 44%, respectively, at 20 m/s wind speed (Kane and Smiley 2006). Furthermore, they found that the assumption of crown area as a triangular shape causes the overestimated the drag coefficient by 14% at 20 m/s wind speed.

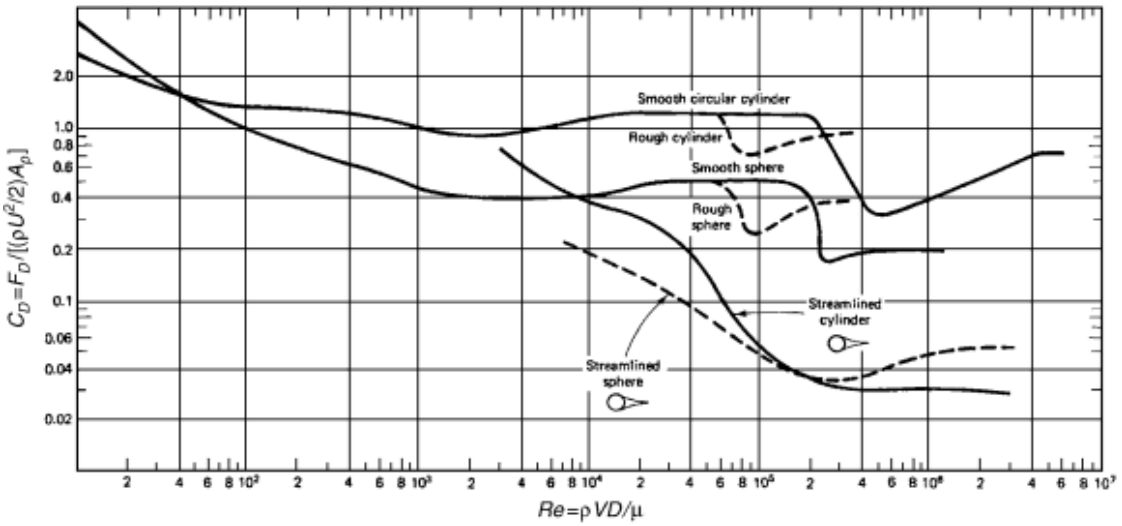

Figure 2.9: Drag coefficient (CD) as a function of Reynolds' number (Re) for different object shapes (Potter et al. 2011).

Moreover, when two different tree species which have similar leaf shape are compared to see the effect of leaf shapes on the drag coefficient (C_D), it is interesting that the average C_D value for the red maples at 11 m/s from the research of Kane and Smiley (2006) is approximately identical to the C_D value of a London-plane tree at 10 m/s from the research of Roodbaraky et al. (1994).

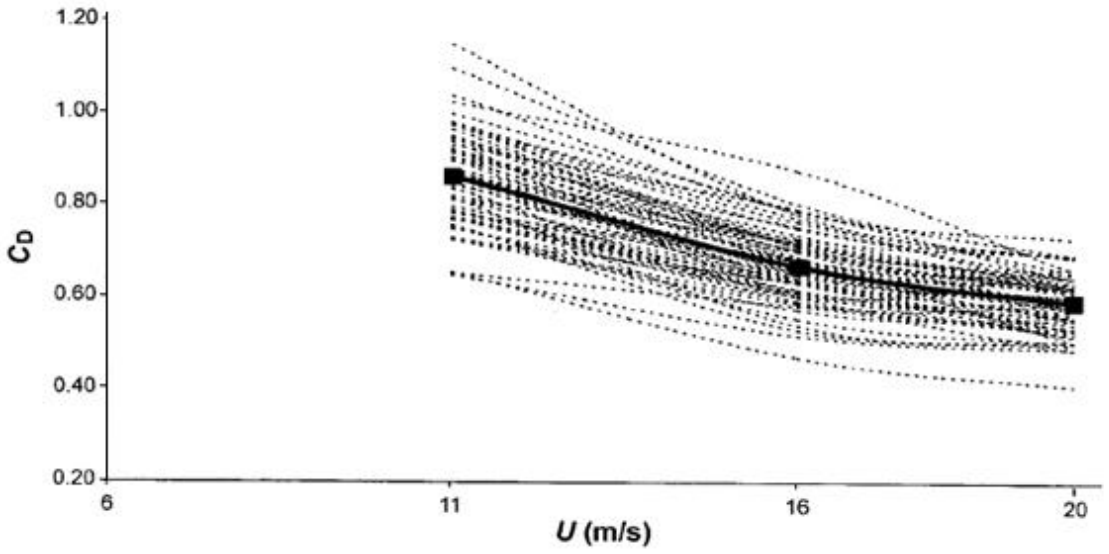

Figure 2.10: Graphical representation of the relationship between drag coefficient (C_D) and velocity (U) (Kane and Smiley 2006).

2.3 Tree Dynamic Response under Wind Induced Excitation

This section generally covers the literature about the dynamic characteristics of oscillatory motion of trees. These intrinsic characteristics are mode-frequencies, which MDOF systems will inherently oscillate at free vibrations, and damping ratio values of the system. Mode frequencies of this motion will be mentioned in the next section. The other intrinsic characteristic, damping processes of this oscillatory motion has already been addressed in section 2.2.2.2.

2.3.1 Dynamic Mode Frequencies in Trees

Trees have a number of modes (is related to the number of degree of freedom of each defined mass in trees). For the each mode they have an eigenfrequency, because they are a kind of multi degree of freedom system. In other words, each element (e.g.

main stem, first branch, and second branch in trees) has infinite mode numbers due to continuing mass distribution on these elements of trees. Furthermore, these mode-eigenfrequency values depend on stiffness and the mass of the system (system refers to any member of trees which have a periodic motion). The effect of the stiffness and the mass on the mode frequencies of the systems can be seen in the next sections.

2.3.1.1 Stiffness Effect on Dynamic Mode Frequencies

To see the effect of the stiffness on a SDOF system (basically), the proportional relation between the stiffness and the natural frequency of this system can be explained by Eq. 2.8 that the higher stiffness, the higher natural frequency.

$$\omega_n = \sqrt{\frac{k}{m}} \tag{2.8}$$

in which k is the stiffness, m is the mass for the SDOF systems.

Eigenfrequency of each mode in relation to the varying architectures of different species of trees were investigated in some research (Roodbaraky et al. 1994, Gardiner 1995, Peltola 1996, Speck and Spatz 2004, Sellier and Fourcaud 2005, Brüchert and Gardiner 2006) by doing some `pull and release` experiments on trees and in other theoretical studies (Sellier et al. 2006, Rodriguez et al. 2008). They found that the first mode frequency values of the trees are much more significant than the other mode frequencies, because the second mode can be seen only when the free vibration motion was initiated by pulling the stem at the location of one third of the stem height, and this second mode is not active when the motion is started by other initial conditions (Sellier et al. 2006). The results of these studies (first mode frequency values) are written in Table

2.3 to compare and see the effects of the different species of trees on fundamental frequency.

Table 2.3: Natural frequencies of trees from selected studies. W and S represent the winter and summer seasons, respectively, for the experimental research of Baker (1997).

Citation	Tree Species	Natural Frequency (Hz)
Castro-Garcia et al. 2008	Olive trees	20.2
Hassinen et al. 1998	P. Sylvestris	0.20
Sellier et al. 2006	Maritime Pine	0.60
Baker 1997	Lime trees	$0.71^{(W)}$ - $0.42^{(S)}$
Moore and Maguire 2004	Sitka Spruce	0.44
Moore and Maguire 2004	Lodgepole Pine	0.49
Moore and Maguire 2004	Douglas-fir	0.41
Kane and James 2011	Chestnut Oak	0.71

2.3.1.2 Mass Effect on Dynamic Mode Frequencies

Again, Eq. 2.8 is a good explanation for the inverse proportion between the mass and the mode frequencies of a system. Therefore, to estimate the varying of mode frequencies of trees with constant stiffness, it is important to focus on the variation in mass matrix of trees. For example, the mass matrix of deciduous trees can be change within the seasons. Baker in 1997 found that same deciduous trees have substantial lower fundamental frequencies for the summer terms than for the winter seasons. It can be explained by inversely proportion between the mass and the natural frequency of trees.

Additionally, Kane and James (2011) agree with Baker (1997) with their results that leafless trees have about 2.5 times greater frequency than in-leaf trees. Thus if it is focused on that the lower the natural frequency, the lower the failure wind force or wind speed (Baker 1997), it can be supposed to be that the summer terms might be more dangerous for trees because of the property of the spectral density function of wind speed. (An example exists in the Chapter 4 for the spectra of wind speeds to see the property of this function.) On the other hand, decrease in drag (Kane and Smiley 2006) and the increase of the damping due to leaves (Kane and James 2011) also should be considered for the summer terms. Moreover the increasing of the total mass of trees within the case of ice accretion on branches in winter seasons was investigated by Kane and James (2011). They state that a thin layer of ice accretion could alter the system frequency by 2 % of the frequency had existed before the ice accretion.

2.3.1.3 How to Obtain or Estimate Dynamic Mode Frequencies

Various research studies used several methods to obtain the mode frequencies of trees by using some experimental results or applying some mathematical models to represent trees. These methods will be explained in the next sections under the names of ‘experimental methods’ and ‘analytical methods’.

2.3.1.3.1 Experimental Methods

To find the fundamental frequency of trees experimentally, several different methodologies and instruments were used and improved by several studies. For instance, some of them (Milne 1991, Roodbaraky et al. 1994, Gardiner 1995, Flesch and Wilson

1999, James and Kane 2008, Kane and James 2011) used portable dataloggers to take the record of data from sensors which can measure the displacements of trees. Some other ones (White et al. 1976, Blackburn et al. 1988, Peltola and Kellomäki 1993, Peltola 1996) used accelerometers even if they can have some errors due to estimated initial position of trees. Moreover, as another example to the different experimental methodologies, Baker (1997) focused on measuring the power spectrum of tree velocity by using a Laser Doppler Interferometer in order to obtain the natural frequency of trees.

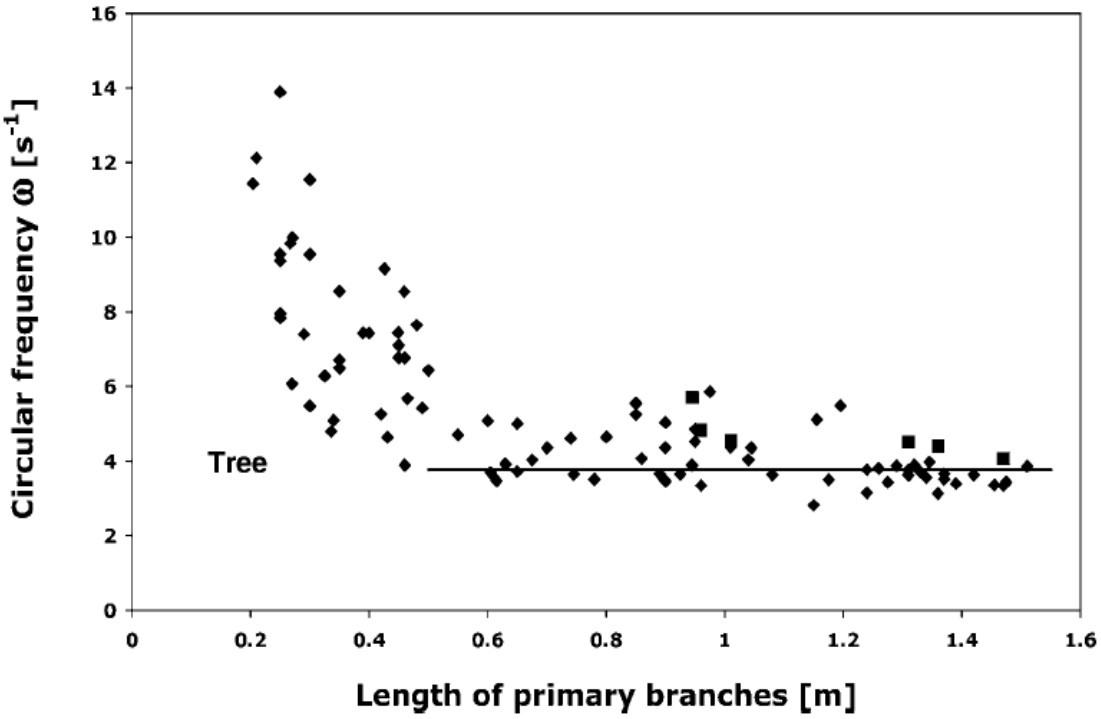

Figure 2.11: Eigenfrequencies of all primary branches of the Douglas fir (*Pseudotsuga menziesii*) tree with a length greater than 0.2 m. The frequency measured for the intact tree is indicated by an unbroken line (Spatz et al. 2007).

To find a relation between the mode-frequency of each element (such as main stem and all primary branches) and the natural frequency of the whole system, Spatz et al. (2007) worked on frequency values of branches of 12 years old Douglas-fir trees in

Germany. They compared these branch frequencies with the oscillation of the intact trees like in Figure 2.11. According to them, all large branches have close frequency to the natural frequency of the main system as can be seen in Figure 2.11. Thus, the combination of all the branches in trees can affect the fundamental frequency of the whole system (trees). For instance, whereas some research (Sellier and Fourcaud 2005, Spatz et al. 2007) found that the intact trees have approximately one third (1/3) of natural frequency of debranched stem cases for the same trees. The research of Milne in 1991 obtained for 26 years old Sitka spruce trees in Scotland that this ratio is nearly equal to 2/3. It means that this ratio may be varied for trees; because, for example, Spatz et al. (2007) states that the dominance or the effect of branches on the natural frequency of trees (Douglas fir) depends on the proportion of branch mass with respect to the trunk mass.

2.3.1.3.2 Analytical Methods

Estimates of the fundamental frequency of trees are useful to compare with detailed models. Several different approaches may be used to determine these estimations. Five of these approaches were chosen as the most common ones from literature and are addressed in this section. By the way, several of these methods are considered as a typical of dynamic analysis.

The first approach is to assume that trees are a kind of single degree of freedom system, so its fundamental frequency is equal to the square root of the ratio of the stiffness of cantilever tree structure to the mass of the tree. This method is describing Eq. 2.8 as in the study of Sellier and Fourcaud (2005).

The second method is based on the application of the principle of conservation of energy. According to this method, the natural frequency of trees can be calculated by using Eq. 2.9 as in the research of Milne (1991).

$$\omega_n = \sqrt{\frac{\sum 0.5\eta_i\theta_i}{\sum 0.5x_i^2 m_i}} \tag{2.9}$$

where the subscript of *i* refers to a vertical section of trees, x_i is the maximum horizontal displacement, m_i is the mass, η_i is the bending moment in the stem, and θ_i is the angular displacement of the stem for the vertical ith section.

The third method is derived from dynamics of distributed property systems (Humar 1990). For this method, the assumptions are to accept that the modulus of elasticity and the mass are uniformly distributed, and the cross-section is constant through the length of stem. Thus, the natural frequency can be found by using Eq. 2.10.

$$\omega_1 = (1.875)^2 \sqrt{\frac{EI}{mL^4}} \tag{2.10}$$

where E is the modulus of elasticity, I is the second moment of area (or moment of inertia), m is uniformly distributed mass along the length (L) of stem.

The fourth method is based on the estimates of Blevins' λ (Blevins 1979) from the measured fundamental frequencies of a specific species. His expression (Eq. 2.11) can be used to find the natural frequency of slender and tapered beam elements.

$$f_n = \frac{\lambda^2}{2\pi h^2} + \sqrt{\frac{EI_o}{\rho A_o}} \tag{2.11}$$

where f_n is the natural frequency, I_0 is the area moment of inertia, A_0 is the area of the cross-section at the base of the cantilever beam (cantilever stem), h is the height of trees, E is the modulus of elasticity, and ρ is the material density. The unitless parameter, λ can

be affected by the varying of the physical properties of trees (such as shape, mass distribution, vertical or horizontal orientation, type of the supporting point, mode of bending, taper of the beam, and so on). On the other hand, this dimensionless parameter can be estimated by using some experiments for a specific species under some certain shapes. For instance, Milne (1991) estimated its average value as 2.08 with its low standard deviation (0.06) for Sitka spruce trees.

Finally, the fifth empirical method is developed by the research of Mayhead (1973) thanks to the data collected during the 1960s by the British Forestry Commission. This empirical equation includes not only a main part (as seen in Eq. 2.12) but also an expansion part which may vary with tree species. But this expansion part could be neglected unless they had been obtained for a specific species. Thus, the natural period of trees can be estimated approximately by using Eq. 2.12.

$$T = 0.86 + 0.74\frac{H\sqrt{MH}}{DBH} \tag{2.12}$$

where M is the total mass of tree, H is the height of tree, and DBH is the diameter at breast height (approximately 1.4 m). Additionally, Moore and Maguire (2004) also combined the results of several previous studies and re-analyzed the data on the relationship between tree height, tree diameter, and tree natural frequency by using eight different species (totally 602 trees), and they plotted their results which are comparable with the empirical formula (Eq. 2.12) as can be seen in Figure 2.12.

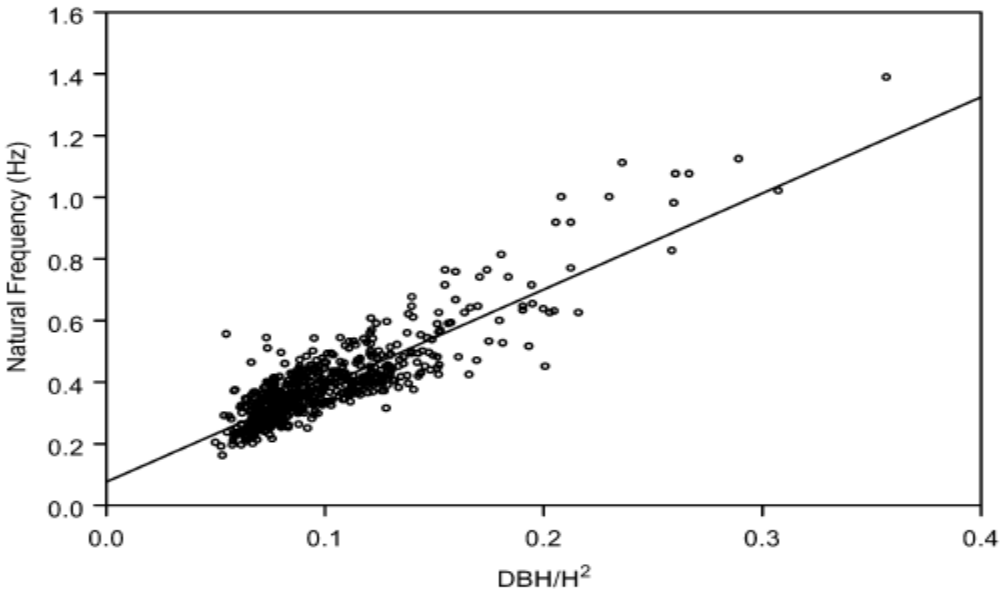

Figure 2.12: Relationship between natural frequency and the ratio (DBH/H^2). The equation of the fitting line on the data points is $fn = 0.0766 + 3.1219(DBH/H^2)$ (Moore and Maguire 2004).

Baker (1997) studied on season effects on tree natural frequency as in Figure 2.13. According to him, there is an inversely correlation between the DBH and 1/T (natural frequency of trees) under different conditions such as winter and summer terms. This study also shows the importance of tree height on the natural frequency, because this inversely correlation between DBH and the natural frequency can be converted to directly proportionality after concerning the effect of tree height as in the study of Moore and Maguire (2004) (Figure 2.12).

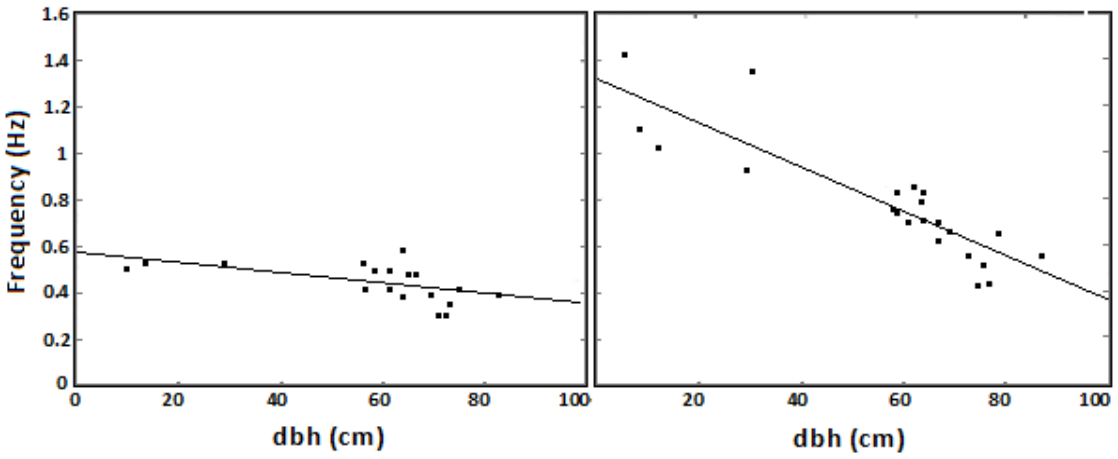

Figure 2.13: Natural frequency versus dbh (tree diameter at breast height) for healthy limes. The graph at the left is for summer conditions, the latter one is for winter conditions (Baker 1997).

Up to here, the first natural frequency of trees can be estimated by using these different five methods. Then to find the other mode frequency values of trees, some mathematical formulas can be used as in the research of Rodriguez et al. (2008). They improved these formulas by utilizing of that trees are assumed like a general fractal structure. For the sympodial shape trees,

$$\frac{f_N}{f_I} = \lambda^{\frac{(N-1)(\beta-2)}{2\beta}} \tag{2.13}$$

For the monopodial shape trees,

$$\frac{f_{N,P}}{f_{I,I}} = [\lambda^{N-1}\mu^{P-1}]^{\frac{(\beta-2)}{2\beta}} \tag{2.14}$$

in which N is to represent the nth mode, β is the slenderness coefficient, μ and λ are respectively the lateral and axial branching ratios, and α is the branching angles which are used to illustrate the two idealized trees (the sympodial and the monopodial shape trees) as in the research of Rodriguez et al. (2008). The values of these parameters can be

selected from Table 2.4. Moreover the representing of the different mode shapes in their mathematical models can be seen clearly in Figure 2.14.

Table 2.4: The parameters in the equations of Rodriguez et al. (2008) for idealized tree shapes.

Idealized Tree Shapes	β	λ	μ	α
Sympodial	3/2	1/2	0	20^o
Monopodial	3/2	1/6	2/3	30^o

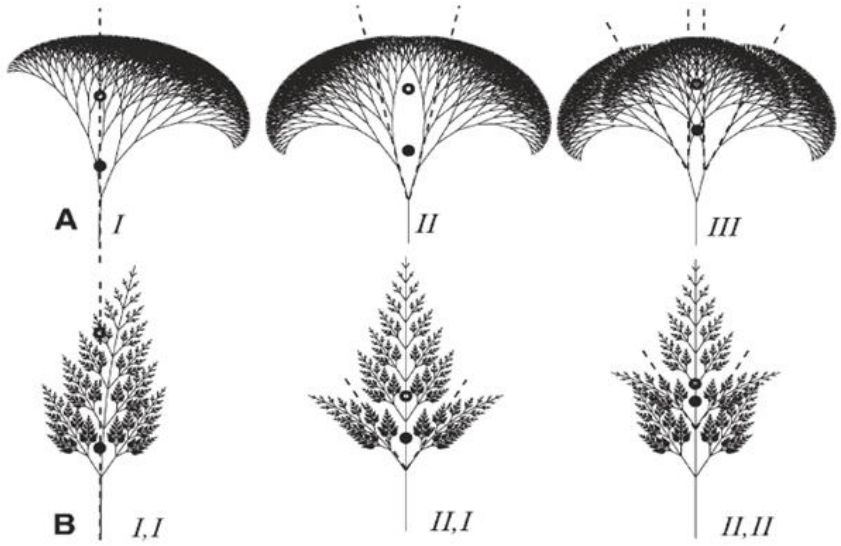

Figure 2.14: (A) Modes of groups I, II, and III of the sympodial model tree. (B) Modes [I,I], [II,I], and [II,II] of the monopodial model tree (Rodriguez et al. 2008).

2.4 Tree Mechanics and Tree Failures

Mechanical properties of wood (tree material) are orthotropic, that is, material properties are different depending on the direction considered. For example, strength depends on the direction of forces with respect to the direction of the grain and it also

depends on the type of forces applied (compression or tension). Therefore, strength of wood is often defined as parallel or perpendicular to the grain direction. Tensile strength parallel to the grain ($\sigma_{||}^{Tension}$) is generally the highest one, parallel compressive strength ($\sigma_{||}^{Comp.}$) is higher than the parallel shear strength ($\sigma_{||}^{Shear}$). Moreover, the perpendicular tensile strength ($\sigma_{\perp}^{Tension}$) is lowest one. Additionally, when the perpendicular compression strength ($\sigma_{\perp}^{Comp.}$) is moderate, the perpendicular shear ($\sigma_{\perp}^{Shear}$) is high with respect to all strength values of wood. The ranking of these strength values can be seen in the inequality below (Hoadly 1980, Green 2001, Kretschmann 2010). For example, while the parallel tensile strength (highest one) of Western hemlock is 89600 kPa, the perpendicular tensile strength (lowest one) is 2000 kPa for the same tree species (Kretschmann 2010).

$$\sigma_{||}^{Tension} > \sigma_{\perp}^{Shear} > \sigma_{||}^{Comp.} > \sigma_{\perp}^{Comp.} > \sigma_{||}^{Shear} > \sigma_{\perp}^{Tension}$$

Of all these strength values, the parallel tensile and compression strength values play the most important role for bending failure of trees under wind forces. As it can be easily seen from the inequalities above between the different strength types that wood is stronger in tension at the direction of parallel to grain than in compression at the same direction. Additionally, many experimental data (Richard et al. 1999, Kretschmann 2010) about the different strength properties of different species state that this tensile strength is approximately two times as greater as the compressive strength in a number of trees. Thus, failures in general occur on the leeward or the compression side of the cross-section of stems or branches (Wagener 1963, Hoadly 1980, Mattheck et al. 1994). Before completely failure, the material in tension side tries to compensate for the compressive

strength loss by changing the place of the neutral axis of bending, even if some portions of compression wood has been failed (Mergen 1954, Mattheck et al. 1994).

How to obtain the wood strengths is conducted by several standard tests (American Society for Testing and Materials, 1971). The most common test is to determine wood strength of beams in use is the static bending test called as ASTM D-143 standard test. This test can also be used to obtain a value for the modulus of rupture (MOR) of the materials. The meaning of MOR is the bending stress of the materials to have maximum load-carrying capacity under bending (Kretschmann 2010).

Hankinson's formula may be used to determine strength of wood in any direction knowing the direction of applied loading relative to the direction of the grain. Thus the strength of wood in any direction depends on the angle of the direction, and the parallel and the perpendicular tensile strength of the wood as in the formula in Figure 2.15 (Hankinson 1921). Thus only by using or finding the compressive or tensile strength to perpendicular to grains, the other strength (parallel to the grains) can be estimated due to the Hankinson's formula by considering angle phase is 90^0, and vice versa.

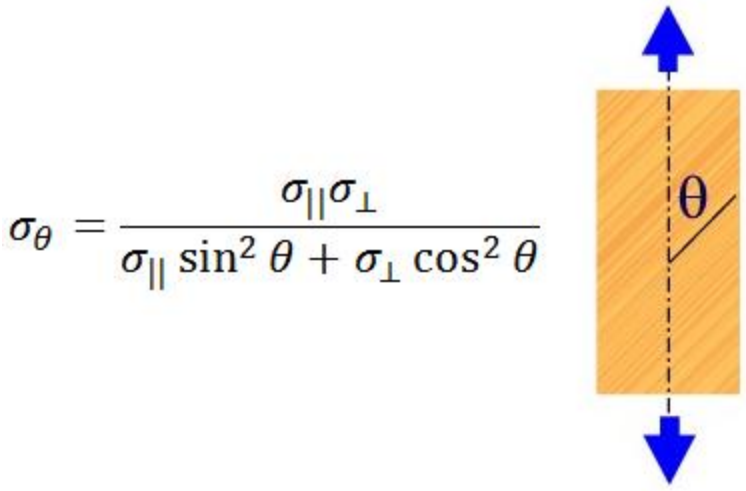

Figure 2.15: Hankinson's formula (www.worldwideflood.com/ark/design_calculations/wood_strength.htm).

2.4.1 Decay Effect on Tree Mechanics

The data of the USDA Wood Handbook (Kretschmann 2010) submits all strength values for each strength type of many tree species, and these strength values are for healthy trees. But, in general, trees might have some loss of strength because of some defects. These defects result from decays (such as, usually, hollow decays, cavities) in wood material, effect of included barks (especially for v-attachments and codominant stems) and imperfection on attachment-angles of branches (Kane et al. 2008). Gilman (2003) has the similar results on Acer Rubrum trees about the effect of included barks in codominant stems with the results of Kane et al. (2008), again, on the same tree species. Additionally, the investigations of Gilman (2003), Kane (2007), and Kane et al. (2008) were on some experiments about the strength loss can be changed with the ratio of branch diameter to trunk diameter (D_b/D_t). Gilman (2003) improved an empirical linear equation

about to find the strength of branch attachments by using the ratio of branch diameter to stem diameter. To represent this formula, it is plotted as in Figure 2.16.

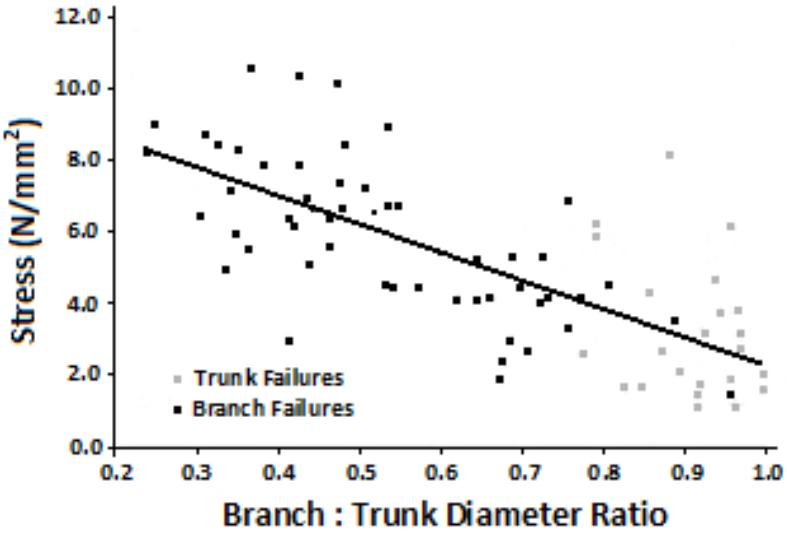

Figure 2.16: Stress (in N/mm^2) required separating a branch from the trunk for a variety of the aspect ratios (Gilman 2003).

The strength loss at branches with respect to the aspect ratio is also plotted in the experimental research of Kane (2007) in Figure 2.17, and Kane et al. (2008) in Figure 2.18. They improved three equations to approximately find the new failure stress of the attachments of three different trees (sawtooth oak, callery pear, and red maple trees) in terms of D_b/D_t ratio of the attachments. The results of these graphs in Figure 2.17 and Figure 2.18 are consistent with the concept that the strength of any elastic material may change with the effective slenderness ratio of the material under stresses. As an example to these elastic materials, changing of the compression design stress of a steel material can be seen in Figure 2.19 (Kumar and Kumar 2005).

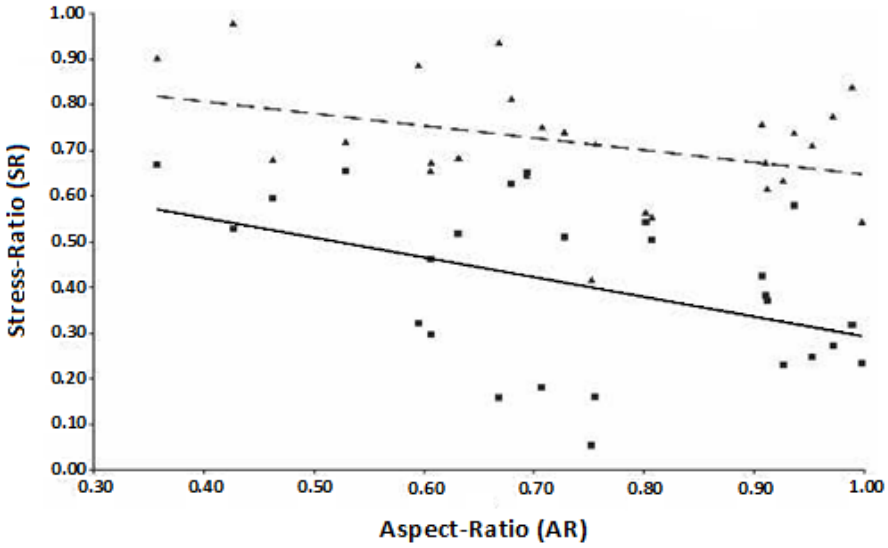

Figure 2.17: Scattered plot and best fit lines between stress ratio and aspect ratio. Stress ratio was calculated using inside bark branch depth and width (triangular data) and outside bark branch diameter (square data) (Kane 2007).

There are also another experimental study (Kane and Clouston 2008) obtained amounts of stress failures and calculated strength loss by considering the difference between these stress failures and capacity strength of perfect healthy trees (MOR). According to Kane and Clouston (2008), their experimental data shows that strength loss is about 55 % due to codominant stems, whereas non-codominant stems have 21 % strength loss.

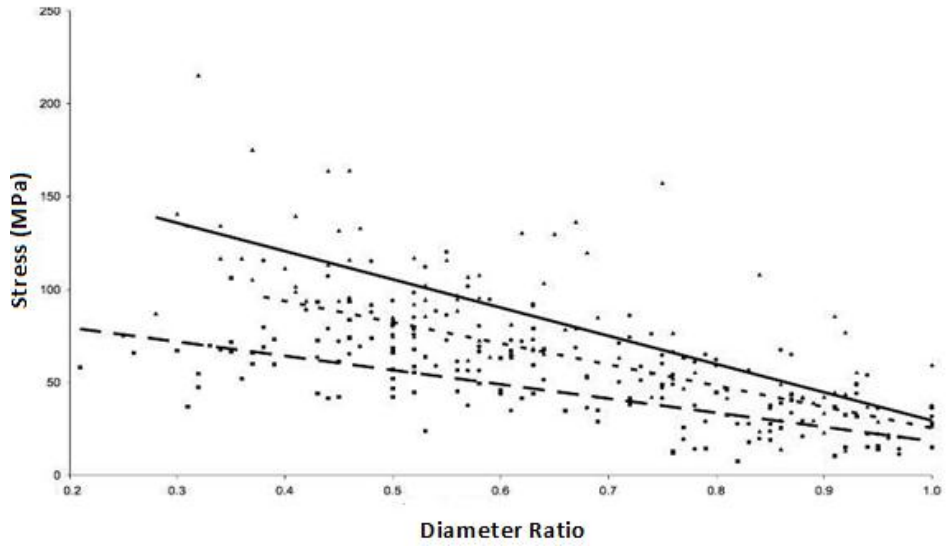

Figure 2.18: Scattered plots for the prediction of stress from the ratio of branch diameter to trunk diameter (Kane et al. 2008).

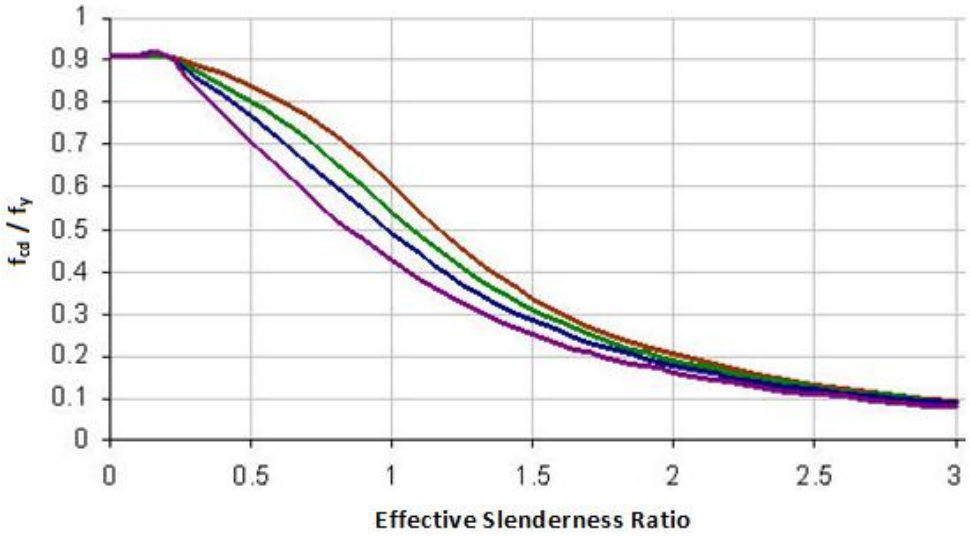

Figure 2.19: Column buckling curves for different buckling classes. Whereas f_{cd} is the design stress in compression, f_y is the yield stress (Kumar and Kumar 2005).

2.4.1.1 Assessing Strength Loss due to Decays

However, to predict the loss of strength is really complicated, because trees are individuals, and so it is quite difficult to obtain a "one size fits all" calculation or estimation of strength loss. According to some research (Mills and Russel 1984, Lucas et al. 1984, Robbins 1986, Matheny and Clark 1991, Smiley and Fraedrich 1992, Albers and Hayes 1993, Kennard et al. 1996), experience of foresters and arborists, and observations (Wagener 1963), some thresholds can be developed by using several approximate estimations of strength loss due to decays (Kane et al. 2001). There are four important formulas commonly used in the literature survey of tree failures in order to estimate this strength loss in percentage. Whereas two of them are about the effect of only concentric decays, the third one [Figure 2.20 from Smiley and Fraedrich (1992)] has the effect of concentric decays with open cavities. The last one (belongs to "offset hollow" in Figure 2.20) is related to the off-centric decays. The definition of decays for these formulas can be seen separately in Figure 2.21. Additionally, all of these formulas have some thresholds in order to give some information and alerts about the potential failure of trees for the hazard tree managers. By using these thresholds, managers can have some ideas about the distinctions between a hazardous tree which needs to be pruned or removed and a nonhazardous tree which can remain standing. The behavior of these formulas can be seen in Figure 2.20.

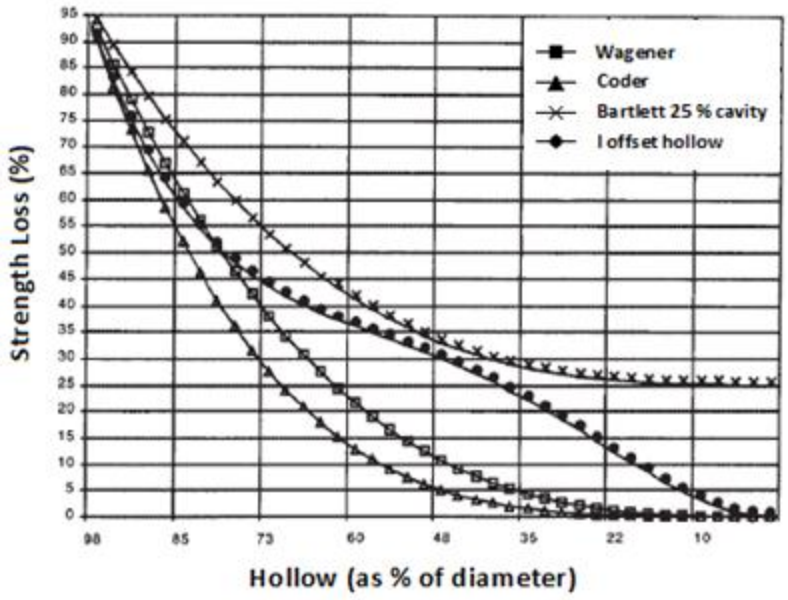

Figure 2.20: Graph of strength loss as a function of stem hollow percentage (Kane et al. 2001).

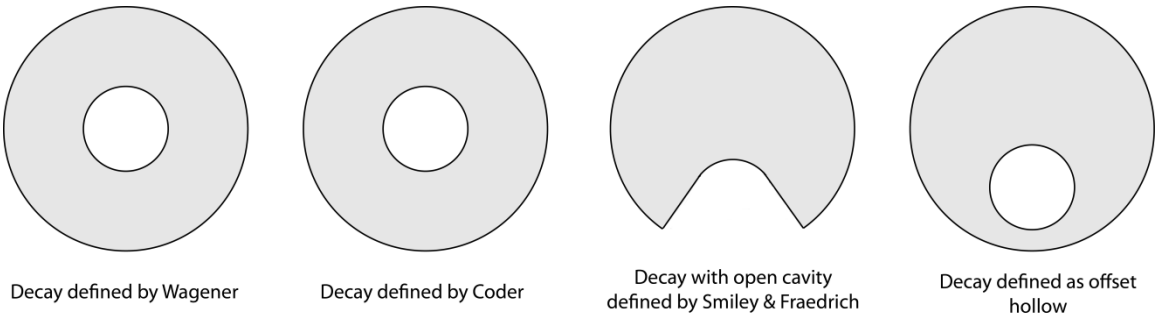

Figure 2.21: Simple definitions of decays which used for the curves in Figure 2.20.

Wagener (1963) assumed that the materials of trees are like a pipe due to concentric hollow decays, and then he traced not to only Eq. 2.15 which is used in solid mechanics but also his experiences and observations to estimate and calculate the strength loss of trees. His anecdotal study states that the loss of strength in conifers depends on the formula d^3/D^3 as in Figure 2.20, where d is the diameter of hollow decay column and D is the average stem diameter inside bark (Wagener 1963). For instance, if a

10 in. diameter tree has a 5 in. diameter decay column, the loss of strength can be calculated as 12.5 % by using Eq. 2.15.

$$loss\ in\ I_{Stem} = \frac{d_H^3}{D_S^3} \tag{2.15}$$

in which d_H is the diameter of hollow to represent the decays in cross-sections, D_S is the diameter of this cross-section.

According to mechanics of solids formula, the loss in moment of inertia of cross sections due to decays can be derived by using Eq. 2.16.

$$loss\ in\ I_{Stem} = \frac{I_{decay}}{I_{Stem}} = \frac{0.25\pi d_H^4}{0.25\pi D_S^4} = \frac{d_H^4}{D_S^4} \tag{2.16}$$

Coder (1989) used the ratio of d^4/D^4 as in Eq. 2.16 for his research to create a hazardous threshold graph for wind induced tree failures. He states that the d^4/D^4 formula can be applicable only to perfect circles of decays and stems under ideal test conditions, so the outcome of the formula must be judged carefully.Coder (1989)

At the Barlett Tree Lab, Smiley and Fraedrich (1993) improved Wagener's formula by adding the effect of cavities to estimate the strength loss. This inclusion is important, because an open cavity (an example of an open cavity can be seen in Figure 2.21) is generally at the outer tree rings, and the outer rings have the significant portion of the total strength of trees. According to Barlett's empirical formula, the percent of strength loss can be calculated by Eq. 2.17.

$$SL\ (\%) = \frac{d^3 + R(D^3 - d^3)}{D^3} x100 \tag{2.17}$$

where *d* and *D* are respectively average of the diameter of decay and sound wood, and *R* is the ratio of cavity opening to stem circumference. Again, the decay and the stem are assumed concentric circles like in the formulas of Wagener and Coder.

As another type of decays, non-concentric (off-center) decays, Mattheck et al. (1994) studied with some experiments on 800 broken and standing trees. According to the results of these experiments, they noticed an empirical inequality for tree risk assessment that when t/R (t is the thickness of sound wood remaining in a stem and R is the radius of the stem) is less than 0.3, in general trees were failed. For standing trees after the experiments, the ratio of t/R is greater than 0.3. Additionally, what the authors did not take into account of the effect of cavities less than one-third of the stem circumference is mentioned in the research of Kane et al. 2004.

Moreover, in the light of each 4 formulas mentioned before about the strength loss of trees due to decays, the authors decided to have some thresholds for the hazard tree managers by using their experiences and observations on real tree data. For instance, whereas the decision of Wagener is that the hazardous case of tree failures starts after strength loss is 33 %, Coder decided that annual review required under 20 % strength loss, caution case is for the interval of 20 % and 44 % strength loss, and the hazardous case begins after strength loss is 44 %. The statistical figure (Figure 2.22) below shows us the thresholds for each of 4 formulas (Kane et al. 2001).

Moreover, about the defect and decay thresholds for the hazard tree managers, some researchers ((Smiley and Fraedrich 1992), (Kane et al. 2001) accept that if the diameter of defect or decay exceeds the 70 % of the trunk diameter, the tree can be considered as severe hazard.

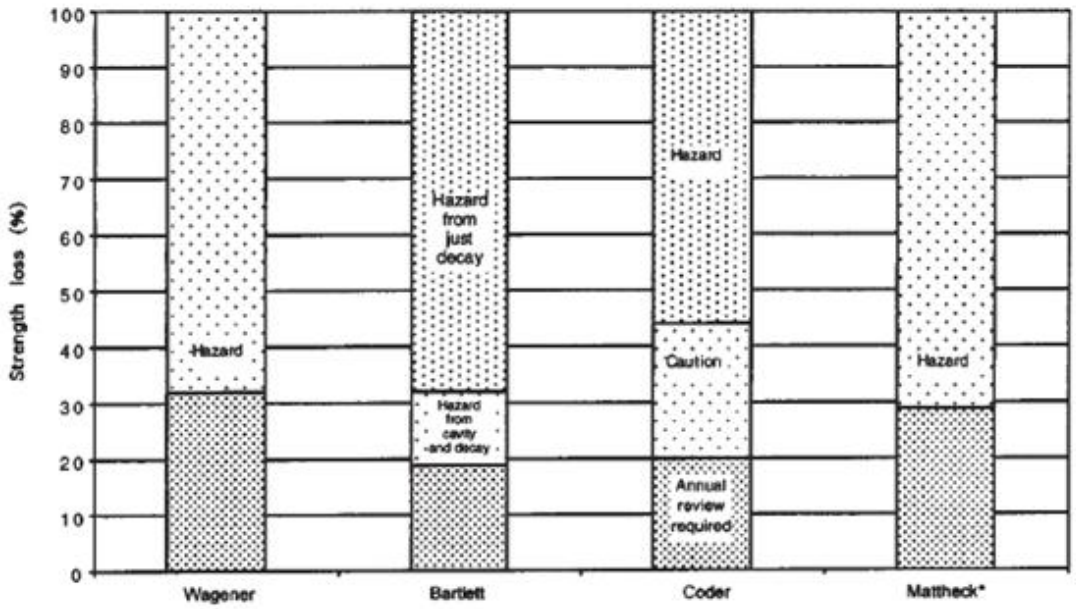

Figure 2.22: Hazard tree strength loss thresholds (Kane et al. 2001).

2.4.2 Tree Failure Types under Wind Forces

Failures can be written under the common types which are called stem breakage, branch breakage, attachment breakage, and uprooting failure types. These failures depend on many factors are like wind speed and frequency, precipitation, soil strength, and tree characteristics (material, geometric, and mechanical properties of trees) (Kane 2008). For instance, the effect of various species on tree failure types was examined by Kane (2008). In this research, he emphasized the complexity of these factors with respect to tree species as can be seen in Figure 2.23. As another example to tree failure types, Kane (2007) concluded that Bradford pear trees have a reputation about their branch breakages.

Additionally, the influences of these factors, which can cause to various tree failure types, were conducted as very complicated phenomenon in many experimental

studies (Cutler et al. 1990, Gibbs and Greig 1990, Smiley and Fraedrich 1992, Fransic and Gillespie 1993, Putz and Sharitz 1996, Duryea et al. 1996, Jim and Liu 1997, Fransic 2000, Luley et al. 2002, Duryea et al. 2007), because the ideas and results of some researchers may have conflicts with the results of some other investigators. For instance, whereas Luley's results (Luley et al. 2002) state that there is no significant effect of pruning trees on reducing the number of branch breakage as a failure type in New York, other researchers (Duryea et al. 1996) found that pruning could reduce the chance of the branch breakage in another place, Florida.

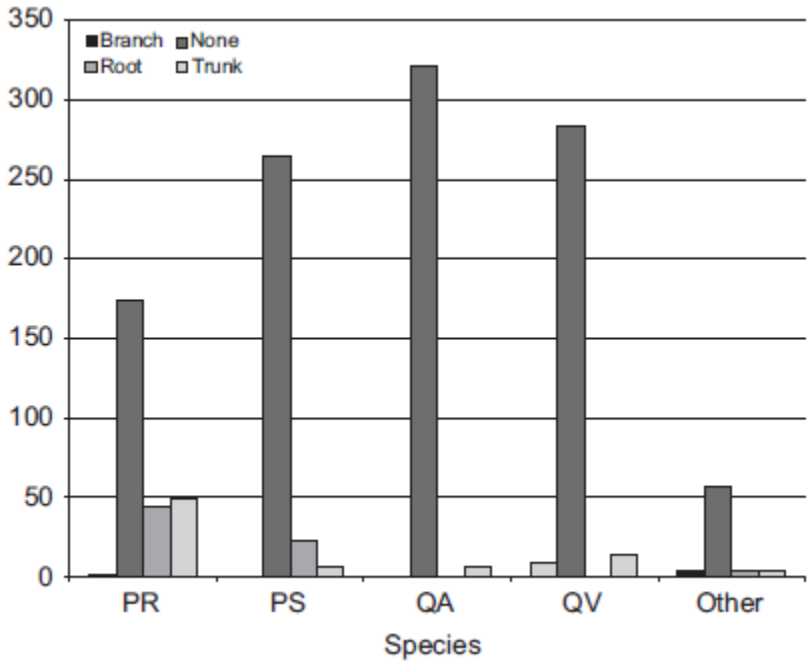

Figure 2.23: Frequency of each failure type for each species (PR: *Pinus rigida*, PS: *Pinus strobes*, QA: *Quercus alba*, QV: *Quercus velutina*, Other: *Acer rubrum*, *Carya glabra*, *Robinia pseudoacacia*, *Sassafras albidum*) (Kane 2008).

Branch breakage (as a tree failure type) does not seem to be affected by angle of attachment (Gilman 2003). In addition to Gilman's research, Kane (2007) and Miller (1959) emphasized that aspect ratio (the ratio of diameter of branches to the trunk

diameters which are the closest to those branches) is a good predictor instead of the angle of attachment. Moreover, Kane (2007) states the importance of the ellipse shape instead of the circle shapes of the branches on this failure type.

The difference between defining failures as branch breakage or branch attachment breakage is discussed by Kane (2007). To categorize as branch failure type more than 50 % of the total failed fibers must have originated in the branch. If less than 50 % of the total failed fibers originate in the branch, then failure is categorized as a branch attachment failure. In general, attachment failures occur when bark is included at the attachment, so if the failure type is branch attachment breakage, the presence of the included bark can be checked at the attachment point (Kane 2007).

Figure 2.24: Examples of the failure modes for (A) the embedded branch failure mode, and (B) the flat surface failure mode (Kane et al. 2008).

There are three important failure sub-categories for the attachment breakage failure (Kane et al. 2008). These are embedded branch failure mode, flat surface failure mode with included bark, and ball-in-socket failure mode (Figure 2.24 and Figure 2.25).

In addition, Kane (2007) states that aspect ratio of trees is a good predictor on the branch attachment strength. Therefore, it can be accepted that the aspect ratio of trees has an important role on causing to the attachment breakages.

Figure 2.25: An example of the ball in socket failure mode (Kane et al. 2008).

2.4.2.1 Risk Assessment on Tree Failures

Tree risk assessment has been investigated, especially, under the wind loads. Three different approaches were developed and commonly used over the last 25 years: (1) qualitative assessments, (2) empirical or statistical models, (3) mechanistic models (Gardiner et al. 2008). All these approaches were developed for, generally, trees in forests. The first model is based on observational tools (e.g. Miller 1985, Mitchell 1998). The second one is mentioned by several researchers (e.g. Valinger and Fridman 1997, Lanquaye-Opoku and Mitchell 2005), and the advantage of the second approach with respect to the first approach is that this second one may be quite accurate and reliable for various locations (Gardiner et al. 2008). The third approach is the newest and most common one which was developed by Peltola et al. (1999) (HWIND mechanistic models)

and Gardiner and Quine (2000) (GALES mechanistic models). HWIND and GALES use a static analysis for trees in stands by using empirical gust factors in order to attempt to catch the effect of the dynamic response of the trees under fluctuating wind. But, the disadvantage of these mechanistic models is that they may not accurately calculate the critical wind speed for the trees in various locations elsewhere the empirical tests were done. Additionally, it is possible to see the cumulative distribution function diagrams in a few studies (Gardiner and Quine 2000, Ancelin et al. 2004, Schelhaas et al. 2007) for the tree failures in stands.

2.5 Conclusion

All the information in this literature review (Chapter 2) have been searched to see significant studies on understanding tree language and to have some important ideas about tree risk assessments, and to obtain some ideas to reduce the likelihood of tree failures under wind forces. To mention the importance of the literature review section by section:

Section 2.2 has the important information utilized in the other chapters, especially in the details of tree modeling approach in Chapter 3. In other words, this section is a good source for Chapter 3 to find a combination of the important computational studies with their methodologies, results, and discussions. For example, dynamic approach on trees subjected to wind loading has been, in detail, addressed in this section to give an idea how to correctly do a model in a FE modeling.

Section 2.3 is related to tree dynamic response under wind excitation forces. This section is also so important to validate tree modeling, which will be defined in Chapters

3, 4 and 6, because of that this section has many significant discussions about various tree responses. Thus it is possible to discuss the results of Chapters 3, 4 and 6 with all these information in this section.

Section 2.4, finally, is about the tree mechanics and failures. The importance of this section is that it is inevitable to learn tree mechanics and failures for doing research on tree risk assessment as applied in Chapters 4 and 5. For example, in this section, it is possible to find several important studies about how they have addressed decay effect on tree failures and tree risk assessment.

Furthermore, as can be seen in this chapter (literature review), it is easier to find many computational studies conducted on forest trees than open-grown trees. Thus, the current research in this Thesis will consider open-grown trees.

CHAPTER 3

FINITE ELEMENT MODELING OF AN OPEN-GROWN MAPLE TREE

3.1 Introduction

A large body of knowledge has investigated windthrow and trunk breakage for forests under static loading (Peltola 2006), but very few studies have considered large and open-grown trees (Kane and Clouston 2008) with dynamic loading. It has also long been recognized that predictions of critical wind speeds from static analyses are overestimates, presumably from the dynamic interaction of wind and tree (Oliver and Mayhead 1974). Thus, to investigate the dynamic behavior of large and open-grown trees subjected to dynamic wind loading, as the first goal of this chapter, a finite element (FE) model was constructed in a computer package program, ADINA 8.5 from ADINA R&D, Inc. in located at Watertown, MA by using field measurements taken by Kane et al. (In preparation) of a large, decurrent sugar maple (Acer saccharum), a common amenity tree in the northeastern United States. Then, as a second goal of this chapter, this FE model was validated by comparing the calculated modal frequency results with experimental values, determined from the tests of Kane et al. (In preparation), and with several empirical and numerical formulae.

Investigations of tree dynamics have been both empirical (Blackburn et al. 1988, Baker 1997, Moore and Maguire 2005, James et al. 2006, Spatz et al. 2007, Rodriguez et al. 2008, Kane and James 2011) and theoretical (Baker 1995, Kerzenmacher and Gardiner 1998, Saunderson et al. 1999, England et al. 2000). In this chapter, FE modeling has also been used to computationally (theoretically) investigate the wind-induced

dynamic response of trees. This dynamic response of trees was characterized by using a single dynamic displacement amplification factor, Rd, which is described in Section 3.5, as has previously been used to investigate the dynamic response of trees in the research of Sellier and Fourcaud (2009).

3.2 Tree Selected for FE Modeling (Prototype Tree)

A sugar maple (Acer saccharum) growing in Belchertown, MA, USA (72.413º W longitude and 42.277º N latitude) was chosen as an example to large and open-grown trees in the northeastern United States. This location was formerly an institutional property with streets and buildings, and the size and crown architecture of trees (Figure 3.1) were typical of those growing in residential settings in the northeastern United States. In addition, this tree will be used as the base model (denoted M100) for all the parametric models described in Chapter 6.

The diameter of the main stem is 53 cm at a height of 1.4 m above the ground (diameter at breast height, DBH) and the overall tree height is 17.1 m. Its crown is 13.7 m in height and 12.1 m in width; the ratio of minimum to maximum crown width, measured orthogonally, is 0.74. The height, diameter, attachment angle, and azimuth of all eleven primary branches were also measured by Kane et al. in preparation (see Table 1). Branch length was not measured due to time constraints. The seventh branch of the tree (Table 1) effectively served as a co-dominant stem. This characteristic has important consequences on the dynamic response as will be discussed later.

Figure 3.1: Maple tree in Belchertown, MA which is used for the base model, M100.

In August 2006, strain meters that measured trunk axial displacements accurate to 0.001 mm were attached orthogonally to the stem (north or south and east or west sides) of the prototype tree approximately 1.4 m above the ground as described by James and Kane (2008). A skidder with a cable winch (John Deere model 440D) was used to apply a point load at approximately 40% of tree height, where the diameter of the trunk was large enough to sustain the applied load without failing. The tree was pulled and released three times, incident with each strain meter (six tests total); loads were always applied to place the strain meters in tension. Axial displacements during free sways were recorded on both strain meters (incident and orthogonal) and plotted with respect to time. The time (t) and amplitude (y) of four successive maximum displacements (i = 1, 2, 3 and 4) were used to

determine fn (1/Tn) and damping ratio (ζ), which was calculated using the logarithmic decrement method (Eq. 3.1):

$$\frac{y_i}{y_{i+1}} = exp\left(\frac{2\pi\zeta}{\sqrt{1-\zeta^2}}\right) \tag{3.1}$$

3.3 Finite Element Modeling

The FE modeling program ADINA-8.5 (ADINA Software, Watertown, MA, USA) was used to conduct the analyses of all tree models. The stem and branches of M100 were divided into longitudinal elements of constant geometry and modulus of elasticity (MOE). For each branch or stem element, MOE and diameter were separately defined before meshing the elements. The concept of local averages of random fields introduced by Bucher (2009) was used to define the properties of each element. In this method, each element is assigned properties of a homogenous material instead of using heterogeneous material properties, but the overall material variations are captured by dividing the tree model into sufficient elements.

Table 3.1: Diameter, estimated mass, mass-weighted mean MOE, attachment height, azimuth, attachment angle, and the first modal frequencies of the stem and each branch of M100. The first modal frequencies were calculated using Eq. 3.11 (Mabie and Rogers 1972). The first mode frequencies calculated by using Eq. 3.11 are close to the natural frequencies from the results of the FE modeling as illustrated in Figures from 3.6 to 3.12 for selected elements (Stem, each branch).

M100	Diameter (m)	Mass (kg)	MOE (GPa)	Attachment Height (m)	Azimuth Angle (º)	Attachment Angle (º)	Natural Frequency (Hz)	1st Mode Frequency (Hz)
Stem	0.53	1235	9.00	n/a	n/a	n/a	2.37	2.332
Top Branch	0.13	69	4.60	12.80	0	0	1.07	1.641
1st Branch	0.28	393	5.08	3.23	83	44	0.69	0.756
2nd Branch	0.27	320	5.03	3.96	230	23	0.73	0.811
3rd Branch	0.27	338	4.95	5.33	68	27	0.70	0.786
4th Branch	0.08	8	4.29	5.36	180	37	1.29	1.752
5th Branch	0.11	21	4.50	5.94	22	13	1.15	1.471
6th Branch	0.06	4	3.97	6.10	354	62	1.34	2.049
7th Branch	0.32	563	5.08	6.19	298	80	0.59	0.652
8th Branch	0.19	118	4.83	7.38	157	88	0.85	0.983
9th Branch	0.17	81	4.74	7.62	47	85	0.91	1.106
10th Branch	0.12	30	4.52	8.60	109	47	1.09	1.395
11th Branch	0.06	5	4.03	9.66	111	90	1.31	2.003

M100 was modeled using a sufficient number of beam elements of constant cross-sectional dimensions to model the branch taper approximately. Branches were divided into 12 elements of equal length. The stem was divided into elements as follows: nodes were established on the stem at the height of each branch; if the distance between two successive nodes exceeded 0.5 m, additional nodes were added at equal lengths midway between them so that no nodes were more than 0.5 m apart. The MOE of the proximal stem element was set to 10.7 GPa (Kretschmann 2010). For each subsequent element, MOE was adjusted in accordance with the slope of an empirical relationship for branches of Norway maple (Dahle and Grabosky 2010). For the elements in the distal 4.3 m of the stem (the top branch), MOE was held constant at the value of the first element in the top branch. Spatz and Bruechert (2000) noted a decrease in MOE of branches with branch height, so MOE of the proximal element of each branch was initially assigned the MOE of the stem element to which the branch was attached. After assigning the MOE of the proximal element of each branch, MOE of the other elements of each element was adjusted in accordance with the empirical relationship for branches of Norway maple in the study of Dahle and Grabosky in (2010) (see Figure 2.4). Then mass-weighted mean values of MOE for branches were calculated by considering the mass and assigned MOE of each element of branches. In order to have approximately a linear relationship between the branch diameter and MOE like in the empirical relationship developed by Spatz et al. (2007) (see Figure 2.6), the MOE values conducted to the seventh branch were adjusted. After this adjusting, all the mass-weighted mean values of MOE with respect to branch diameter can be seen in Figure 3.2.

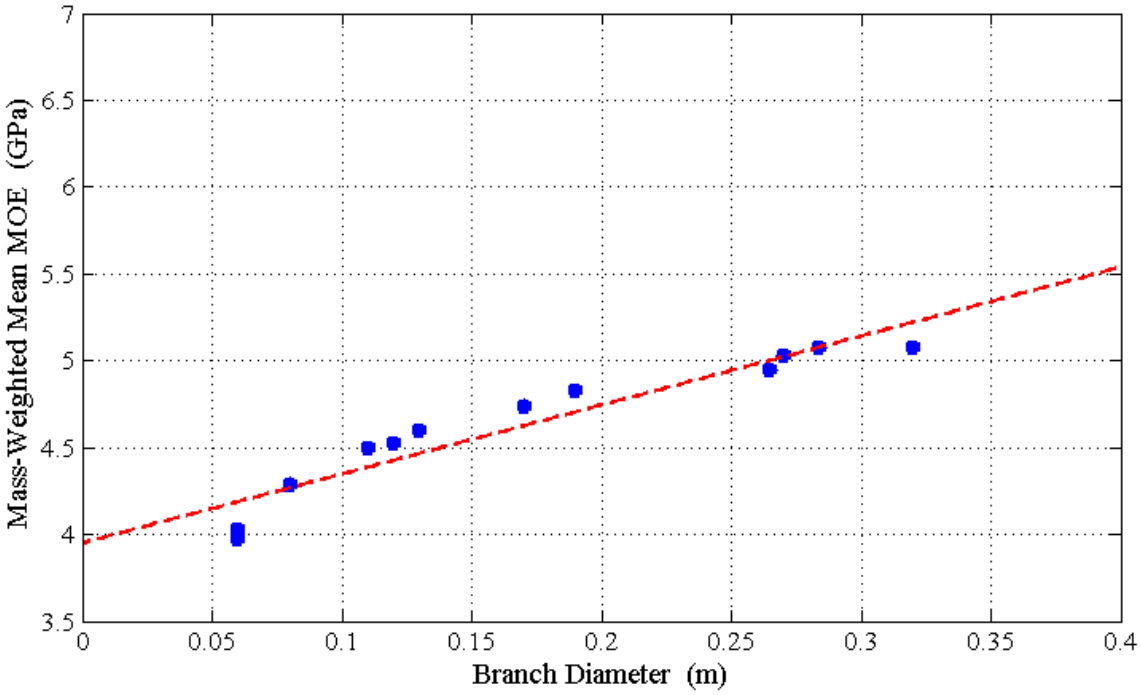

Figure 3.2: Adjusted and assigned mass-weighted mean MOE of the branches in the modeling.

Stem was assumed to be fixed at the base, and connections between branches and the stem were assumed to transfer moment at the attachments. Previous work has demonstrated that modeling branches as lumped masses attached to the stem can lead to errors of modeled natural frequencies of trees (Sellier et al. 2006, Moore and Maguire 2008).

The mass of the stem and branches were estimated assuming mean wood density of green wood specimens from the USDA Wood Handbook (Kretschmann 2010) and volume of the stem or branches. This method will slightly overestimate branch mass because diameters were measured outside the bark, which is not as dense as the wood itself. The FE models only considered the stem and primary branches. However, the estimated mass of secondary and tertiary branches was included by increasing the density

of the primary branches using a ratio. The ratio of stem volume to the total volume of primary branches was calculated for M100. Assuming that M100 follows a fractal structure as described by Rodriguez et al. (2008), the ratio was applied to each primary branch to estimate the additional mass of secondary and tertiary branches.

Empirically-determined damping ratio, ζ, for M100 was 16%, which was rounded down to 15% assuming Rayleigh damping. In order to emphasize damping for the first two modes of vibration, the Rayleigh damping coefficient (β) was assumed to be 0.001, as previously proposed (Sellier et al. 2006, Castro-García et al. 2008). If β is known, α can be calculated from Eq. 2.3 where ω_k is known from the undamped dynamic analyses and ζ is 15%.

Material nonlinearity was ignored in the FE model because the tree response did not exceed the yield stress, so displacements and stresses remain within the elastic region. Geometric nonlinearity was neglected, because stiffness reduction caused by P-Delta effects is negligible given the relatively small mass near the top of trees. Although the lateral deflections of trees may be large near the top, gravity loads are generated by self-weight, which is distributed along the components of the system. The largest gravity loads occur near the bottom of trees where deflections are small.

Newmark's time history linear acceleration method used to conduct the dynamic analyses is stable if the ratio of time step to natural period of the model ($\Delta t/Tn$) is less than or equal to 0.551 (Chopra 2007). To avoid any stability problems, particularly for higher modes, a sufficiently small time-step of 0.05s was selected for the analyses. To verify the accuracy of the prototype model, the undamped natural frequency was

calculated in the FE program as 0.59 Hz (so Tn = 1.69). Thus the ratio of the time-step increment to the natural period of the model is $\Delta t/Tn = 0.05/1.69 = 0.029 < 0.551$.

3.4 Assumed Wind Loading

Since wind speed varies with height (z) above the ground (Hsu et al. 1994, Zhu et al. 2000), for each element of the trees in the FE models, wind profile (u) was determined by Eq. 2.7 (Panofsky and Dutton 1984), which is commonly used in engineering texts for land based and for the neutral stability of the atmosphere. Wind speed profiles used in forest stands were deemed inappropriate because of the substantial reduction in wind speed below the top of the canopy. The harmonic drag (F_D) on each tree element was calculated as:

$$F_D = \frac{\rho_{air} U^2 A C_D}{2} \tag{3.2}$$

where ρ_{air} is air density (assumed to be 1.226 kg/m^3), A is the frontal area of the tree, and C_D is the drag coefficient, which was assumed to vary with wind speed in accordance with Kane and Smiley's (2006) empirical relationship (see Figure 2.10) for small red maples (*Acer rubrum*). The distribution of drag on the tree and individual branches is shown in Figure 3.3. Each model was run 38 times for wind excitation frequencies ranging between 0 and 5 Hz. Wind frequencies were incremented by 0.05 Hz for frequencies up to 1.20 Hz, 0.1 Hz for frequencies between 1.20 and 2.00 Hz, and 0.50 Hz for frequencies greater than 2.00 Hz. Multiple frequencies were investigated because of the highly variable air flow and turbulence associated with wind in developed settings (Kastner-Klein et al. 2004). Smaller increments were used at lower frequencies to better capture the low frequency response of the trees, where greater wind energy can be

transferred to the tree (Baker 1995). Additionally, plots of Rd vs. wind frequency in this chapter and Chapter 6 include interpolated values between tested wind frequencies.

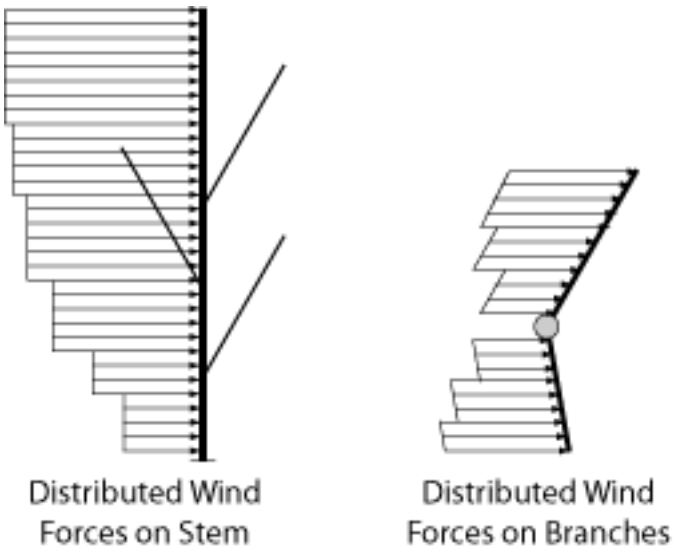

Figure 3.3: Illustration of distributed wind forces on stem and branches of trees. The figure on the left is an elevation view, and the one on the right is a plan view.

3.5 Dynamic Amplification Factor (Rd)

To capture the characteristics of dynamic response using a single parameter, the dynamic displacement amplification (or deformation response) factor (Rd) was analyzed as the output of the FE models. Rd is the ratio of the maximum displacement computed from the dynamic response of a structure to the maximum displacement computed from the static response of the structure. It is a unitless function that depends on characteristics of the structure (the mass, damping, and stiffness of the tree in this case) and the forcing function (frequency in the case of a harmonic load). For a single degree of freedom (SDOF) system subject to harmonic loading, the steady-state displacement of the system can be calculated as:

$$u(t) = C\sin(\omega t) + D\cos(\omega t) \tag{3.3}$$

where

$$C = \frac{P_0}{k}\frac{1-(\omega/\omega_n)^2}{[1-(\omega/\omega_n)^2]^2 + [2\zeta(\omega/\omega_n)]^2} \tag{3.4}$$

and

$$D = \frac{P_0}{k}\frac{-2\zeta(\omega/\omega_n)}{[1-(\omega/\omega_n)^2]^2 + [2\zeta(\omega/\omega_n)]^2} \tag{3.5}$$

and ω is the frequency of the excitation force, ω_n is the natural circular frequency of the system, ζ is the damping ratio, *k* is the stiffness of the system, and P_0 is the amplitude of the excitation force. The ratio of P_0/k gives the maximum displacement, $[(u_{st})_0]$ induced by the amplitude of static loading. Given that the sine and cosine functions are bound between -1 and 1, and are out of phase by an angle of π/2, the maximum dynamic displacement (u_0) of a SDOF system is:

$$u_0 = \sqrt{C^2 + D^2} \tag{3.6}$$

Thus,

$$Rd = \frac{u_0}{(u_{st})_0} = \frac{u_0}{P_0/k} = \frac{1}{\sqrt{[1-(\omega/\omega_n)^2]^2 + [2\zeta(\omega/\omega_n)]^2}} \tag{3.7}$$

For SDOF systems, Rd is plotted as a function of the frequency ratio (ω/ω_n), as in Figure 3.4. There are often multiple peaks for MDOF systems, however, so Rd was plotted as a function of ω for this study, as in Figure 3.5. Modal frequencies of M100 were identified where peaks in plots of the damped and undamped Rd for Node-10 (located on the stem 1.4 m above the ground) occurred at the same excitation frequency. Modal frequencies of each branch of M100 were identified where peaks in the plot of the undamped Rd for a node near the base of the branch exceeded the Rd plotted for Node-10. Figure 3.5

includes these plots for Node-27, near the base of the first branch, which is closest to the ground.

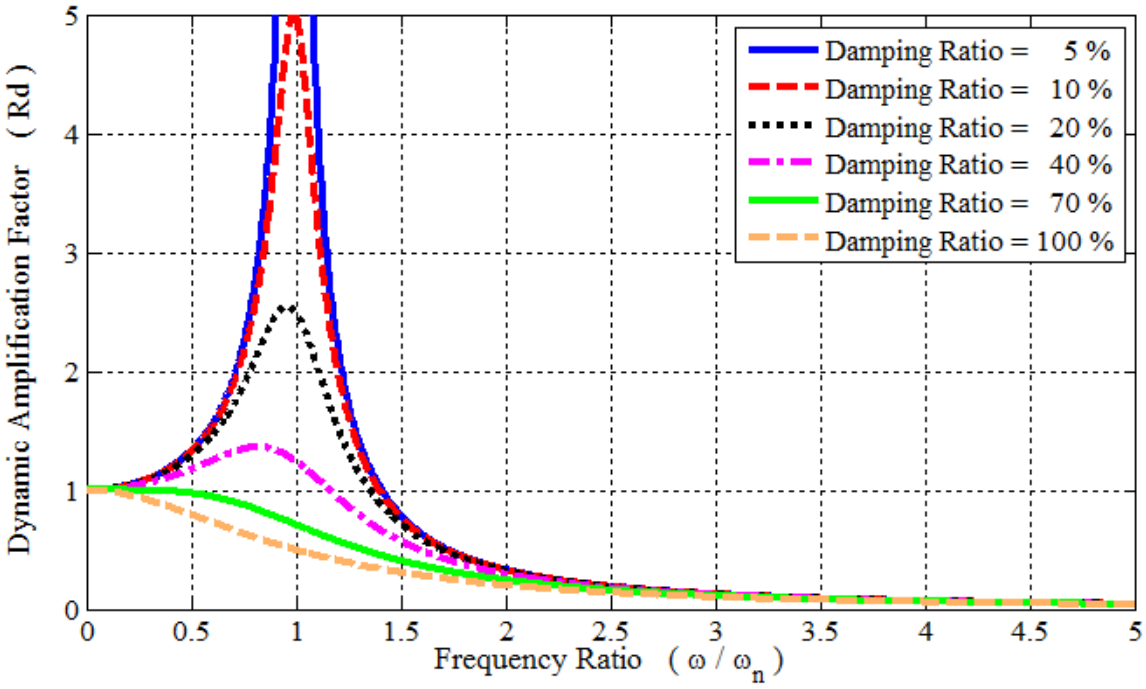

Figure 3.4: Dynamic amplification factor of SDOF systems excited by harmonic forces for several different damping ratios.

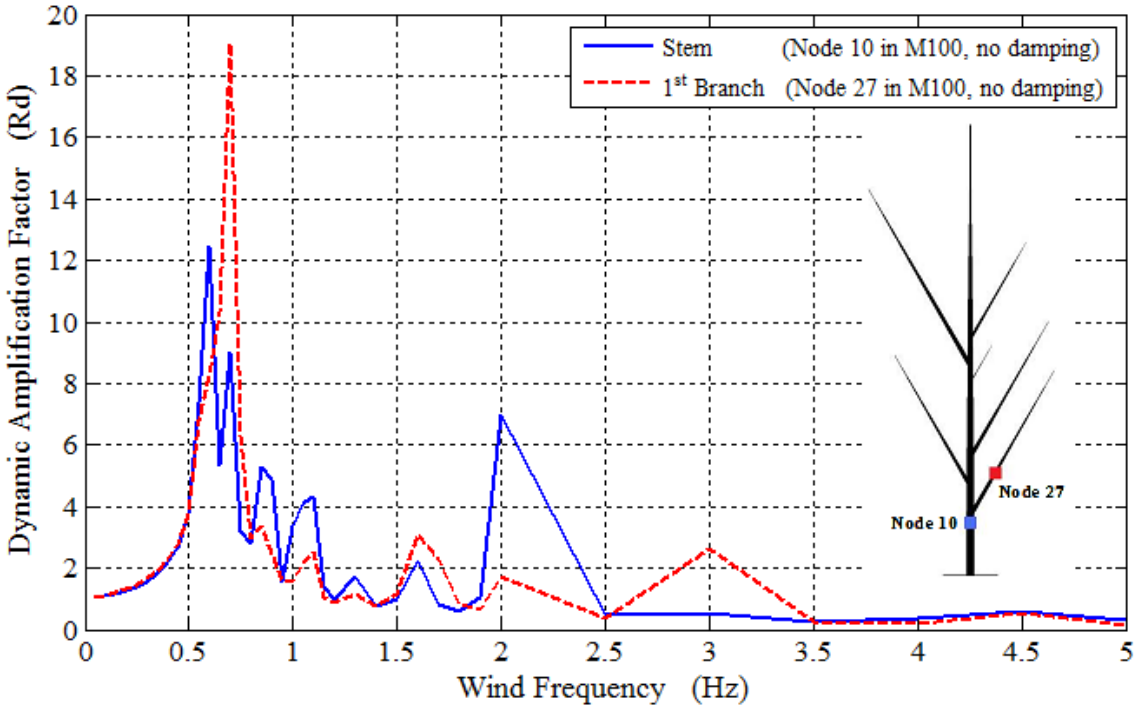

Figure 3.5: Comparison of the dynamic amplification factors of the first branch and the main-stem in the prototype tree. The blue (solid line) one belongs to the Node 10 whose height is close to the breast height (1.4 m). The other curve is for the Node 27 which is one of the nodes on the first branch of the tree.

3.6 Validation of FE Modeling

To validate the FE model, modal frequencies of the whole tree, the branchless stem, and each branch were determined by several other ways. Natural frequency of the whole tree was determined from field tests conducted by Kane et al. (In preparation), as described above, and by using two empirical relationships from two different studies (Baker 1997, Mayhead 1973). Baker (1997) developed an empirical relationship, Eq. 3.8, for the natural frequency of in-leaf *Tilia europea*:

$$f_n = \left(0.569 - 0.0021(DBH)\right) \pm 0.043\sqrt{1 + 0.0026(DBH - 58.4)^2} \qquad (3.8)$$

where DBH is measured in cm and the right-hand term is the 99% confidence interval. Substituting 53 cm into Eq. 3.8 yields 0.50 Hz. Mayhead (1973) empirically developed Eq. 3.9 for conifers:

$$f_n = \left[0.86 + 0.74\left(\frac{H\sqrt{MH}}{(DBH)^2}\right)\right]^{-1} \tag{3.9}$$

where DBH is given in cm, H is total tree height (m) and M is tree mass (kg). Entering values of M100 into Eq. 3.9 gives:

$$f_n = \left[0.86 + 0.74\left(\frac{(17.1)\sqrt{(3185)(17.1)}}{(53)^2}\right)\right]^{-1} \approx 0.52\ Hz \tag{3.10}$$

The first four modal frequencies of the branchless stem and each branch were determined by using Mabie and Rogers' (1972) equation (Eq. 3.11) for double-tapered cantilever beams (second, third, and fourth frequencies). These determined first four modal frequencies can be seen in Table 3.1.

$$f_n = \frac{(lk)^2}{2\pi\left(\frac{l^2}{h_1}\right)}\sqrt{\frac{Eg}{12\rho}} \tag{3.11}$$

where $(lk)^2$ is a constant associated with a particular beam taper, l is the length of the element, h_1 is the thickness at the distal point of the element parallel to the direction of the applied load, E is the elastic modulus, g is gravitational acceleration, and ρ is the density of the element. Imperial units were used for these parameters to be consistent with Mabie and Rogers (1972). In addition, the modal frequencies of each element in M100 can be obtained from the FE modeling using shapes obtained through modal analysis. For example, the modal frequencies and the mode shapes of each element (branches and main stem) can be seen in Figures from 3.6 to 3.12.

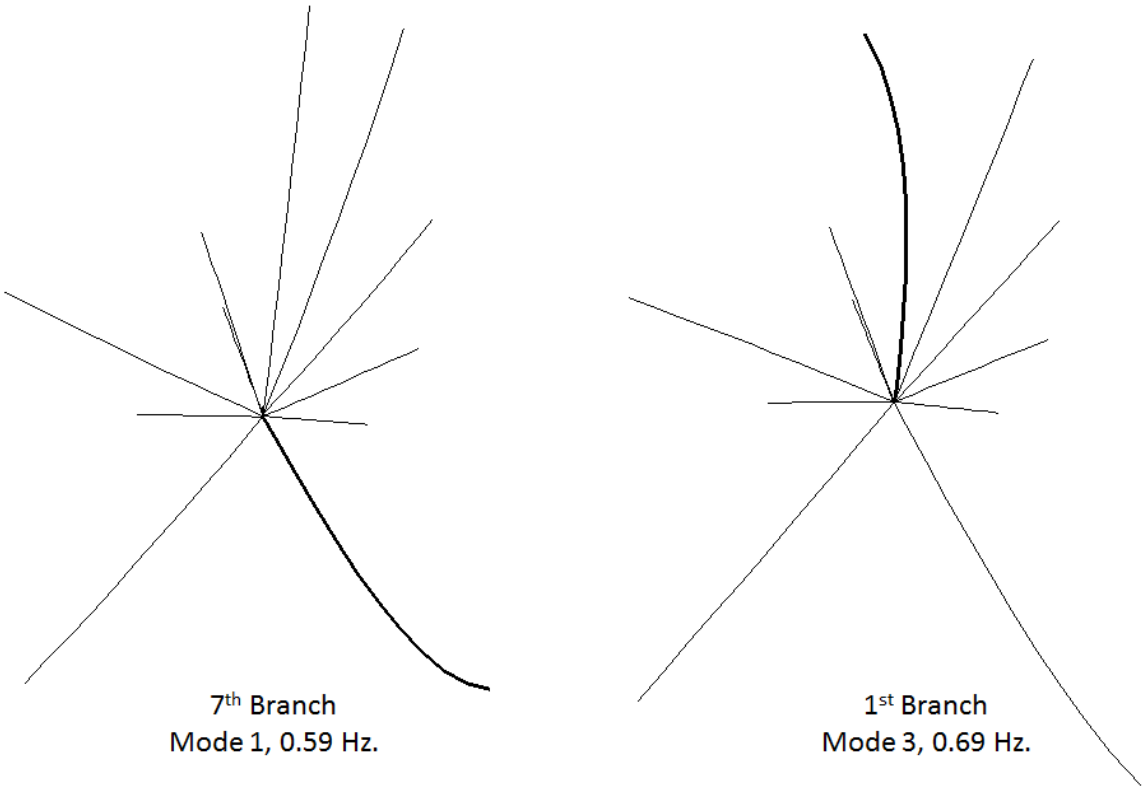

Figure 3.6: Mode shapes and modal frequencies of 7th (left) and 1st (right) branches from the top view of the model, M100.

FE modeling result (0.59 Hz) is comparable with all the values (0.50 Hz from Eq. 3.8, 0.52 Hz from Eq. 3.10, 0.59 Hz from Eq. 3.11 and the experimental result, 0.42 Hz) for the natural frequency of the tree.

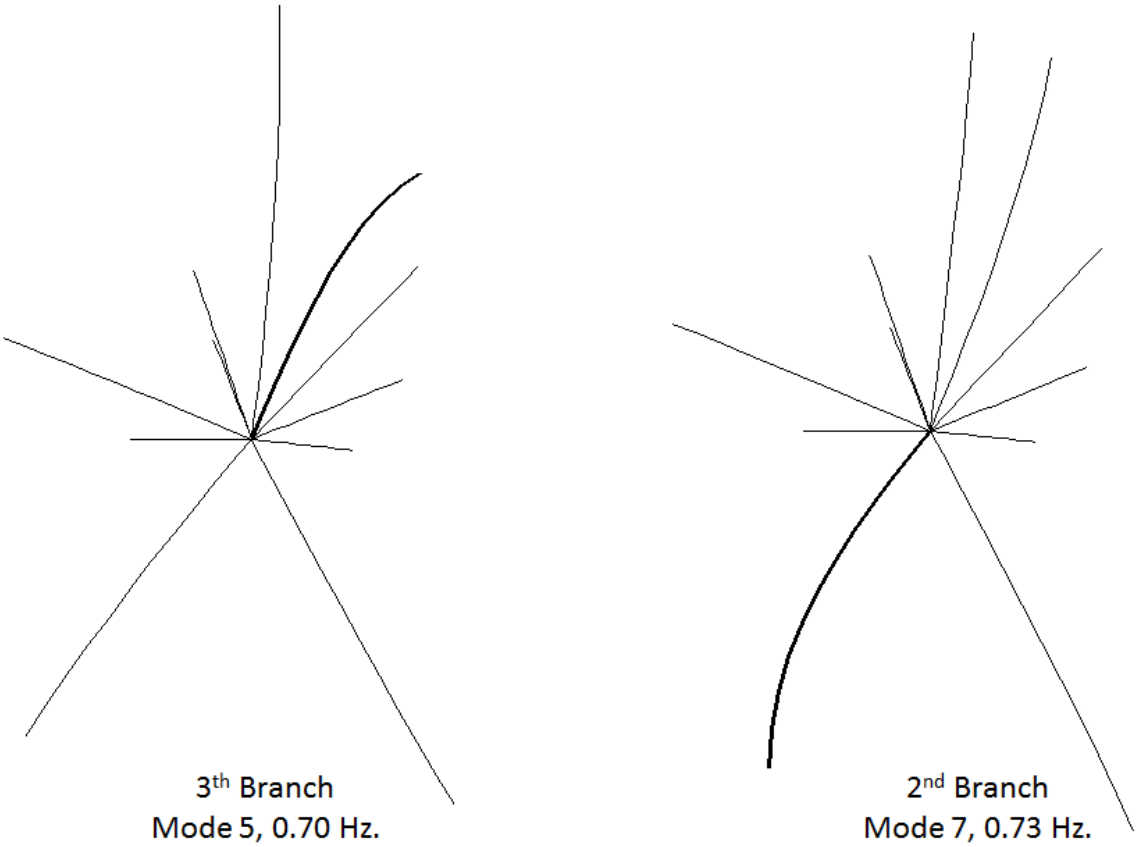

Figure 3.7: Mode shapes and modal frequencies of 3rd (left) and 2nd (right) branches from the top view of the model, M100.

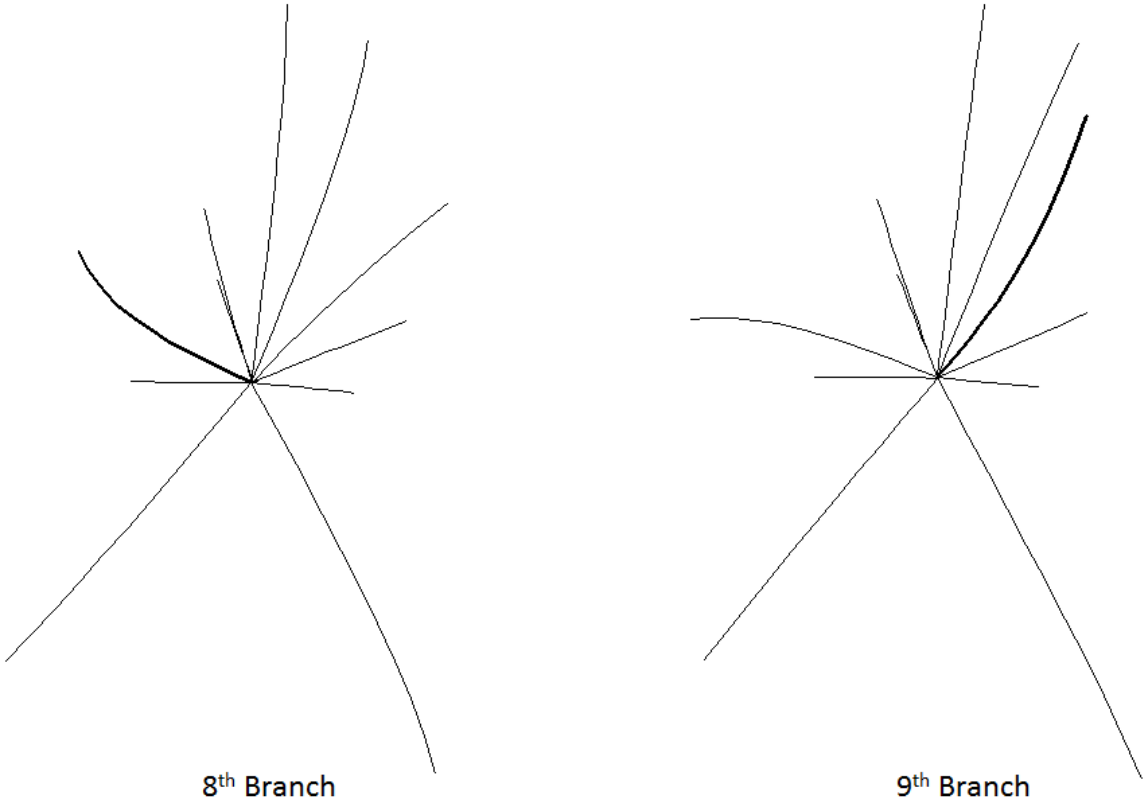

Figure 3.8: Mode shapes and modal frequencies of 8th (left) and 9th (right) branches from the top view of the model, M100.

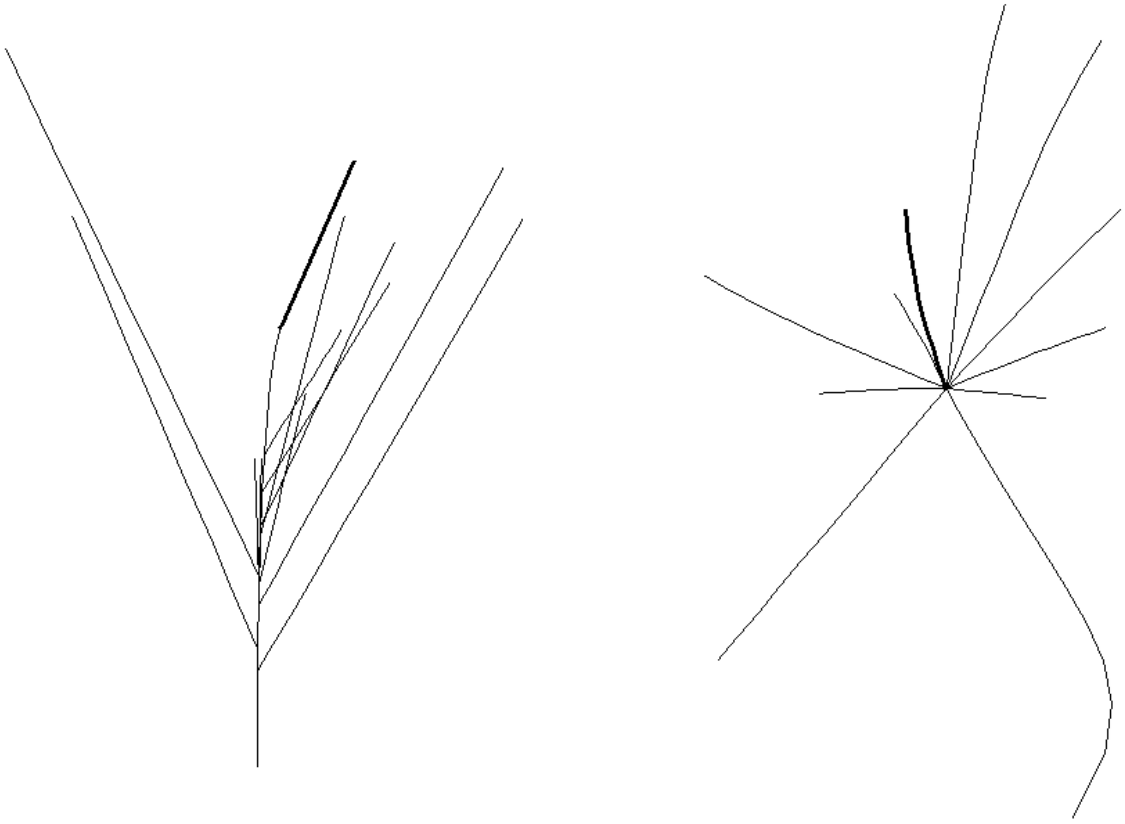

Figure 3.9: Mode shapes and modal frequencies of the top (left) and 10th (right) branches from the side (left) and top (right) view of the model, M100.

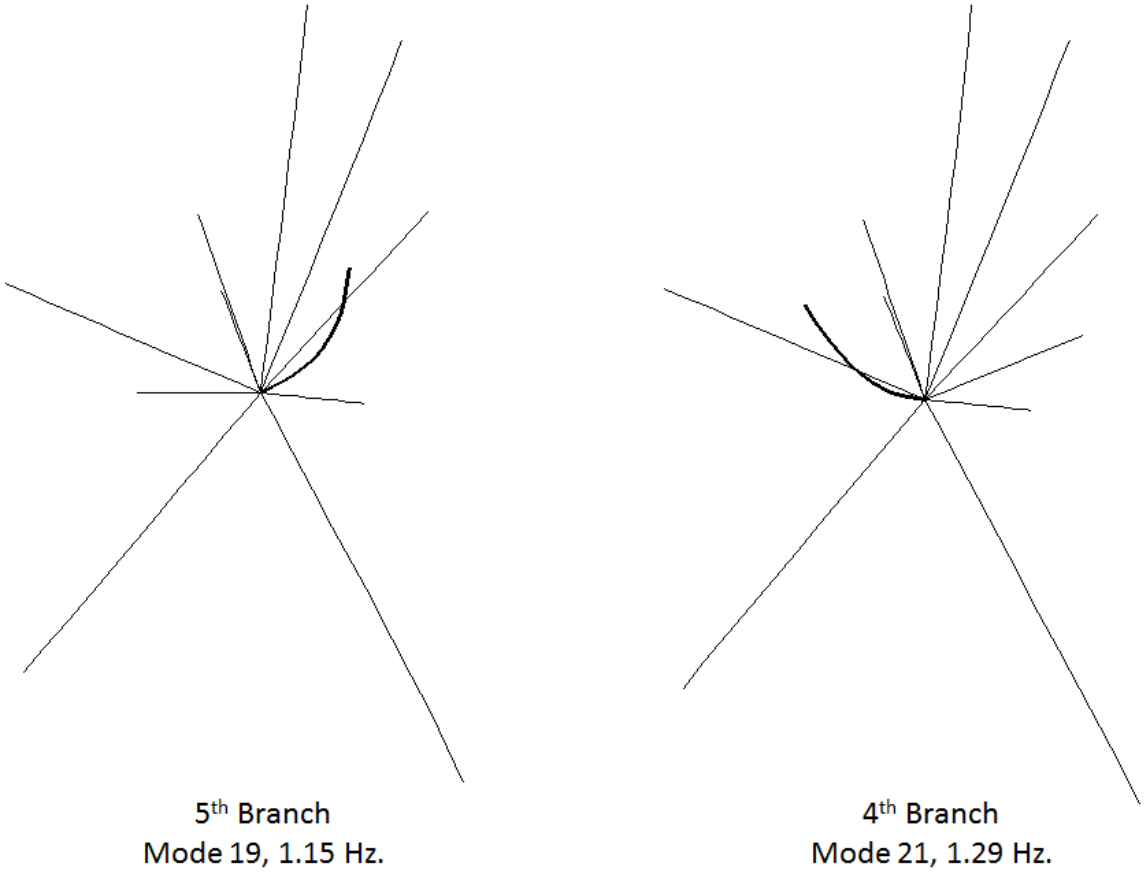

Figure 3.10: Mode shapes and modal frequencies of 5th (left) and 4th (right) branches from the top view of the model, M100.

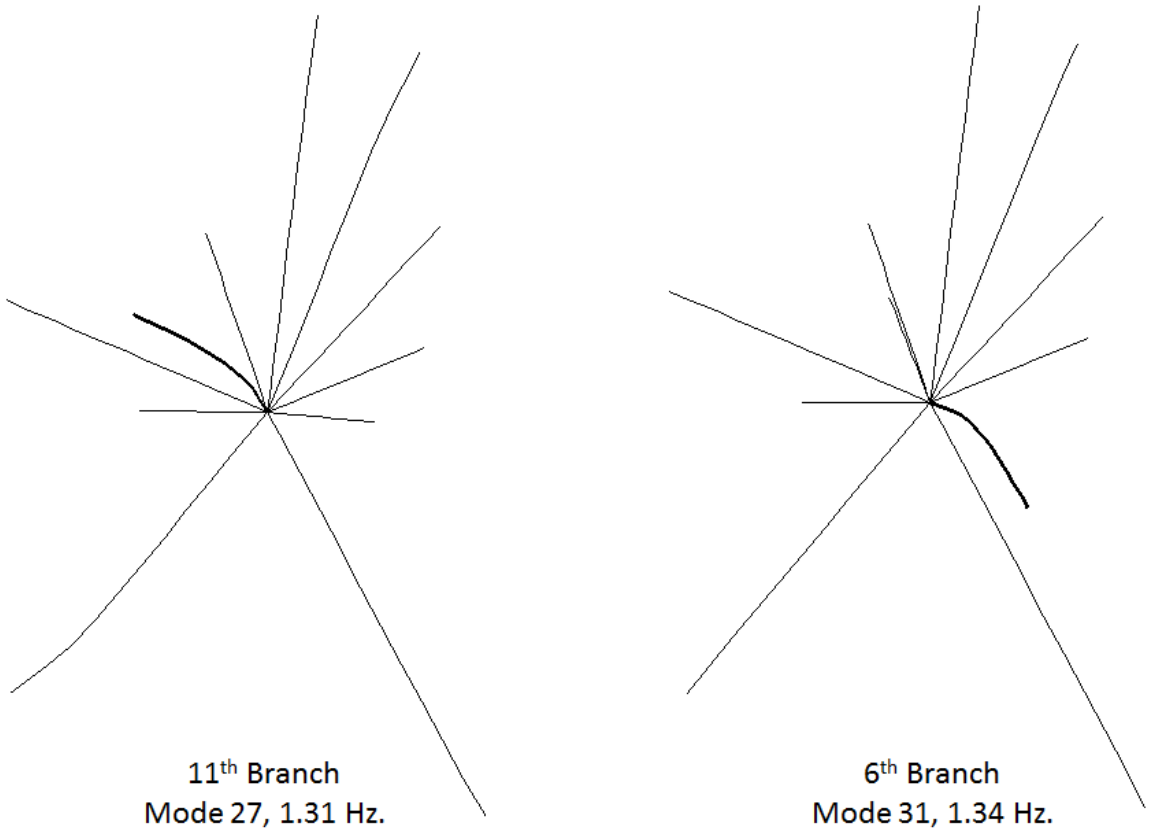

Figure 3.11: Mode shapes and modal frequencies of 11th (left) and 6th (right) branches from the top view of the model, M100.

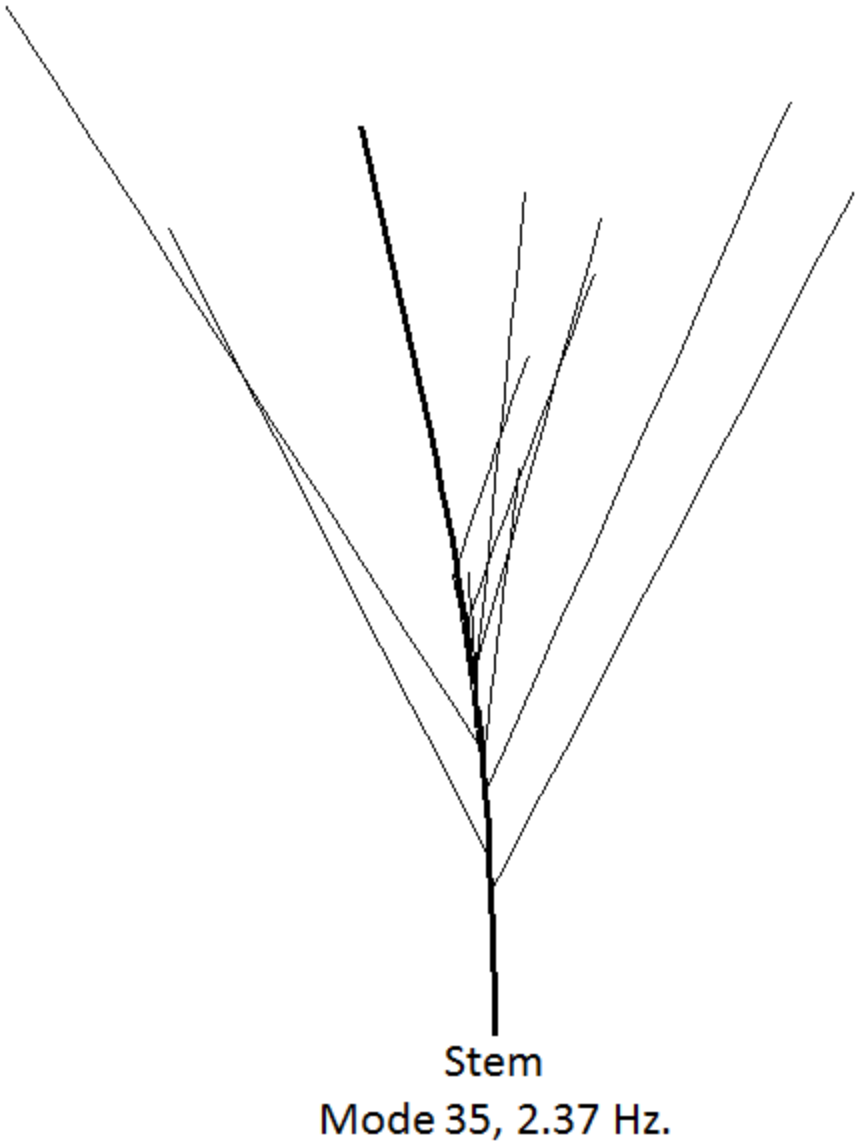

Figure 3.12: Mode shape and modal frequency of the stem of M100.

It can be said that several same frequencies are coupled, for example the natural frequency (1.09 Hz) of tenth branch is coupled with a higher frequency of seventh branch as can be seen in Figure 3.9.

3.7 Discussion of Measured and Calculated Dynamic Parameters

In Table 3.1, it can be seen that smaller natural frequencies correspond to branches of greater diameter because natural frequency is inversely proportional to the diameter of a beam (Eq. 3.12). The circular frequency (ω_n) of a branch is the square root of the ratio of stiffness (k), which increases linearly with diameter (D) because length depends linearly on the slenderness ratio (λ) of the branches, and mass (m), which increases as a function of diameter cubed and wood density (ρ):

$$\omega_n = \sqrt{\frac{k}{m}} \propto \sqrt{\frac{\frac{EI}{L^3}}{\rho L D^2}} \propto \sqrt{\frac{\frac{E\pi D^4}{(\lambda D)^3}}{\rho \lambda D^3}} \propto \frac{1}{D} \tag{3.12}$$

Thus, circular frequency and frequency will be inversely proportional to branch diameter. Figure 3.5 reveals the first and second modal frequencies of the first branch (see Table 1) in comparison with modal frequencies of M100. Unless stated otherwise, Rd values refer to those at Node 10 in the FE model, which is on the stem, 1.4 m above ground.

Table 3.1 also includes the estimated mass of each branch and stem and mean MOE of branches and the stem, weighted by the mass of each element in a branch or the stem. The estimated mass of M100 (3185 kg) and the ratio of branch mass to stem mass (1.4), were significantly larger than medium-sized Douglas-firs previously considered in FE analysis (Moore and Maguire 2008). Slenderness of the stem including (32) or excluding (24) the top branch was smaller than previously reported (Moore and Maguire 2005, Sellier and Fourcaud 2005, Jönsson et al. 2007, Rodriguez et al. 2008, Sellier and Fourcaud 2009).

Figure 3.13 shows Rd of M100 as a function of wind frequency for damping ratios of 0% and 15%. The damped model shows a peak at 0.59 Hz, which is greater than the value determined from pull and release tests (0.42 Hz) conducted by Kane et al. (In preparation). As it will be evaluated in Chapter 6, changing the assumed value of branch slenderness from 50 to 60, however, caused a peak at 0.42 Hz (see Figure 6.8), which lends confidence that the assumptions used to develop the model (M121 will be defined in Chapter 6) were reasonable. The natural frequency determined by FE modeling (M100) fit within the 99% confidence interval of Eq. 3.8 (Baker 1997), but was 19% less than the values calculated in Eq. 3.10 (Mayhead 1973). The disparity is not surprising because Eq. 3.10 was developed from trees of excurrent form.

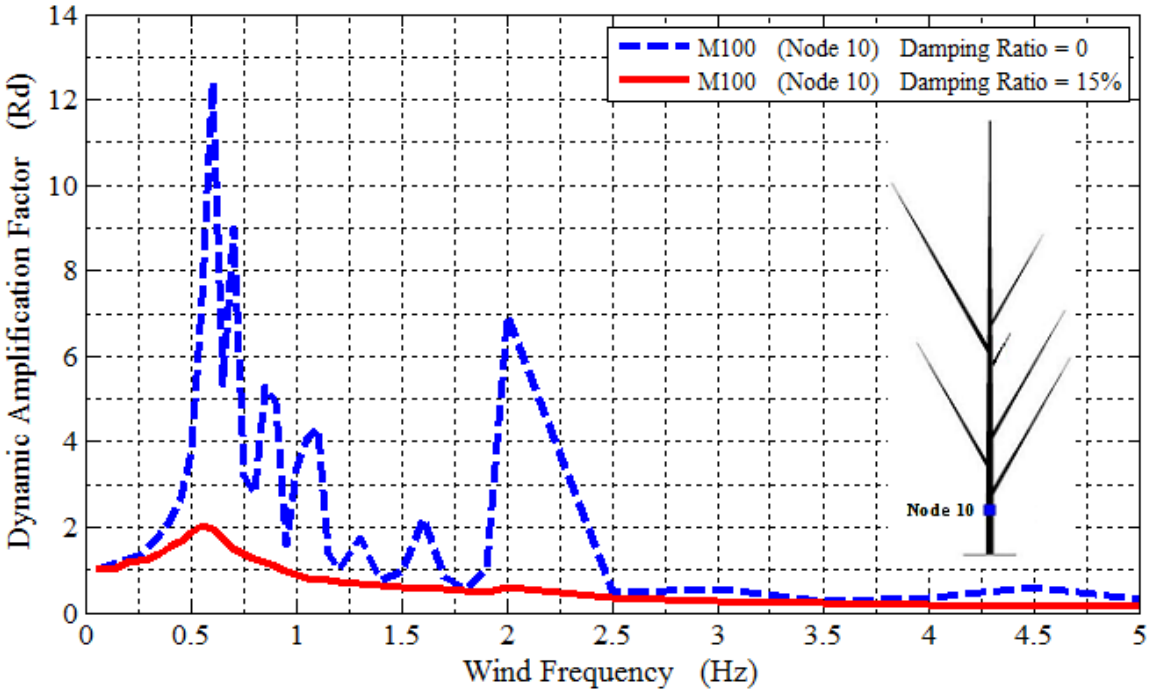

Figure 3.13: Dynamic amplification factors in terms of wind frequency for the undamped and damped (15 %) MDOF systems of the prototype tree subjected to harmonic wind forces.

The peak at 0.59 Hz is close to the natural frequency of the seventh branch, which is the largest, of M100. The natural frequencies of three other large branches (first, second, and third) are slightly greater than that of the seventh branch, and all of these were different from that of the stem (Table 3.1). It was not surprising that the natural frequency of M100 was similar to that of the four largest branches because their cumulative mass (1614 kg) exceeded that of the stem and top branch (1304 kg). It appeared that the portion of the stem proximal to the seventh branch effectively functioned as a rigid element in the model because of its reduced slenderness and greater MOE.

The effect of crown architecture on natural frequency has been illustrated previously (James et al. 2006, Spatz et al. 2007, Sellier and Fourcaud 2009) and previous works have shown a similar difference between natural frequency of the stem compared to the whole tree (Moore and Maguire 2005, Sellier and Fourcaud 2005, Spatz et al. 2007). Results of the current study demonstrate the significant effect of large branches on sway response, which has made it more difficult to fit empirical data to theoretical expectations (Baker 1997, Kane and James 2011).

Although 0% damping is unrealistic, it is included to illustrate peaks in the Rd curve (Figure 3.13) that would otherwise not be visible. The peaks of the undamped plot of Rd at 0.59 and 2.0 Hz correspond to the first and the second modal frequencies of the tree; the first modal frequency is close to the first modal frequencies of the large branches and the second modal frequency is close to the first modal frequency of the stem, the second modal frequency of the medium and small sized branches and the third modal frequencies of the largest branches (Table 3.1). Other peaks in the undamped model

correspond to modal frequencies associated with branches, but these peaks disappear once damping is considered. The number of branches and the number of peaks in the plot are not equal because several branches have natural frequencies that are approximately equal (because they have similar diameters). For example, the first modal frequencies of the first, second, and third branches are similar (Table 3.1), which caused the peak in Rd near 0.70 Hz (Figure 3.5).

3.8 Summary

A FE model was developed for a prototype tree in Belchertown, MA by using several assumptions and information from the literature in Chapter 2. By using this FE modeling, two important results are obtained for use in subsequent chapters (Chapter 4 and Chapter 6, respectively). First, the favorable results of selected response parameters (mainly frequencies) between the FE model and field testing validate the assumptions used in FE modeling. This is required before conducting the Monte Carlo simulations in Chapter 4. The second important implication of the analysis results presented in this chapter is that with a validated model one can now incorporate variations of the base model to create parametric models to investigate the effects of model variations on dynamic response. These analyses are presented and results are discussed in detail in Chapter 6.

CHAPTER 4

RISK ASSESSMENT OF MAPLE TREES SUBJECTED TO RANDOMLY GENERATED WIND LOADING

4.1 Introduction

Trees have some important roles for human lives due to their many environmental and sociological benefits (Nowak and Dwyer 2000). If they fall down due to uprooting or breakage failures of stems or branches, these benefits sometimes may be replaced by significant damages such as deaths, personal injuries, cold-sicknesses, traffic jams and economic losses owing to litigations (Kerzenmacher and Gardiner 1998, Gardiner and Quine 2000, Kane and Ryan 2004, Mortimer and Kane 2004, Fournier et al. 2006, James et al. 2006). That is why, risk assessment of trees is important for arborists.

According to the studies (Milne 1991, Rodriguez et al. 2008, James and Kane 2008), wind forces have the important role on falling down of trees. Thus, tree risk assessment has been investigated under the wind loads and three different approaches were developed and have been commonly used over the last 25 years: (1) qualitative assessments, (2) empirical or statistical models, (3) mechanistic models (Gardiner et al. 2008). The first model is based on observational tools and it was mentioned in some studies (e.g. Miller 1985, Mitchell 1998). The second one is mentioned by several researchers (e.g. Valinger and Fridman 1997, Lanquaye-Opoku and Mitchell 2005), and the advantage of this approach with respect to the first approach is that this second one may be quite accurate and reliable for different locations (Gardiner et al. 2008). The last approach is the newest and most common one which was developed by Peltola et al. in

1999 (HWIND mechanistic models), and Gardiner and Quine in 2000 (GALES mechanistic models). All these approaches were developed for, generally, trees in forests. Additionally, the other important example of the mechanical models (FOREOLE mechanistic models) was developed by Ancelin et al. (2004) not only for wind loading but also for snow loading on trees in forest areas about the risk assessment.

As for the important differences between the research in this chapter and the previous studies, large and open-grown trees will be addressed instead of trees in forests. The other difference is to use FE modeling as the methodology to study tree risk assessment. The third important difference relates to the methodology that 1000 different wind speed samples of a mean wind-speed were randomly generated for the wind loading on tree models in this chapter in order to concern the randomness of the wind loading in nature. But the randomness of the wind loading in the mechanistic models cannot be seen, or in other words each wind speed has a specific gust factor for a specific tree, so the critical wind speed of that specific tree is calculated specifically and deterministically. The final important difference is that dynamic analysis approach was used to calculate the probability of tree failures. Mechanical models, however, use empirical gust factor to attempt to catch the effect of the dynamic response of trees under fluctuating wind, these models may not calculate the critical wind speed dynamically for the trees in different locations elsewhere the empirical tests were done, because the gust factor might be different for such different locations.

Currently, by using Monte-Carlo (MC) simulation algorithm in order to attempt to capture the variance of wind turbulence, totally 1000 different samples could be generated and applied to two specific trees (in Belchertown and Amherst, MA) for each

wind speed (from 13 m/s to 39 m/s) with the interval of 2 m/s (≈ 4.5 mph). The disadvantage of MC simulations is to be expensive computationally (Arwade and Deodatis 2011), because it takes time to do FEMs and to apply all the varied inputs into these models. However, in probabilistic approaches, MC is a common method in engineering for fragility analysis which is a standardized methodology for performance-based structures subjected to loads. The objective of this fragility analysis is to see the conditional probability of exceedance of deterministically defined indicator (such as maximum lateral drift or maximum bending moment in structures or any other indicator corresponding to a specific feature of the response of the structures) (Smith 2009). Thus, in this paper, maximum bending moment at breast height of two trees was used as the indicator of the fragility analyses. After that, the annual probability of tree failures in a specific location can be calculated by using the probability density function of annual wind speed or wind speed for a reference period which belongs to that specific location.

4.2 FE Modeling Maple Trees

The finite element (FE) modeling program, ADINA 8.5 was used to conduct the dynamic analyses of two different real trees, which are located (1) near the police station in Belchertown, MA and (2) in the campus of University of Massachusetts-Amherst, MA. All the modeling methodologies have already been described in Chapter 3, thus it is not necessary to mention how to model the trees in ADINA, again.

The morphological information of the second tree can be seen in Table 4.1, because these information do not exist in Chapter 3. Additionally, Figure 4.1 is also show a picture of Tree-2 with its model shape from ADINA.

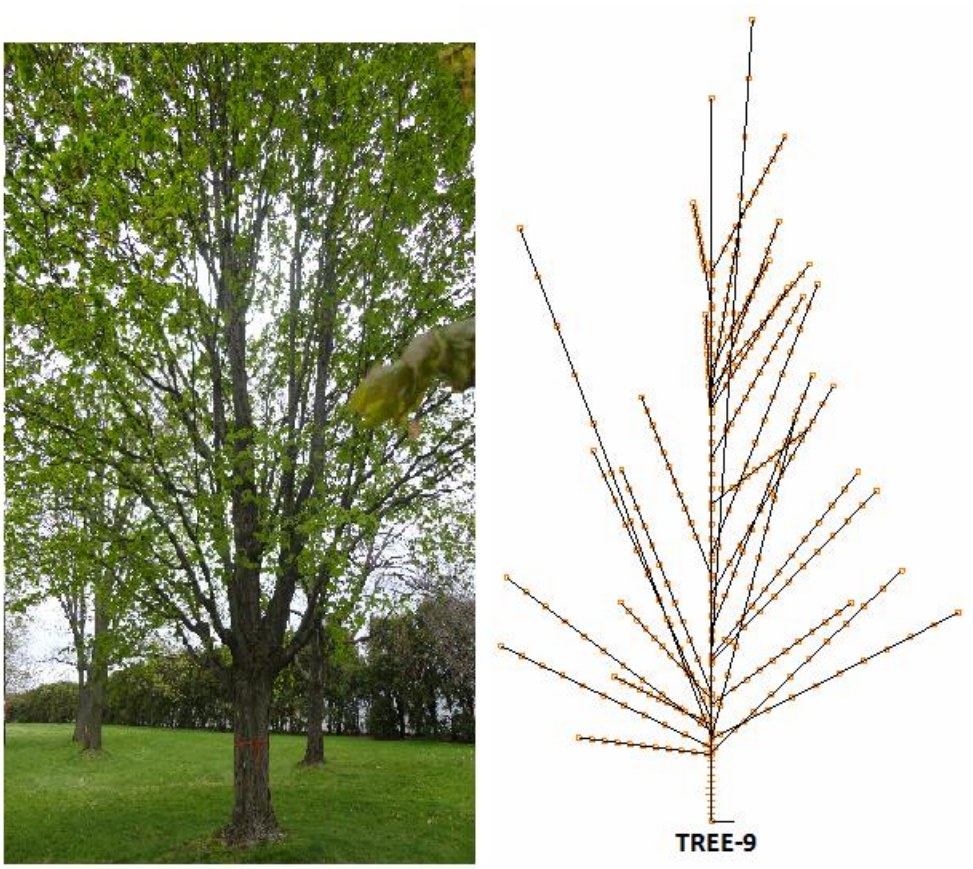

Figure 4.1: A photo from the real TREE-9 (left one) and its model in ADINA (right one).

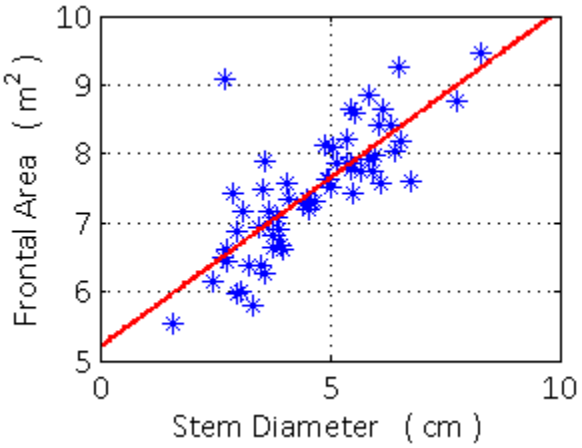

Figure 4.2: The relationship between stem diameter and foliage area with leaves. The equation of the linear fitting on the experimental data is y=0.49x+5.22.

Table 4.1: Field measurements for the morphological properties of the second tree.

	2nd TREE	Diameter (m)	Attachment Height (m)	Azimuth Angle (º)	Attachment Angle (º)
	Stem	0.66	n/a	n/a	n/a
Branch #	1	0.13	2.21	228	89
	2	0.23	2.29	308	59
	3	0.21	2.44	134	71
	4	0.23	2.74	28	15
	5	0.20	2.75	28	65
	6	0.38	2.79	138	26
	7	0.17	2.97	198	53
	8	0.09	3.20	225	69
	9	0.21	3.38	225	30
	10	0.17	3.86	305	66
	11	0.15	4.06	114	65
	12	0.16	4.24	188	19
	13	0.15	5.31	7	41
	14	0.17	5.44	316	45
	15	0.44	5.51	282	16
	16	0.19	6.32	40	24
	17	0.16	7.54	26	29
	18	0.13	8.15	143	21
	19	0.19	8.86	25	20
	20	0.08	10.52	322	52
	21	0.12	12.07	337	26
	22	0.08	13.06	265	22
	23	0.10	13.72	308	40
	24	0.13	13.84	50	25
	25	0.10	14.35	346	33
	26	0.14	14.36	75	29
	27	0.08	15.01	349	21
	28	0.07	17.12	240	13
	29	0.10	18.21	360	24
	Top	0.10	18.22	n/a	0

In modeling, two different seasons, which are called as winter season and summer season were investigated because they have different drag forces and so different responses for these seasons. All the reasons of the differences due to these seasons can be collected under two definitions like ‘internal effects of seasons’ and ‘external effects of

seasons'. The important external effect is air density which was assumed to be 1.226 kg/m3 and 1.326 kg/m3 in tree models for the summer season and the winter season, respectively. The first important internal effect is changes in foliage area of trees in Eq. 3.2. Whereas foliage area for the winter season was defined as the exposure area of the trunks and the branches in trees without leaves, the foliage area for the summer season was estimated by using the relationship between stem diameter at breast height and the total area of the whole trees which had been investigated in the research of Kane as can be seen in Figure 4.1. The other internal effect is drag coefficient in Eq. 3.2, and for winter season it was approximately selected as 1.0 from fluid mechanics under the assumption is that branches and tree trunk are a kind of rough circular cylinders along their length. For the summer season, it was assumed to vary from 0.6 to 0.9 as a function of wind speed as in the study of Kane and Smiley (2006).

4.3 How to Generate Random Wind Loading for MC Simulations

To generate, randomly, 1000 samples for the time-history of each wind speed in Eq. 3.2, it might be necessary to obtain a function of spectral density with respect to wind speed frequencies. Thus, Ochi-Shin Equation (Eq. 4.1, from Ochi and Shin (1988)) was modified in order to correspond to a new equation for lands, because Eq. 4.1 is for offshore areas. For this modification, the spectral densities of the time-histories of several wind speeds, which are field data measured from Amherst, MA in September of 2006, were calculated by taking Fourier Transformation of these wind speed data. Then these spectral densities were compared with the Ochi-Shin equation, and the surface drag coefficient of Eq. 4.1 was modified as long as the differences between the numerical

integration of the modified Ochi-Shin equation and the spectral densities of the field data are the smallest value. The spectral densities of the field data can be seen in Fig. 4.2 with the modified Ochi-Shin equation. Moreover, it has already been expected that the surface drag coefficient of the modified equation for land areas should be larger than the surface drag coefficient of the equation for offshore areas because of the effect of the higher friction at land areas than offshore areas.

$$S_{Vw}(\omega) = \frac{CV_w^2 F_g}{f} \tag{4.1}$$

in which C (defined by Eq. 4.2) is the surface drag coefficient and is related with the roughness of surface, V_w is the average wind speed at a reference level of 10 meter, f is the wind frequency in Hz, and F_g is the gust factor as defined in Eq. 4.2. The modified surface drag coefficient, C^M in Eq. 4.4 is for the modified Ochi-Shin equation, and it is for the land areas like in Amherst, MA.

$$F_g = \begin{cases} f/V_W & 0 \le f \le 0.0003V_W \\ \dfrac{420(f/V_W)^{0.7}}{(1+(f/V_W)^{0.35})^{11.5}} & 0.0003V_W \le f \le 0.01V_W \\ \dfrac{838(f/V_W)}{(1+(f/V_W)^{0.35})^{11.5}} & 0.01V_W \le f \end{cases} \tag{4.2}$$

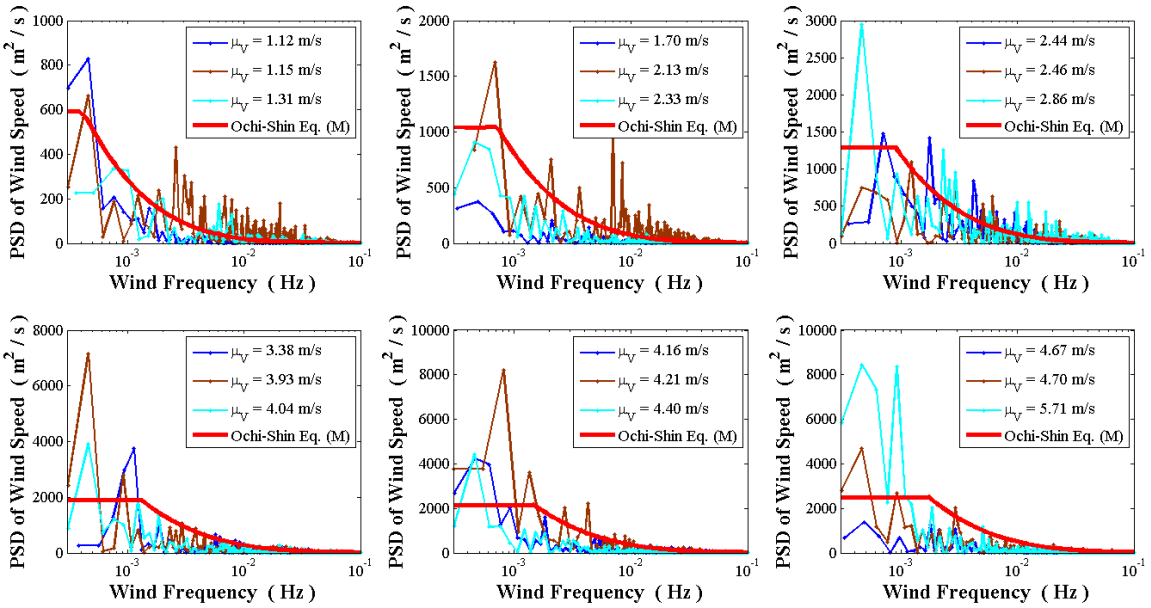

Figure 4.3: Comparison of wind spectral densities of field data and modified Ochi-Shin equation.

$$C = (750 + 69V_w)(1.0x10^{-6}) \tag{4.3}$$

$$C^M = (20000 + 69V_w)(3.7x10^{-6}) \tag{4.4}$$

After obtaining a modified Ochi-Shin equation, it is time to generate 1000 samples for the time-history of several specific mean wind-speeds which were incremented by 2 m/s (≈4.5 mph) from 13 m/s (29 mph) to 39 m/s (87 mph). Thus, a matlab code were applied to generate the time history samples of $V_w(t)$, a stochastic process, by using the methodology of the spectral representation (Shinozuko 1972). According to this spectral representation, Gaussian stochastic processes can be obtained by using Eq. 4.5.

$$V_w^G(t) = \sum_{r=1}^{n} A_r \sin(\omega_r t) + B_r \cos(\omega_r t) \tag{4.5}$$

where A_r and B_r are independent Gaussian random variables with zero mean and the variance (σ^2) which can be calculated by using Eq. 4.6, t represents the time in the time-history wind samples, and ω_r is the wind speed frequencies which are at the middle of the number of n which is the number of equally divided parts of the spectral density of the modified Ochi-Shin Equation. In this chapter, the spectral density was divided to 430 equal parts (n=430) from zero to approximately 0.48 Hz in order to obtain approximately 30 minutes time-history of the stochastic processes.

$$\sigma^2 = G_{VV}(\omega_r)\Delta\omega \tag{4.6}$$

where $G_{VV}(\omega_r)$ is the range value of the domain of ω_r in the wind spectral density function, and $\Delta\omega$ is the interval of frequencies for the equally divided parts in the spectral density function.

These Gaussian time history samples can be transformed to Log-Normal distributions by using Nataf-model (Nataf 1962) in Eq. 4.7, because of the assumption that winds blow with the property of a kind of Log-Normal distribution.

$$V_i^G = \Phi^{-1}\left[F_{V_i}(V_i)\right] \tag{4.7}$$

in which V_i^G is Gaussian variables of wind speed, Φ^{-1} is the inverse of Gaussian cumulative distribution function, and F_{Vi} is the cumulative distribution function of log-normally distributed random variables (V_i) which can be written in terms of Gaussian cumulative distribution function as in Eq. 4.8.

$$F_{V_i}(V_i) = \Phi\left(\frac{ln\left(\frac{V_i}{\mu}\right)}{s}\right) \tag{4.8}$$

where the parameters s and μ can be written in terms of the mean (μ_{Xi}) and the standard deviation (σ_{Xi}) of the log-normally distributed random variables as follows (Eq. 4.9 and Eq. 4.10):

$$s = \sqrt{ln\left(\frac{{\sigma_{X_i}}^2}{{\mu_{X_i}}^2} + 1\right)} \tag{4.9}$$

$$\mu = \mu_{X_i} exp\left(-\frac{s^2}{2}\right) = \frac{{\mu_{X_i}}^2}{\sqrt{{\mu_{X_i}}^2 + {\sigma_{X_i}}^2}} \tag{4.10}$$

In Eq. 4.7, the terms (Φ^{-1} and F_{Vi}) can be cancelled each other out because of Eq. 4.8. Thus Eq. 4.7 can be rewritten as follows;

$$V_i^G = \Phi^{-1}\Phi\left(\frac{ln\left(\frac{V_i}{\mu}\right)}{s}\right)$$

$$= \frac{1}{s} ln\left(\frac{V_i}{\mu}\right) \tag{4.11}$$

Then, Eq. 9 and Eq. 10 can be plugged into Eq. 11 as follows;

$$V_i^G = \frac{1}{\sqrt{ln\left(\frac{{\mu_{X_i}}^2 + {\sigma_{X_i}}^2}{{\mu_{X_i}}^2}\right)}} ln\left(\frac{V_i\sqrt{{\mu_{X_i}}^2 + {\sigma_{X_i}}^2}}{{\mu_{X_i}}^2}\right) \tag{4.12}$$

Finally, the log-normally distributed random variables (V_i) of wind speeds can be generated by using Eq. 4.13 which is another form of Eq. 4.12. As an example, in Figure 4.3, the histogram of 1000 samples, which have 21 m/s (≈ 47 mph) mean wind speed, matches to the perfect log-normal distribution whose mean is 21 m/s and standard deviation was calculated from the modified Ochi-Shin's equation for this specific wind speed. Additionally, the time history of one of these samples can be seen in Figure 4.4.

$$V_i = \frac{{\mu_{X_i}}^2}{\sqrt{{\mu_{X_i}}^2 + {\sigma_{X_i}}^2}} exp\left(V_i^G \sqrt{ln\left(\frac{{\mu_{X_i}}^2 + {\sigma_{X_i}}^2}{{\mu_{X_i}}^2}\right)} \right) \tag{4.13}$$

The limitation of the Nataf model is that the correlation function of the Gaussian random field of wind speed, which is obtained by using the methodology of the spectral representation (Eq. 4.5), might not equal to the correlation function of the generated log-normal random field of wind speed because of the distortions of using Eq. 4.13. But, these distortions can be ignored, because they are small as can be seen in Figure 4.6.

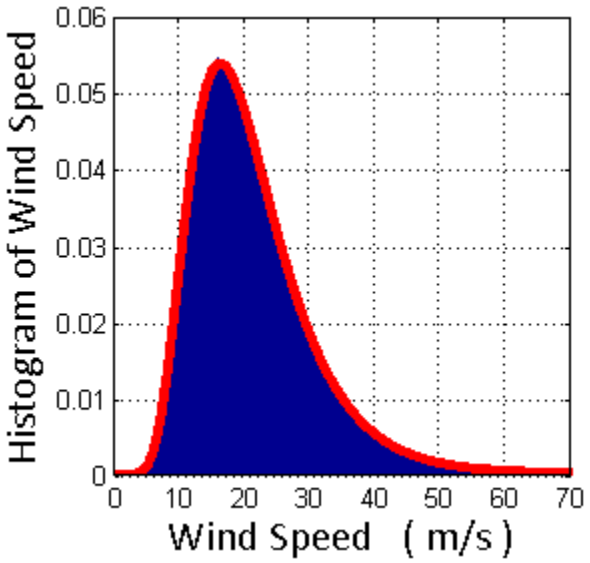

Figure 4.4: Matching of the generated samples (blue shaded area) with the perfect Log-Normal distribution (solid red line). The mean of the samples is 21 m/s.

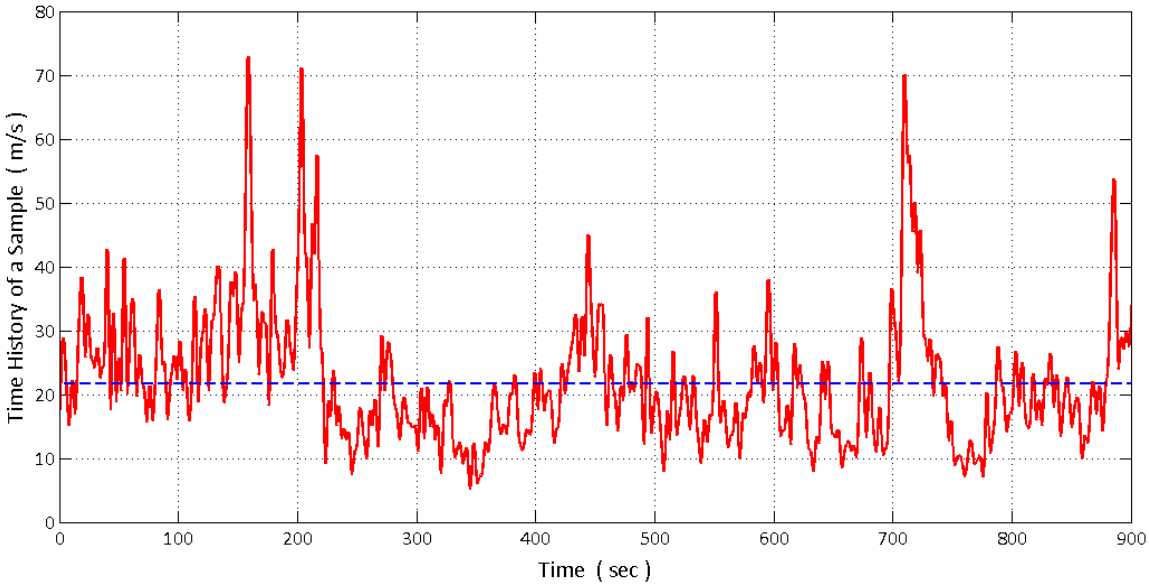

Figure 4.5: Time-history for one of the generated 1000 samples. Dashed line is to represent the mean of the sample at 21.6 m/s.

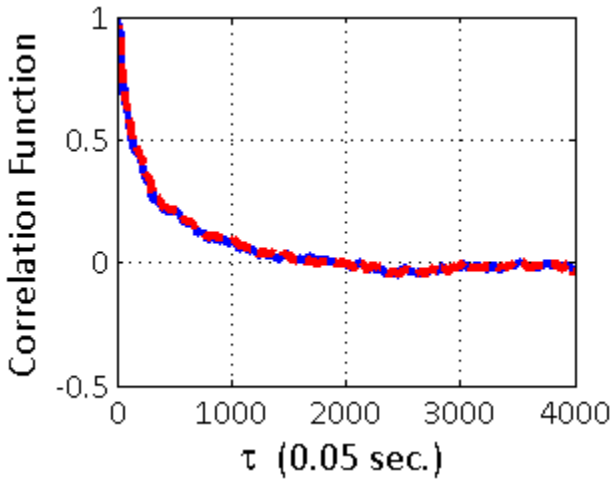

Figure 4.6: Correlation functions for the random field of generated Gaussian and Log-Normal wind-speeds.

4.4 Probability of Exceedance for MC Simulations

To be broken at once in a given time, or not to be broken over this time region, that is the question about the failure of trees. Thus, it can be defined that a tree will be broken down in this time region if a bending moment at anywhere on its trunk exceeds the threshold (maximum bending moment for that location on its trunk not to reach to the compressive yield point of the stress-strain behavior of the trunk) at least once. In the light of this definition, probability of exceedance can be calculated as in Eq. 4.14.

$$P_E(\xi, T) = Prob\left[\max_{t\epsilon[0,T]} M(t, ns) \geq \xi\right] \tag{4.14}$$

in which ξ is the threshold, T is the given time period, M(t,ns) is the random field which could be obtained as the outputs of the FEMs for 1000 number of samples (ns). The application of Eq. 4.14 for the MC simulations in this research can be explained by using Figure 4.6. The threshold value of the bending moment in Figure 4.6 can be calculated by using Eq. 4.15 (bending stress formula in a cross-section) for trees. To explain Figure 4.6, if the bending moment of the tree trunks (at breast height, 1.4 m) for any sample in total of 1000 samples reaches to the threshold (ξ) in Figure 4.6 at least once, tree will break down at that location. Then, the ratio of the number of the samples, whose bending moments have at least one up-crossing with the threshold, to the total number of the samples (1000 for this research) is the probability of exceedance in Eq. 4.14 (or maybe called as probability of failures) for the specific mean wind speed.

$$M_b = \frac{\sigma I}{y} \tag{4.15}$$

where σ is the compression strength parallel to grain (27700 *kPa* for green sugar maple trees from Kretschmann 2010), y is the distance between the neutral-axis and the

point which has the maximum bending moment (M_b), and I is the second moment of inertia for the cross-section of the trees. This inertia can be calculated by using Eq. 4.16 under the assumption that the tree cross-sections are a kind of circular shape.

$$I = \frac{\pi D^4}{64} \tag{4.16}$$

where D is the diameter of the cross-section of the trees.

If it is assumed that the neutral-axis goes through the diameter of the cross-section of the tress, y will be equal to the half of the diameter of the cross-sections. Thus, Eq. 4.15 can be rewritten as follows;

$$BM_y = \frac{\sigma_y \frac{\pi D^4}{64}}{\frac{D}{2}} = \frac{\pi \sigma_y D^3}{32} \tag{4.17}$$

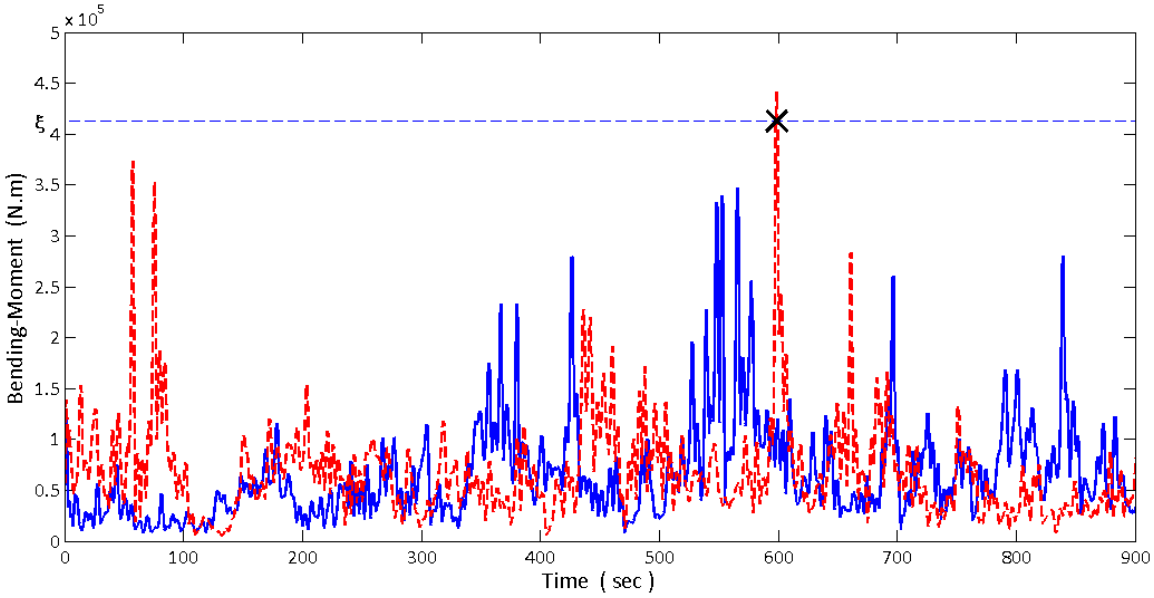

Figure 4.7: Bending moments at breast height (1.4 m) of Tree-1 for two different samples which were generated to have 21 m/s mean wind-speed on the trees.

4.5 Results and Discussion

To determine the time region for the record of the generated wind samples, the MC simulation time intervals (900 sec.) were assumed to represent the characteristics of life time for storms. This assumed time length may be increased for hurricanes by concerning their life time.

Figure 4.7 shows a plot of fragility curves for the different strength-loss scales due to decay in Tree-1 under the winter conditions. Figure 4.8 is for the same tree, but for the summer conditions. For example, when Tree-1 is subjected to wind blows whose mean speed is 56 mph and standard deviation (std) is 24 mph (80-56=24 in Figure 4.7) under the zero decay condition of this tree, the probability of exceedance of the bending moment at breast height (1.4 m) to the threshold value (for the stem breakage) is approximately 7 % and 40 % for the winter and summer seasons, respectively. For the same conditions of Tree-9, these probabilities are 68 % and 36 % for, again, the winter (Figure 4.9) and summer (Figure 4.10) seasons, respectively. The comparison of these probabilities for these trees can be seen in Figure 4.11 as well.

The fragility curves (with respect to decay levels in the trees) in each figure (Figures 4.7 through 4.10) can be calculated by using an assumption that the new moment capacity (new threshold value, ξ) of the cross-section of the tree trunk is equal to 90% (for SL=10%), or 80% (for SL=20%) of the original moment capacity due to particular decays in the cross-section. This moment capacity loss depends on the size and the location of the decays in cross-sections of the trunks. This relationship between the moment capacity loss and the decay size and location will be addressed in Chapter 5 in detail.

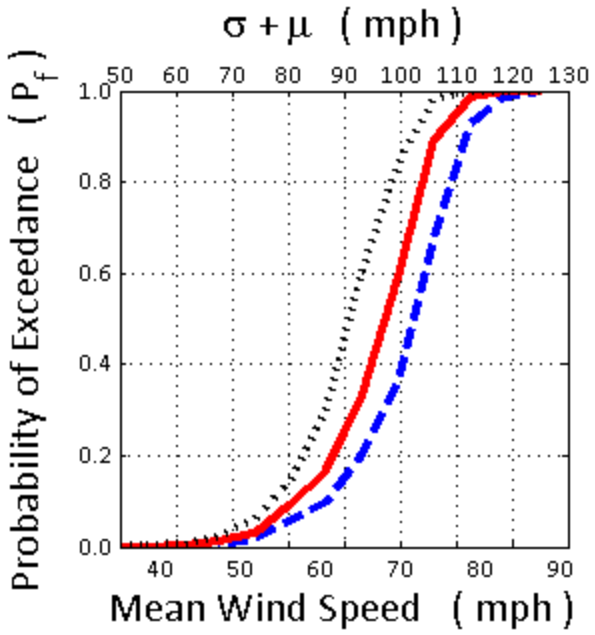

Figure 4.8: Winter season for Tree-1. Dashed line, solid line, and dotted line represent fragility curves of Tree-1 with zero, 10 %, and 20 % moment capacity loss, respectively, due to an assumed decay in the tree.

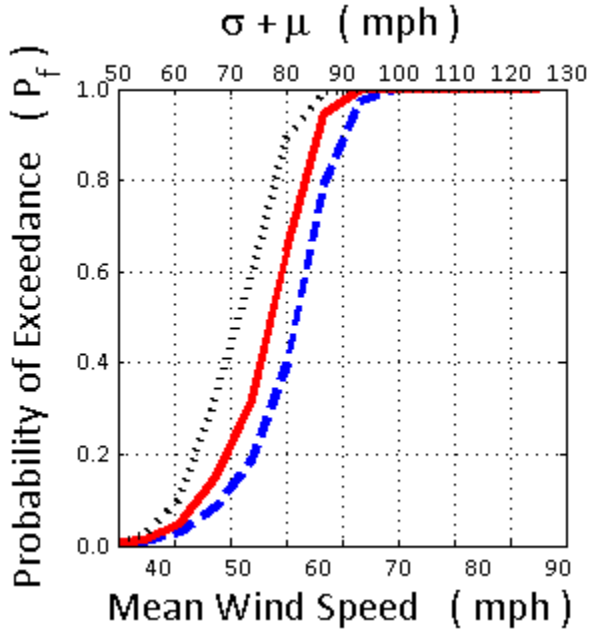

Figure 4.9: Summer season for Tree-1. Dashed line, solid line, and dotted line represent fragility curves of Tree-1 with zero, 10 %, and 20 % moment capacity loss, respectively, due to an assumed decay in the tree.

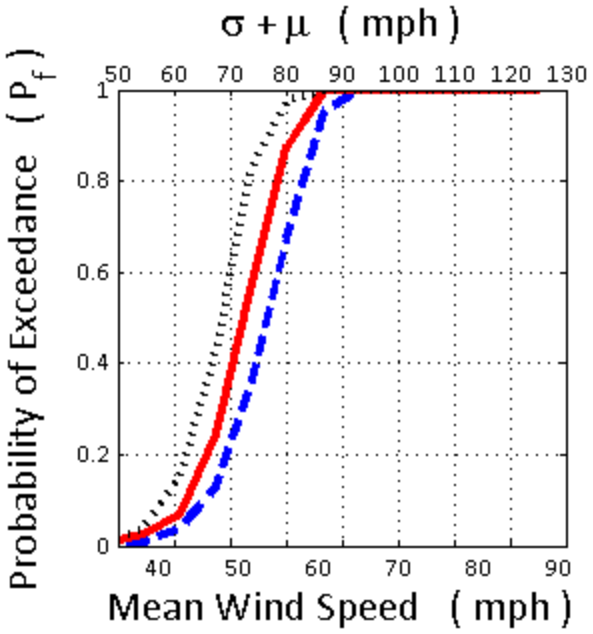

Figure 4.10: Winter season for Ttree-9. Dashed line, solid line, and dotted line represent fragility curves of Tree-9 with zero, 10 %, and 20 % moment capacity loss, respectively, due to an assumed decay in the tree.

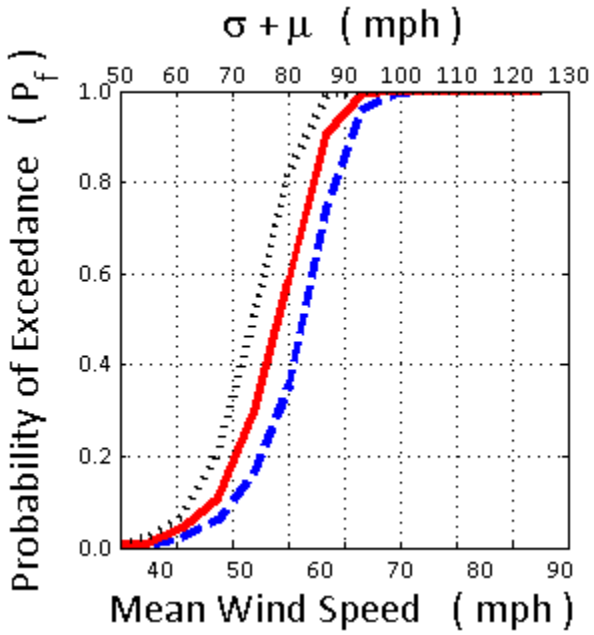

Figure 4.11: Summer season for Tree-9. Dashed line, solid line, and dotted line represent fragility curves of Tree-9 with zero, 10 %, and 20 % moment capacity loss, respectively, due to an assumed decay in the tree.

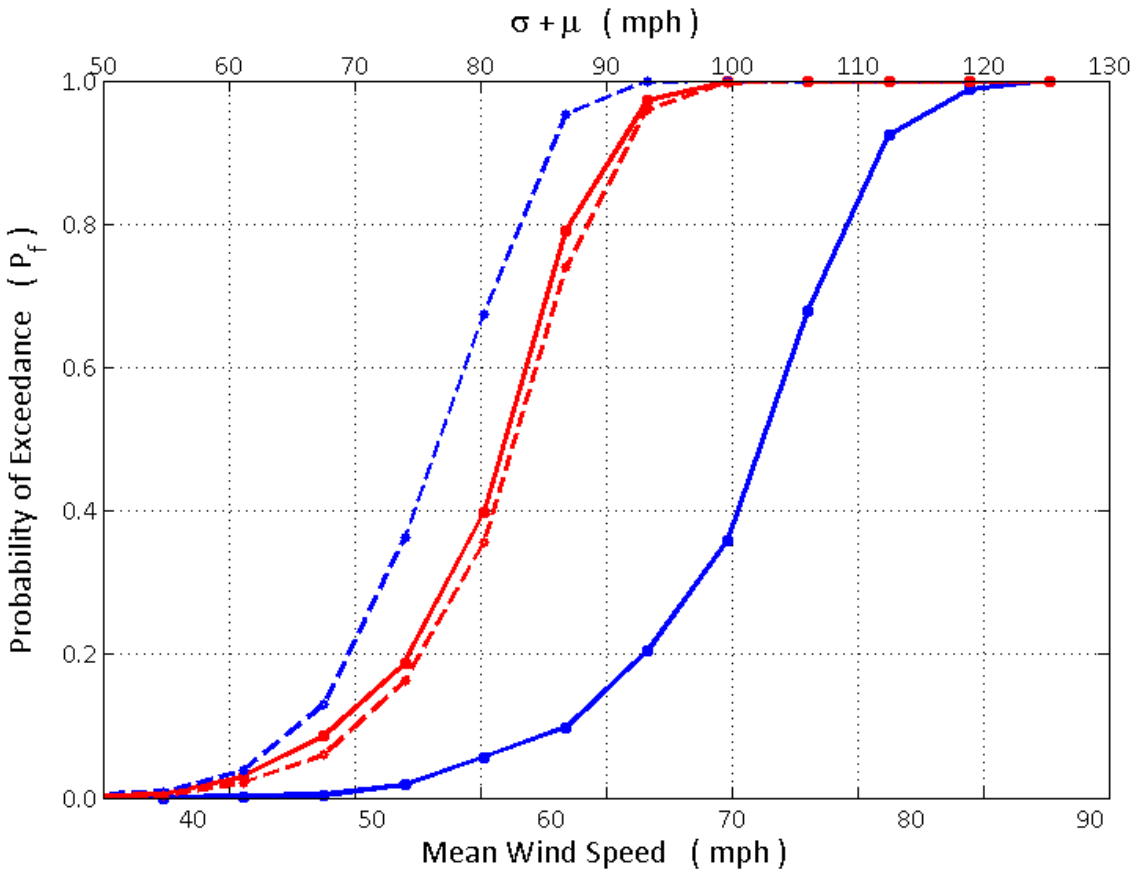

Figure 4.12: All seasons for Tree-1 (solid curves) and Tree-9 (dashed curves) without any decay. Red and blue curves represent the summer and winter seasons, respectively.

Although dynamic analyses can be viewed as a nonlinear transformation from the inputs to outputs, a nearly linear relationship between the maximum bending moments for the winter and summer seasons for each of the trees (Tree-1 and Tree-9) can be seen in Figure 4.13 and Figure 4.14, respectively. After applying MC simulations only for winter season, the maximum bending moments for summer season would have been generated by using the slope of the linear relationships between the maximum bending moments for the different seasons, because the constant values in these linear functions of Figure 4.12 and Figure 4.13 can be neglected due to their small values with respect to the

amount of summer bending moments at the y-axes in these figures. To obtain the slope of the linear functions in the figures can be estimated by using Eq. 4.18.

$$\frac{BM_S}{BM_W} = \frac{[\rho A C_d \zeta]_S}{[\rho A C_d \zeta]_W} \tag{4.18}$$

where BM_S and BM_W are for the maximum bending moment data from the MC simulations for the summer and winter seasons, respectively. The ratio of these maximum bending moments in Eq. 4.18 is close to the slope of the linear functions in Figures 4.12 and 4.13. This slope depends on the ratio of the dynamic excitation forces for the summer and winter seasons. ρ, A, and Cd are the same symbols in Eq. 3.2. The damping ratio (ζ) varies from season to season due to leaves on the trees.

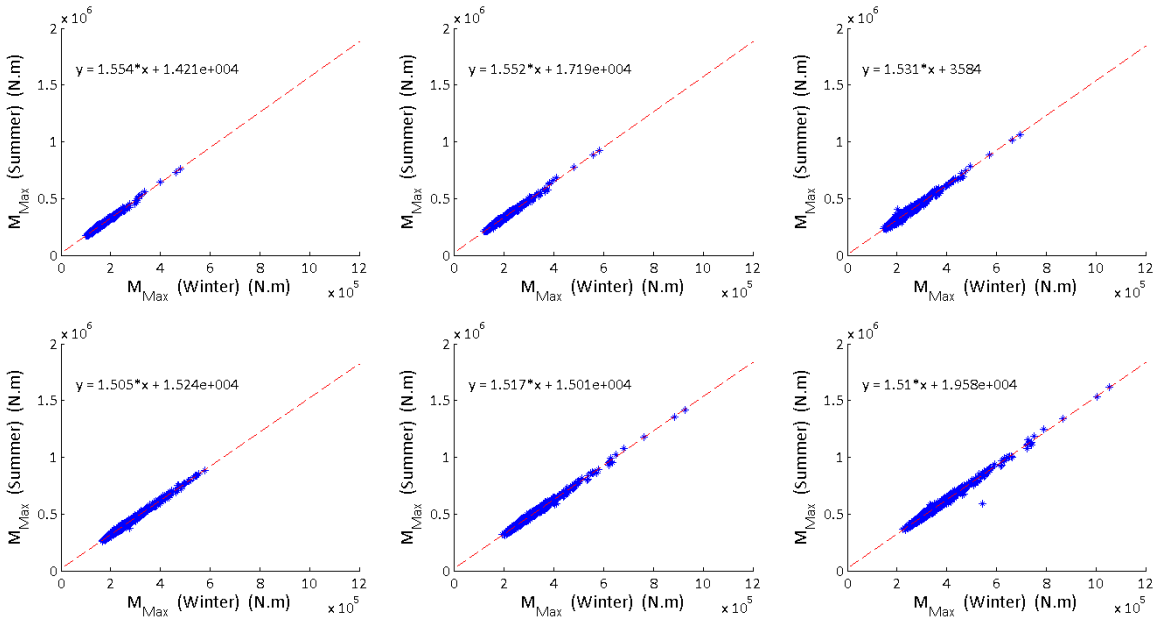

Figure 4.13: The relationship between the maximum bending moments of the winter and summer seasons for Tree-1.

For example, the effect of the ratio (Eq. 4.20) of the damping ratios on the dynamic response of Tree-1 for the summer and winter seasons can be estimated by using

Eq. 4.18 and Eq. 4.19 to obtain that the slope of the linearity in Figure 4.12 is averagely 1.53 for the Tree-1.

$$\left[\frac{[\rho AC_d\zeta]_S}{[\rho AC_d\zeta]_W}\right]_{Tree-1} = \frac{(1.226)(3.9A_W)(0.6)(\zeta_S)}{(1.326)(A_W)(1.0)(\zeta_W)} = 1.53 \tag{4.19}$$

$$\left[\frac{\zeta_S}{\zeta_W}\right]_{Tree-1} = 0.71 \tag{4.20}$$

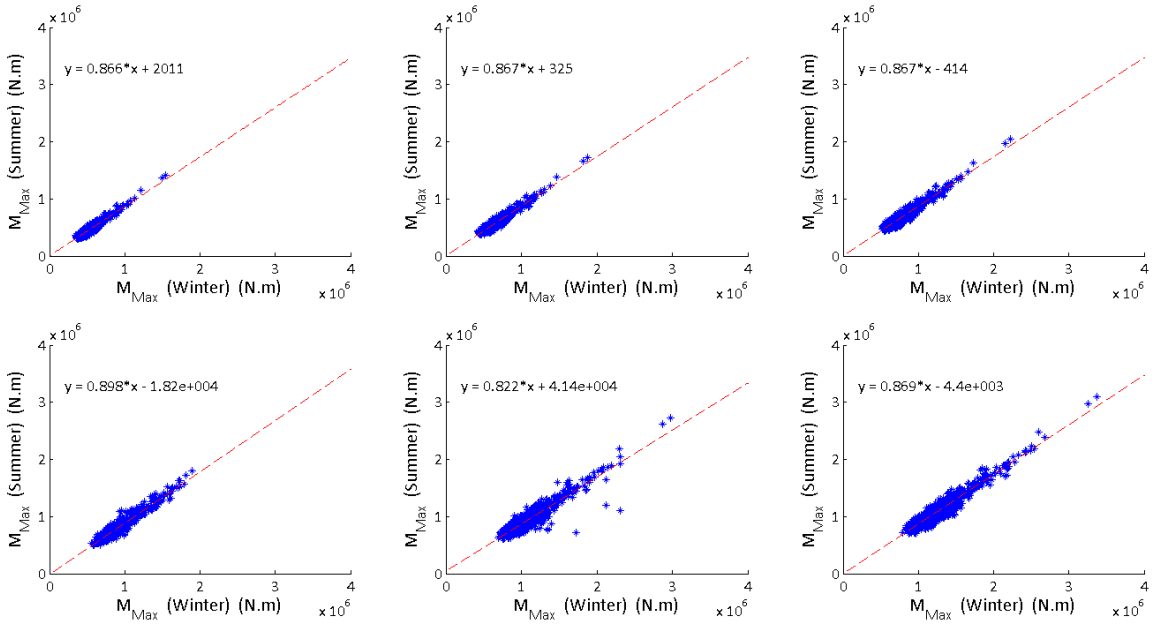

Figure 4.14: The relationship between the maximum bending moments of the winter and summer seasons for Tree-9.

For another example, again, the effect of the ratio (Eq. 4.22) of the damping ratios on the dynamic response of Tree-9 for summer and winter seasons can be estimated by using Eq. 4.18 and Eq. 4.21 to obtain that the slope of the linearity in Figure 4.13 is averagely 0.87 for the Tree-9.

$$\left[\frac{[\rho AC_d\zeta]_S}{[\rho AC_d\zeta]_W}\right]_{Tree-9} = \frac{(1.226)(2.5A_W)(0.6)(\zeta_S)}{(1.326)(A_W)(1.0)(\zeta_W)} = 0.87 \tag{4.21}$$

$$\left[\frac{\zeta_S}{\zeta_W}\right]_{Tree-9} = 0.63 \tag{4.22}$$

It is interesting that the ratios (0.71 in Eq. 4.20 and 0.63 in Eq. 4.22) of the damping ratios of the summer and winter seasons are in the range of 0.58 (Rd_{15} / Rd_5 = 0.58 for the dashed curve in Figure 6.11) and 0.84 (Rd_{15} / Rd_5 = 0.84 for the dotted curve in Figure 6.11).

Additionally, the probability of tree failures can be expanded for various tree locations and for various time periods by using Eq. 4.23 which is a common formula used in several recent studies (e.g. Yue and Ellingwood 2006, Smith 2009).

$$P_f^T = \int_0^\infty F_R(v) f_V(v) dv \tag{4.23}$$

where $F_R(v)$ is the fragility curve function (as in the figures from Figure 4.7 to Figure 4.10) of trees in terms of wind speed (v), and $f_v(v)$ is the probability density function (pdf) of wind speed. For this fragility analysis, this wind-speed distribution can belong to anywhere and can be expressed with reference to any time period (such as annual wind speed, 10-year wind speed, and 50-year wind speed).

4.6 Conclusion

In this chapter, only two different trees could be investigated because of the difficulties on measuring real tree structures and time concerning of MC simulations. Thus, the randomness of tree structures could not be addressed, but the randomness of the wind excitation force could be addressed successfully, by generating a total of 1000 different wind speed samples for each mean value. For future work, the investigation of

the randomness of tree structures with concerning the randomness of wind forces on those trees may be a good research.

The results discussed in this Chapter are limited to some assumptions used. One of the assumptions is that Ochi-Shin equation was modified by using small mean wind-speeds (from 1.1 m/s to 5.7 m/s), and then wind samples were generated by using this modified Ochi-Shin equation for greater mean wind-speeds (from 13 m/s to 39 m/s). The other important assumption is that decay can only affect the moment capacity of the tree sections by excluding the effect of decays on tree dynamics and the effect of wood orthotropic material property on that moment capacity.

The effect of moment capacity loss due to decays on the fragility curves can be seen in the figures (from Figure 4.7 to Figure 4.10) by assuming that there is a specific decay and this decay causes to a 10% or 20% moment capacity loss for the tree sections. But the important question is to know or calculate the moment capacity loss for any decay. The answer of this question will be addressed with the next chapter, Chapter 5.

CHAPTER 5

MOMENT CAPACITY LOSS IN TREES DUE TO DECAY

5.1 Introduction

Tree risk assessment is an important aspect of arboricultural practice. Tree failures regularly damage property and kill or injure people (Schmidlin 2009). There is also a risk of litigation associated with tree failures (Mortimer and Kane 2004), so their economic cost may be much greater than simply the cost of removing the tree and repairing the damage. Examples can be found in most cities: a recent series of articles in the New York Times detailed multiple lawsuits stemming from fatalities and injuries associated with hazardous trees (Glaberson and Foderado 2012).

Tree risk assessment involves many techniques that range from visual approaches (Fink 2009) to sophisticated methods involving tomography (Nicolotti et al. 2003, Gilbert and Smiley 2004, Wang and Allison 2008), radar (Butnor et al. 2009), strain gauges and inclinometers (Sinn and Wessolly 1989). Assessing decay has been the focus of much research, primarily in the form of decay detection devices (Johnstone et al. 2010). Quantifying the amount of decay has been translated into the probability of failure using strength loss formulas (Wagener 1963, Coder 1989, Smiley and Fraedrich 1992, Mattheck et al. 1994). Kane et al. (2001) reviewed existing strength loss formulas, which [excepting Mattheck et al. (1994)] derive from the moment of inertia (I) of a beam of circular cross-section, and have been modified in accordance with empirical evidence. It should be noted that the level of sophistication and the quantity of investigations of

testing of devices to detect decay far exceeds the sophistication, accuracy and quantity of investigations of the strength loss formulas.

Strength loss formulas suffer from three important limitations. First, they consider only the relative proportion of decay in the cross-section, but strength loss depends also on the location of the neutral axis and distance (c) between it and the location at which stress (σ) is calculated in the flexure formula:

$$\sigma = \frac{Mc}{I} \tag{5.1}$$

The second limitation of the formulas is that they assume a homogeneous and isotropic material: where tensile and compressive stresses develop symmetrically in the cross-section. It is well known that wood is axially stronger in tension than compression (Bodig and Jayne 1993), which is why bending failures of test specimens initially fail in compression (Hoadly 1980). Finally, the formulas assume circular areas of decay, and two of them (Wagener 1963, Coder 1989) do not account for off-center areas of decay, which undermined their ability to predict strength loss (Kane and Ryan 2004).

The objective of this chapter is to develop improved moment capacity loss (MCL) curves that account for areas of decay that vary with respect to size and distance from the perimeter of the cross-section, as well as those of irregular shapes. A secondary objective is to investigate whether the magnitude of disparity between the tensile and compressive elastic moduli of wood affected the performance of the improved strength loss curves.

5.2 Materials and Methods

In deriving the improved MCL curves, several assumptions have been made. First, it was assumed that the stem or branch experienced pure bending stress; the effects

of axial, shear and torsional stresses have been ignored. The reason of this assumption is that wind-induced tree failures typically involve bending stress due to tree swaying motion (James 2003) and experimental verification of the improved formulas involved primarily bending stress. Shear stresses or combination of shear and bending stresses are neglected given the typical slenderness found in branches and stem. Second, cross-sectional areas of the stem and decay were assumed to be circular and defined by radii R and r, respectively, as shown in Figure 5.1. The area of decay, still considered a circle, can also have an open cavity, as in the right-hand side of Figure 5.1. Third, the derivation assumes that the line of application of bending force is along a diameter drawn through the center of both the area of decay and the cross-section of the stem (Figure 5.1). This assumption results in the maximum loss in moment capacity of the cross-section in order to concern the worst case scenario in tree failures.

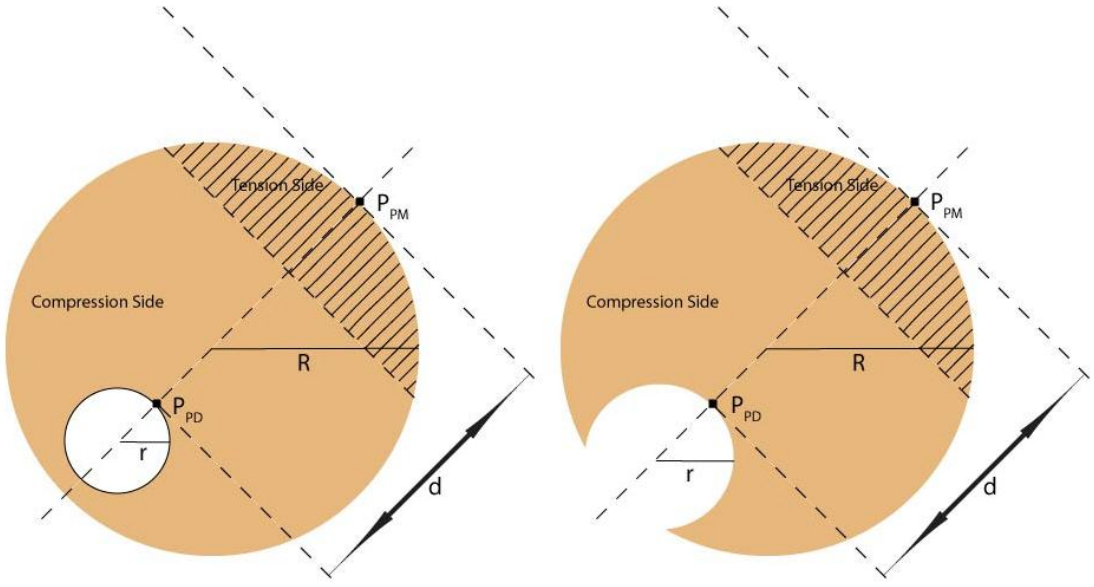

Figure 5.1: Decay definitions in cross-sections of any members in trees. The shaded area refers to the region of tensile stress and strain; the clear area refers to the region of compressive stress and strain. The neutral axis (where there are no bending strains) is the dashed line that separates the shaded and clear areas of the cross-section.

5.2.1 Definition of Circular Decays in Cross-Sections:

The distance (d) in Figure 5.1 quantifies the degree to which an area of decay is offset from the point which has maximum tensile strain and stressin the stem cross-section. It is the distance along a diameter line that bisects the area of decay and the stem from the farthest point of the tension side of the stem (P_{PM} in Figure 5.1) to the closest point on the perimeter of the area of decay (P_{PD} in Figure 5.1). The ratio d/R will be used to plot the loss in moment capacity.

5.2.2 Theoretical Approach and Implementation:

Moment capacity of the stem cross-section (with and without decay) can be calculated as the total moment of compressive and tensile stresses about the neutral axis of the cross-section. Thus, the first step to calculate moment capacity of stems with and without decay is to determine the location of the neutral axis. Figure 5.2 shows a representative stem cross-section with decay, as well as distributions of compressive and tensile strains and stresses [including the resultant compressive (F_C) and tensile (F_T) forces induced by bending moment]. The neutral axis lies at the transition from compressive (ε_c) to tensile (ε_t) strains, where for the case of zero axial force as assumed in this analysis.

$$F_C = F_T \tag{5.2}$$

The location of the neutral axis does not coincide with the geometric centroid of the stem, because it was assumed that the elastic modulus of wood is greater in tension (E_T) than in compression (E_C) due to the knowledge that theratio of E_T to E_C is

approximately 1.1 for two juvenile tree species, Douglas-fir and Western hemlock (Langum et al. 2009).

To determine the location of the neutral axis, eight values of the modular ratio, n, (1.0, 1.1, 1.2, 1.3, 1.4, 1.5, 2.0 and 2.5) were tested, where

$$n = \frac{E_T}{E_C} \tag{5.3}$$

This facilitated a qualitative comparison of the effect of n on MCL. The ratio dictates the proportional disparity between similar triangles representing ε_t and ε_c shown in Figure 5.2. For a given strain distribution, a stress distribution can be calculated (Figure 5.2). The neutral axis was initially assumed to be at 1% of the diameter of the cross-section, an unrealistically small value. Tensile and compressive strains that resulted from the placement of the neutral axis at each value of n were used to calculate σ_c and σ_t from Hooke's Law:

$$\sigma_i = E_i \varepsilon_i \tag{5.4}$$

where *i* designates compressive or tensile values of each parameter. From the distributions of σ_c and σ_t, the resultant forces (F_C and F_T) were calculated by integrating compressive (σ_c) and tensile (σ_t) stresses over the cross-sectional areas in compression and tension, respectively, in Figure 5.2. For each value of n, the preceding steps were repeated after incrementally increasing the distance between the neutral axis and P_{PM} in Figure 5.1 until Eq.5.2 was satisfied, a statement of internal force equilibrium.

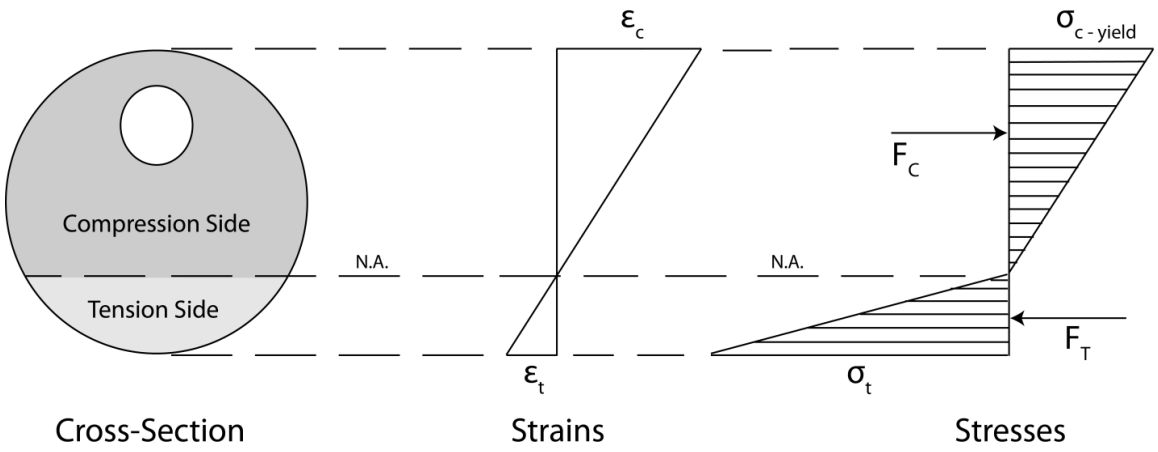

Figure 5.2: Strains and stresses in compression and tension sides of a cross-section.

Once the location of the neutral axis was known, the moment of inertia (I) of the stem about the neutral axis was calculated for stems with and without decay. A program was written in Matlab (Matlab 7.8.0-R2009a) to calculate the moment of inertia of the stem by dividing the cross-section into rectangular areas of incremental width and using the parallel axis theorem to sum the inertia of each rectangle about the neutral axis of the cross-section:

$$I = \sum_{i=1}^{N} \frac{1}{12} b_i h_i^3 + A_i l_i^2 \tag{5.5}$$

where *N*, *b*, *h*, and *A* are the number, base, height, and area, respectively of each rectangle (i); and *l* is the perpendicular distance between the neutral axis and the center of each rectangle.

5.2.3 Experiments on Moment Capacity Loss:

To validate the MCL curves for different amounts and locations of decay, ten red oaks (Quercus rubra) growing in Pelham, MA, USA (USDA Hardiness Zone 5A) were

tested in 2009 by Kane (unpublished data). Morphometric data of the trees are presented in Table 5.1. Branches were removed prior to testing to limit the P-delta effect of the offset mass of the crown during testing. A snatch block (McKissick Light Champion model 419) was attached to the tree with an Ultrex sling (1.9 cm diameter, Yale Cordage, Saco, ME) at approximately 65% of its height. Trees were pulled using a skidder (John Deere model 440D) with a hydraulic winch and 61 m of Vectrus (1.3 cm diameter, Yale Cordage, Saco, ME). The rope was passed through the block and attached to a load cell (Dillon EDXtreme, Weigh-Tronix, Fairmont, MN) that recorded loads (accurate to 44 N) at 10 Hz. Loads had to be adjusted to account for friction and they were resolved into components parallel and normal to the long axis of the trunk. Taking the sine of the mean angle between the applied force and the tree (Table 5.1) indicated that 96% of the load was applied normal to the longitudinal axis of the trunk.

Table 5.1: Morphometric data for ten red oaks tested by Kane (unpublished data)

Parameter	Mean	SD
DBH (cm)	41	4.3
Tree Height (m)	21.6	1.2
Crown Width (m)	11.9	2.3
Block Height (m) *or Pulling Height*	13.8	1.3
Diameter at block height (cm)	18	1.8
Angle between cable and stem (^{o})	73	2.5
% of diameter notched (Type 1)	35	10
% of diameter notched (Type 2)	40	15

A strain meter was attached to the tension side of the tree approximately 1 m above ground as described by James and Kane (2008), which recorded axial displacements at 20 Hz. Displacements were converted to strains and downloaded into a spreadsheet (Excel 2003, Microsoft Corp.). To relate displacements with loads, which were also downloaded into Excel, the mean of two displacements taken every 0.1 s was matched each load taken at the corresponding time. Trees were winched to induce displacements in the trunk of approximately one or two mm to ensure that strains remained in the elastic range. The rate of loading varied with trees of different dimensions and time in the test (initial rates were less). Loading rate ranged from approximately 100-200 N/s, which induced displacements at a rate of approximately 0.1-0.2 mm/s.

After winching, a notch whose long axis was normal to both the direction of winching and the longitudinal axis of the trunk was cut into each tree with a chainsaw. Two types of notches were cut: 1) into the tension face of the trunk, removing all of the wood on the perimeter of the stem (two tested trees); 2) through the tree leaving wood intact at the perimeter of the trunk on the tension and compression faces (eight tested trees) (Figure 5.3). More Type 2 notches were cut because of the variability of the location of the notch relative to the center of the trunk (as measured incident with the applied load). One left equal thicknesses of wood on the proximal and distal sides of the trunk (relative to the position of the skidder); one left a greater thickness of wood on the proximal side of the trunk; and the remaining seven trees left a greater thickness of wood on the distal side of the trunk. The mean thickness of wood on both the proximal and distal sides of the trunk for all trees that received Type 1 notches is included in Table 5.1.

Figure 5.3: Two different drilling types were applied to tree stems.

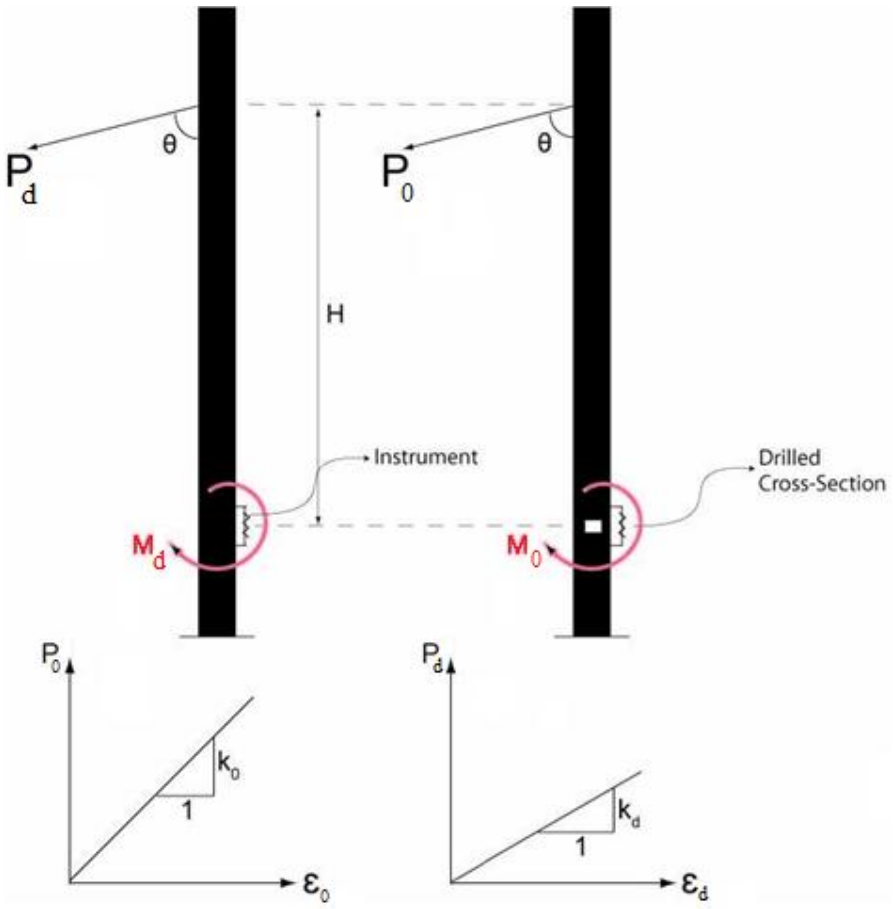

Figure 5.4: Representing the experiments on the trees and the data from these experiments.

The force (P) inducing bending moment (M) was plotted against strain before and after notches which were cut on each tree. The slope of the best-fit line is related to the moment capacity of the tree before (k_0) and after notching (k_d) due to the derivation of Eq. 5.22 (Figure 5.4).

5.2.4 Analyses of Experimental Data:

In the following derivation, the subscripts ($_0$) and ($_d$) refer to before and after notching, respectively, and it was assumed that

$$E_0 = E_d \tag{5.6}$$

Hooke's Law can therefore be used to relate stress to strain of trees before and after notching:

$$\frac{\sigma_0}{\varepsilon_0} = \frac{\sigma_d}{\varepsilon_d} \tag{5.7}$$

Eq.5.7 can be solved for σ_0:

$$\sigma_0 = \frac{\varepsilon_0 \sigma_d}{\varepsilon_d} \tag{5.8}$$

To find moments (M) of the applied force (P), the distance between the center of the strain meter and the block on the tree (H) and θ (in Figure 5.4) must be known:

$$M_0 = HP_0 \sin\theta \tag{5.9}$$

$$M_d = HP_d \sin\theta \tag{5.10}$$

where P_0 and P_d can be found for each tree as shown in Figure 5.4:

$$P_0 = k_0 \varepsilon_0 \tag{5.11}$$

$$P_d = k_d \varepsilon_d \tag{5.12}$$

and substituted into Eq.5.9 and Eq. 5.10:

$$M_0 = Hk_0\varepsilon_0 \sin\theta \tag{5.13}$$

$$M_d = Hk_d\varepsilon_d \sin\theta \tag{5.14}$$

Eq.5.1 can be re-written including nfor tension side of the stem cross-sections (as in Figure 5.5):

$$\sigma_0 = n\frac{M_0 c_0}{I_0} \tag{5.15}$$

$$\sigma_d = n\frac{M_d c_d}{I_d} \tag{5.16}$$

M_0 and M_d from Eq.5.13 and Eq.5.14 can be substituted into Eq.5.15 and Eq.5.16:

$$\sigma_0 = n\frac{Hk_0\varepsilon_0 \sin\theta\, c_0}{I_0} \tag{5.17}$$

$$\sigma_d = n\frac{Hk_d\varepsilon_d \sin\theta\, c_d}{I_d} \tag{5.18}$$

The section modulus (S) before and after damage is calculated using:

$$S_0 = \frac{I_0}{c_0} = \frac{nHk_0\varepsilon_0 \sin\theta}{\sigma_0} \tag{5.19}$$

$$S_d = \frac{I_d}{c_d} = \frac{nHk_d\varepsilon_d \sin\theta}{\sigma_d} \tag{5.20}$$

Substituting σ_0 from Eq. 5.8 into equation Eq. 5.19 yields:

$$S_0 = \frac{nHk_0\varepsilon_d \sin\theta}{\sigma_d} \tag{5.21}$$

Loss in section modulus ($LOSS_{SM}$) of the tension side of tested tree cross-sections due to notching can be calculated for each tree from values of k_0 and k_d:

$$LOSS_{SM} = 1 - \frac{S_d}{S_0} = 1 - \frac{nHk_d\varepsilon_d \sin\theta/\sigma_d}{nHk_0\varepsilon_d \sin\theta/\sigma_d} = 1 - \frac{k_d}{k_0} \tag{5.22}$$

$LOSS_{SM}$ in the tension side of cross-sections of trees tested in situ was also determined as described in Section 5.2.2, except that areas of notches were considered

trapezoidal, not circular, consistent with Figures 5.3 and 5.5. The reason of that $LOSS_{SM}$ in the tension side of the tested tree cross-sections was theoretically obtained instead of the moment capacity loss (described in Section 5.2.2) for each tree is that all the measurements in situ correspond to tension side of the cross-sections of the trees. In addition, it is known that the moment capacity loss is equal to the loss of elastic section modulus in the compression side because trees have a lower compressive strength, and not in the tension side.

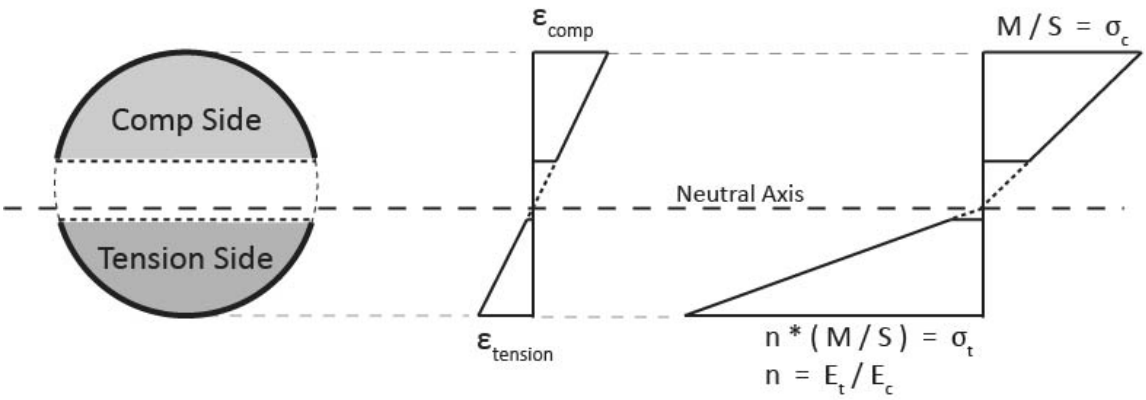

Figure 5.5: Strains and stresses in compression and tension sides of the cross-sections of the trees which have drilling type-2 as in Figure 5.3.

To experimentally and theoretically compare the $LOSS_{SM}$ values in the tension side of the cross-sections of the tested trees, the modular ratio, n, unknown for the tested trees (large, open-grown red oaks), should be assumed first. Thus, two values of n, 1.10 as in the study of Langum et al. (2009), and 2.00 were considered when theoretically determining $LOSS_{SM}$. A one-way analysis of variance was used to investigate whether estimates of $LOSS_{SM}$ differed between the three methods (empirical, theoretical assuming n=1.1, theoretical assuming n=2.0). A regression analysis was used to determine whether

differences between empirically and theoretically determined values of $LOSS_{SM}$ were related to the magnitude of $LOSS_{SM}$.

5.3 Results and Discussion

Figures 5.6 and 5.8 plot moment capacity loss (MCL) of the cross-section of a tree relative to size and location of decay in the cross-section. In both figures, it has been assumed that n = 1.10 (consistent with Langum et al. (2009)). To describe the location of decays, the ratio of d/R was used as illustrated in Figure 5.1. If this ratio is negative, it means that decay creates an open cavity on the tension side of the cross-section, so Figure 5.8 should be used for these decay types. Figure 5.6 should be used for the other possibilities ($d/R \geq 0$) for location of decay. Linear interpolation may be used for values of d/R not included in Figures 5.6 and 5.8. For d/R = 0.40, for example, MCL can be interpolated between the curves for d/R = 0.33 and 0.50.

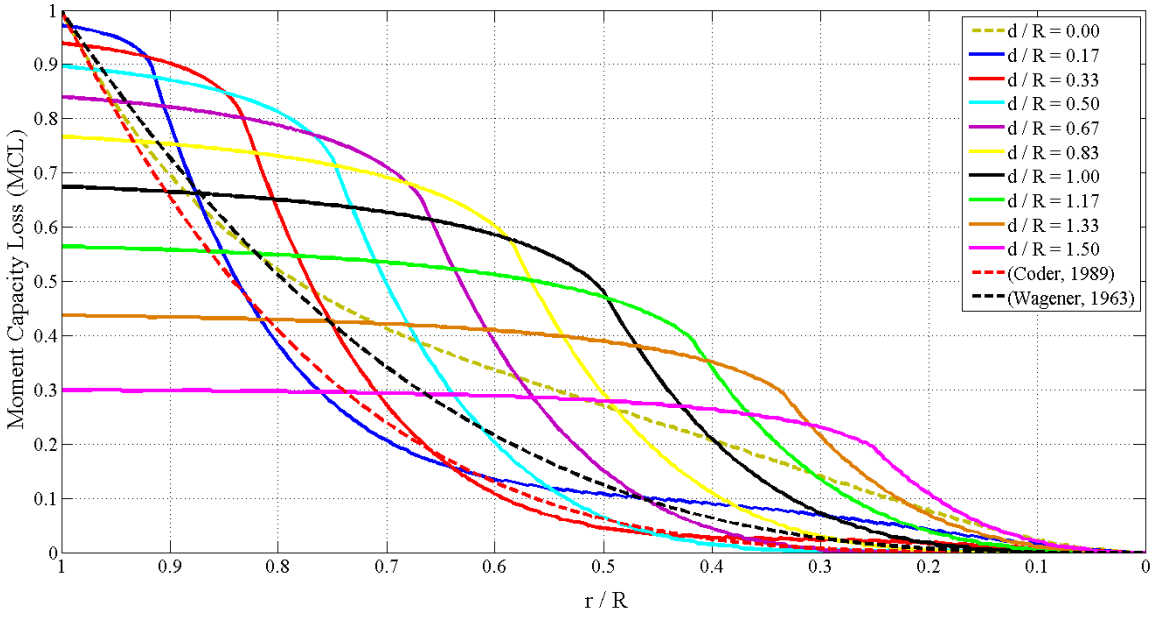

Figure 5.6: MCL for different sizes and locations of decays [n = 1.10].

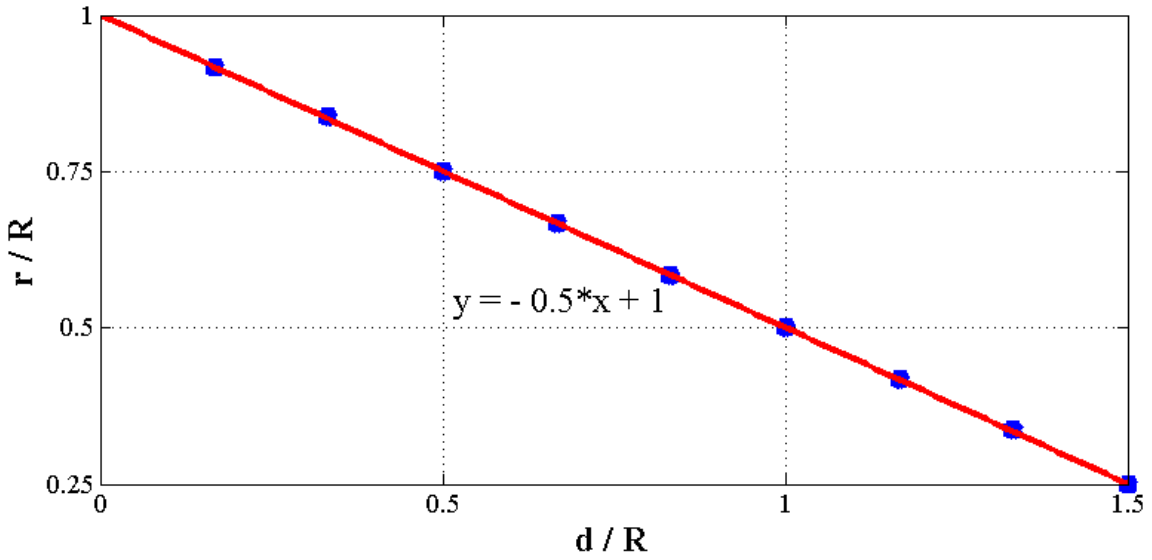

Figure 5.7: Relationship between decay size (r/R) and the yielding points of various d/R ratios in Figure 5.6.

Yield points for various d/R ratios in Figure 5.6 are shown by dots in Figure 5.7. Data in Figure 5.7 fit well to a line with the slope of -0.5 and the r/R intercept of 1. The fitted equation shows that:

$$\frac{r}{R} = -0.5\frac{d}{R} + 1 \tag{5.23}$$

Eq. 5.23 can be rewritten in the following form,

$$2r + d = 2R \tag{5.24}$$

By considering the definition of decay in Figure 5.1, Eq. 5.24 corresponds to the case of the formation of an open cavity in a tree cross-section. The shape of the moment capacity loss curves in Figure 5.6 indicates that for a given decay location (d/R), a critical decay size (r/R) exists above which MCL does not increase significantly. This critical r/R is given by Eq. 5.24.

The interaction of size (r/R) and location (d/R) is underscored by Figures5.6 and 5.8. For example, in Figure 5.6, a specific size of decay (r/R=0.5) can have varying MCL

values depending on location: 27% for d/R=0.00, 4% for d/R=0.33, 7% for d/R=0.50 (concentric decay), and 48% for d/R=1.00. Predicted loss in moment capacity for d/R=0.00 exceeds predictions of loss in moment capacity for all other positive values of d/R (except d/R=1.50) for $r/R \leq 0.2$. As r/R increases, predicted loss in moment capacity for d/R=0 is less than predictions from the largest values of d/R (1.17, 1.33, 1.50), but still greater than predictions from smaller values of d/R (0.17, 0.33, 0.50, 0.67). As r/R continues to increase predicted loss in moment capacity for d/R=0.00 is less than predictions assuming small and moderate values of d/R, but greater than predictions assuming the largest values of d/R (1.33, 1.50). A careless accounting for the location of decay could grossly under- or overestimate the loss in moment capacity of the stem, even for relatively small areas of decay. As an example, Wagener (1963) suggested that when the diameter of an area of decay was 70% of the diameter of the cross-section there was a greater likelihood of failure. Figure 5.6 shows that loss in moment capacity or strength loss (Wagener 1963, Coder 1989, Smiley and Fraedrich 1992) at r/R=0.7 can be quite variable depending on location. Conversely, 0.41, which is the approximate loss in moment capacity for r/R=0.70 and d/R=0.00 can occur at $r/R \approx 0.67, 0.61, 0.64, 0.47, 0.43$ for d/R=0.50, 0.67, 0.83, 1.00, and 1.17, respectively. These findings are explained by the difference in compressive and tensile capacities of the stem. Decays located near the tension side are more detrimental than those found near the compression face.

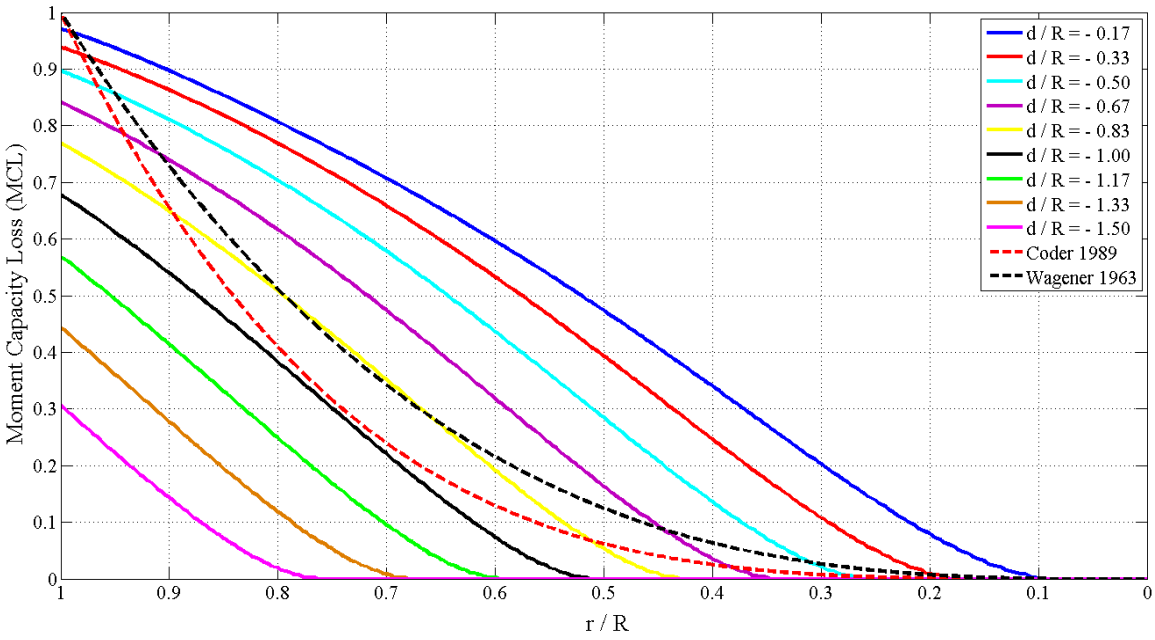

Figure 5.8: MCL values for different sizes and different locations of decays [n=1.10].

Wagener's (1963) and Coder's (1989) predictions of strength loss have been included in Figure 5.6, although both researchers based on reduction of I (moment of inertia). Smiley and Fraedrich's (1992) formula is the same as Wagener's (1963) when no cavity is present. The limitations of the formulas are immediately evident in Figure 5.6. Unless r/R < 0.10, using the formulas will dramatically over- or underestimate the loss in moment capacity. Such disparities are particularly important because the formulas have action thresholds. For example, Wagener (1963) suggested that conifers were more likely to fail when strength loss exceeded 33%. Loss in moment capacity of 35% occurs at r/R values of approximately 0.40, 0.45, and 0.50 for d/R values of 1.13, 1.00, and 0.83, respectively. Wagener's (1963) formula predicted 33% strength loss at r/R of 0.70. Similarly, Coder (1989) described the "caution zone" when strength loss exceeded 20%, which occurs at r/R ≈ 0.66. Loss in moment capacity of 0.20, however, occurred across the range of 0.25 < r/R < 0.70, depending on the value of d/R (Figure 5.6). Large

differences were also noted when values of $d/R < 0$ were considered (Figure 5.8). For $r/R \leq 0.5$, Wagener's (1963) and Coder's (1989) formulas underestimated loss in moment capacity compared to predictions using $d/R = -0.17$, -0.33, and -0.50. For $r/R \leq 0.5$, the formulas overestimated loss in moment capacity compared to predictions using $d/R = -1.17$, -1.33, and -1.50.

Wind-induced motion of some trees does not always result in pendulum-like sways. Some stems are only deflected in the leeward direction before returning to the equilibrium point when the wind stops (see Figures 7 and 8 in James et al. (2006)). This motion may cause areas of decay to occur consistently in the tension or compression sides of the cross-section of the stem, depending on the wind direction as shown in Figure 5.9. A leaning tree would similarly experience bending stress consistently tensile and compressive on opposite sides of the cross-section, relative to the direction of lean. It is noteworthy that the direction of loading produces very different results for certain combinations of r/R and d/R. For example, consider $d/R = 0.17$ and -0.17 in Figures 5.6 and 5.8, respectively: the loss in moment capacity is similar for $0.9 < r/R < 0.2$, but noticeably different throughout the remaining range of r/R. Practitioners would almost certainly reach opposite conclusions regarding the removal of a tree depending on whether wind-induced deflection causes the area of decay to be in compression or tension. The range of disparity is smaller, but the same pattern is true for d/R values of 0.33 and -0.33, as well as 0.50 and -0.50.

5.3.1 Procedure to Estimate MCL

Figure 5.9 shows two different decay sizes for a tree cross-section. According to this figure, the radius (R) of the cross-section of the stem is 20 cm. If wind blows from right to left as illustrated in the left part of the figure, the distances for the two decays (d_1 and d_2) between the points (P_{PM} and P_{PD}) are 10 cm, and the size as defined by their corresponding radii (r_1 and r_2) are 10 and 15 cm.; For wind blowing from left to right (right side of figure), d_1 (for the small decay) will be 10 cm, and d_2 (for the large decay) will be zero for the given radii r_1 and r_2. The vertical dashed lines in Figure 5.9 represent tangents to the tree cross-section on the side where tension is generated due to the direction of wind. Because wind direction can blow from two directions, two estimates of MCL can be obtained for this cross-section for each decay size depending on wind directionality. Sections 5.3.1.1 and 5.3.1.2 present the results from these two cases, where wind blows from right-to-left (leftward), and from left-to-right (rightward), respectively.

5.3.1.1 Wind Blowing Leftward

The ratio of the distances, d_1 and d_2 (between the points, P_{PM} and P_{PD}) to the radius of the cross-section is 0.50, as can be seen at the left side of Figure 5.9. Using the curve in Figure 5.6 corresponding to d/R=0.50 (cyan) and reading vertically from the two decay size ratios (r_1/R=0.50 and r_2/R=0.75) gives the two estimates for MCL. Estimated MCL is 6.6 % and 72.8 % caused by the small and large decays, respectively, highlighting the non-linear relationship between moment capacity loss and decay size. For an increase in decay size of 50%, MCL is obtained greater than tenfold.

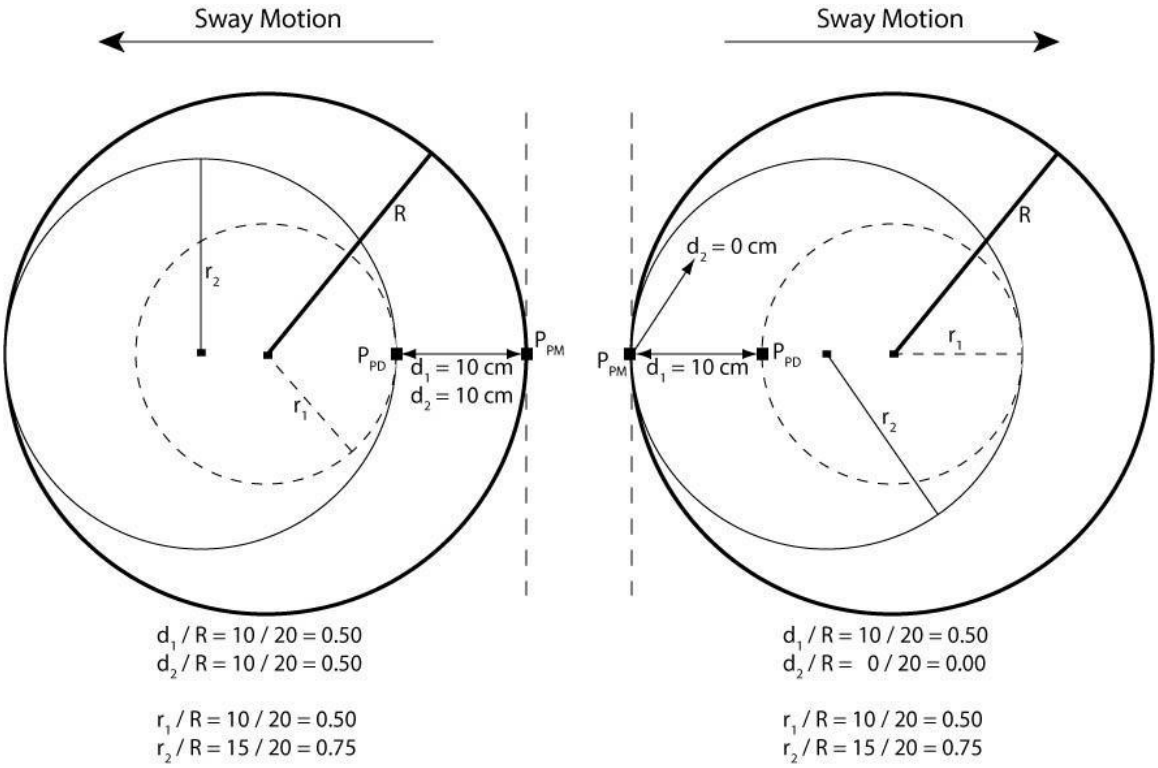

Figure 5.9: Representation of two different decays in a cross-section. The figure at right is for the rightward blowing wind; the figure at left is for leftward blowing wind.

5.3.1.2 Wind Blowing Rightward

The effect rightward wind condition for the same two decay types studied in the previous section references the right of Figure 5.9. Decay position ratios (d/R) in this case are 0.50 and 0.00 for the small and the large decays, respectively. The curves corresponding to these two decay location ratios (cyan for $d_1/R=0.50$ and dashed-tan for $d_2/R=0.00$) are used to determine MCL. For each decay size with r/R of 0.50 and 0.75, respectively, one finds MCLs of 6.6 % and 46.2 %. The effect of the small decay on MCL is the same as the case of leftward blowing wind, but a lower MCL is caused by the larger decay than before. The two examples discussed illustrate the importance of

accounting for wind directionality to find the critical MCL for a given tree stem and size of decay.

5.3.1.3 MCL Envelope for Rightward and Leftward Wind

The small decay produces the same MCL for both directions of induced wind (MCL=6.6%) because of that it is a concentric decay. The large decay, in contrast, produces two different MCLs, with 72.8 % MCL being the critical condition for leftward wind.

Results of the small decay (concentric decay) are compared with the estimations from the formulas proposed by Wagener (1963) and Coder (1989), who only studied the effect of concentric decays. Using Wagener's formula results in a strength loss of approximately 12 % (about twice the value predicted here), while Coder's formula predicts a strength loss of about 6 %, in better agreement with results from the current approach. The discrepancy in results points to the importance of using proper assumptions in the capacity loss models.

As further comparison of the proposed method, consider the diameter of a trunk cross-section is increased to 40 cm (R=20 cm), and the diameter of a concentric decay is increased to 33.2 cm (r=16.6 cm with d=3.4 cm). Using Wagener's and Coder's formula, strength losses are estimated as 57 % and 47 %, respectively. The critical MCL using the proposed method (Figure 5.6) is 47.5 %, again in better agreement with the results Coder's formulas for the assumed modular ratio of for n=1.10. It is conceivable that a larger modular ratio (n), indicating a larger difference between tensile and compressive

capacities would result in larger differences in MCL predictions. The effects of n on the critical MCL values of tree cross-sections will be discussed in Section 5.3.2.

5.3.2 Effects of Modular Ratio (n) on MCL

Figures 5.10 and 5.11 show that different values of n would not dramatically change MCL of decayed sections. Moment capacity loss was defined as $1-MC_d/MC_0$. MC_d refers to the moment capacity of a cross-section with decay; MC_0 is for the moment capacity of this cross-section without decay. Moment capacities with and without decay are calculated using equal values of n, so the resulting ratio is not as affected as the individual capacities are by increasing values of n. The small effect of n on moment capacity loss suggests that a wide range of species could be included using the curves given in Figures 5.6 and 5.8.

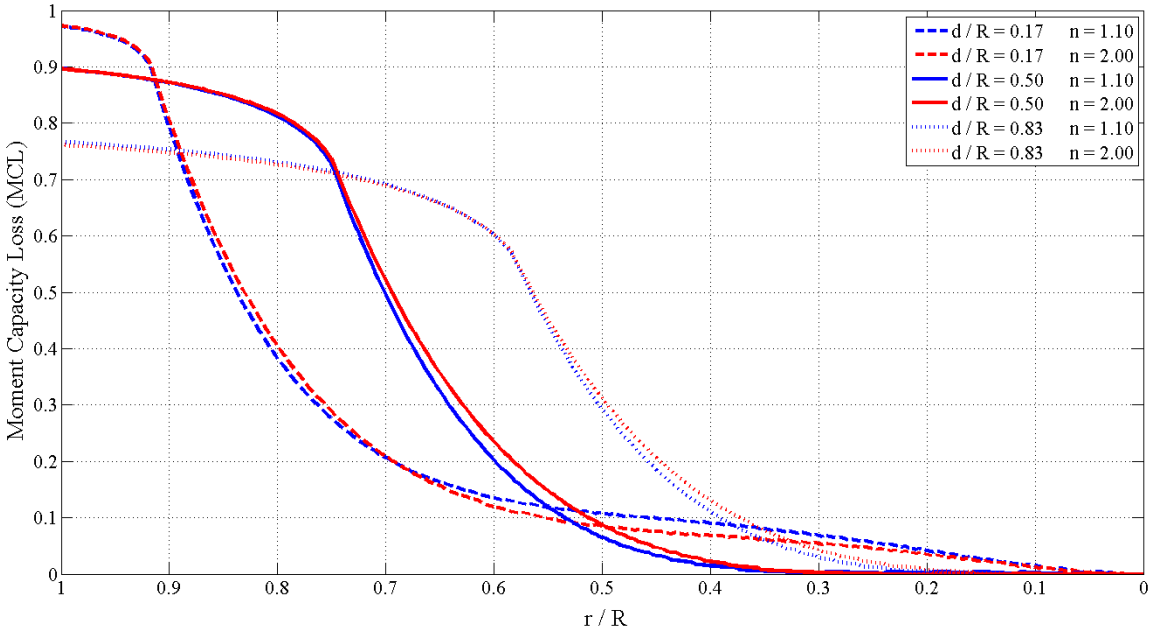

Figure 5.10: Effect of n (1.1, 2.0) on MCL for three values of d/R (0.17, 0.50, 0.83).

Table 5.2: Moment Capacity Loss (MCL) for various values of n (Et/Ec) and decay cases. Cv refers to cavity. T and C are for tension and compression sides of the cross-sections. The symbols (r, R and d) are defined in Figure 5.1. All the percentage columns were calculated by considering that the base case is n=1.0.

r / R = 0.5	d / R													
	1.50		1.17		0.83		0.50		0.17		- 0.17		- 0.50	
n = 1.0	.2822	%	.4732	%	.2890	%	.0625	%	.1129	%	.4732	%	.2830	%
n = 1.1	.2797	0.9	.4719	0.3	.2927	- 1.3	.0657	- 5.1	.1086	3.8	.4745	- 0.3	.2856	- 0.9
n = 1.2	.2772	1.8	.4688	0.9	.2960	- 2.4	.0690	- 10.4	.1048	7.2	.4760	- 0.6	.2880	- 1.8
n = 1.3	.2772	1.8	.4691	0.9	.2990	- 3.5	.0694	- 11.0	.1010	10.5	.4774	- 0.9	.2885	- 1.9
n = 1.4	.2771	1.8	.4678	1.1	.3020	- 4.5	.0758	- 21.3	.1003	11.2	.4771	- 0.8	.2887	- 2.0
n = 1.5	.2748	2.6	.4664	1.4	.3044	- 5.3	.0763	- 22.1	.0940	16.7	.4787	- 1.2	.2914	- 3.0
n = 2.0	.2702	4.3	.4626	2.2	.3129	- 8.3	.0881	- 41.0	.0855	24.3	.4830	- 2.1	.2977	- 5.2
n = 2.5	.2658	5.8	.4588	3.0	.3187	- 10.3	.0947	- 51.5	.0769	31.9	.4879	- 3.1	.3037	- 7.3
Decay case	Cv & C		Cv & C		C		C & T (Concentric)		T		Cv & T		Cv & T	

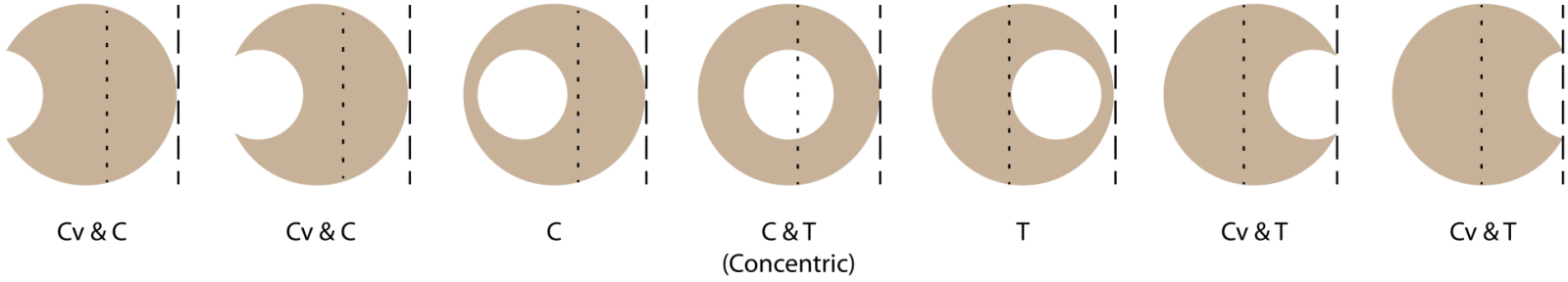

Figure 5.11: Illustration for the decay cases mentioned in Table 5.2. Dotted and dashed lines are for neutral axis and tension face representations (for n=1.10), respectively, for the cross-sections.

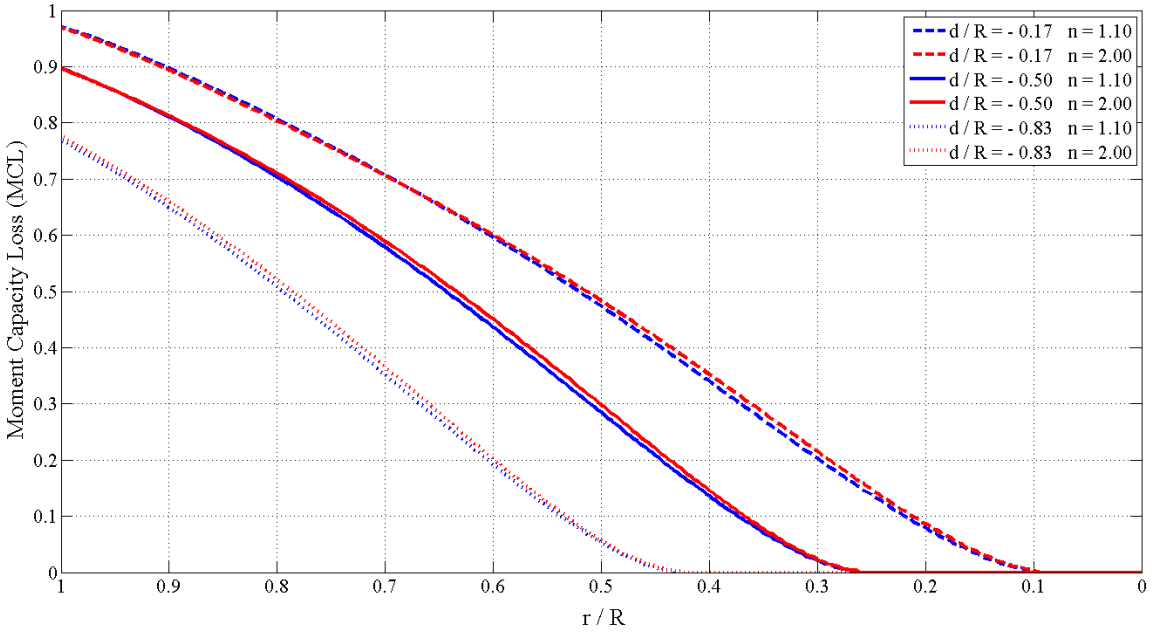

Figure 5.12: Effect of n (1.1, 2.0) on MCL for three values of d/R (-0.17, -0.50, -0.83).

Table 5.2 presents specific values of moment capacity loss for r/R = 0.50 and several values of d/R and n. The second column in each of the cells corresponding to a given d/R indicates the percent difference in moment capacity loss from the value calculated using n=1.0. The disparity between predicted MCLs assuming different values of n from the baseline of n=1.0 varied depending on the value of d/R. For values of n up to 1.4 the differences in MCL do not exceed 4% except for two notable cases of d/R corresponding to concentric and nearly concentric decays. These results suggest that incorrect assessment moment capacity loss will be limited for most situations, unless n is much larger than 1.0 particularly for cases where decay is nearly concentric. It should be noted, however, that cases where the percentage differences are high also correspond to cases where MCL is lowest (less than 12%), so the practical impact of these differences would be quite limited and perhaps negligible.

5.3.3 Assessment of Decay Shape on MCL

Although decay in trees can sometimes adopt an approximately circular or other areas with simple geometry, decays mostly form in irregular shapes (Shigo 1984) and the extent of decay can vary by tree species and presence of fungus (Deflorio et al. 2008). Two methods can be used to estimate MCL of such decayed stems using the curves developed in this dissertation. The first method can be used without excessive calculations, making it suitable for use in the field. The second method requires a more careful accounting of the area and location of decay.

5.3.3.1 Method I

An irregularly-shaped area of decay can inscribe and be inscribed by circles. For example, Figure 5.13 shows a rectangular-shaped decay, but the method can be applied to any other decay shape. The moment capacity loss (MCL) can be determined from Figures 5.6 and 5.8, assuming r and d for the smaller and larger circles. Three estimates of MCL could be obtained using the larger circle, the smaller circle, and a mean value. Depending on the loading conditions (sheltered or exposed trees, for example) or other factors related to risk assessment (such as value or importance of the affected structure), the smallest of largest estimate of MCL could be employed. This approach may offer an advantage over the method described by Mattheck et al. (1994), who suggested using the thinnest remaining wall of sound wood when assessing off-center areas of decay, which tended to over-estimate the loss in I of such stems (Kane and Ryan 2004).

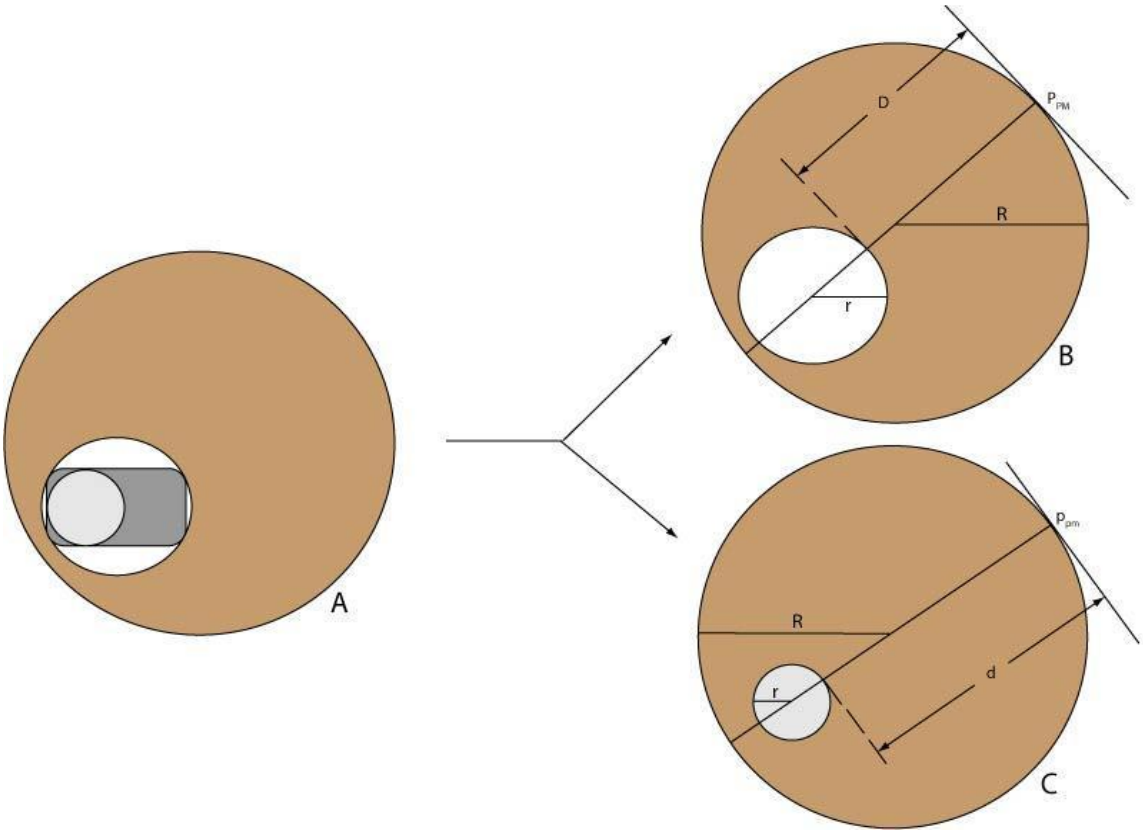

Figure 5.13: Approach for non-circular decay areas (Method I). Actual decay is shown in part-A as a rectangular shaded area. B shows the larger circle inscribing the decay region; C shows the smaller circle inscribed by the decay area. R, r, d, and P_{PM} were described in Figure 5.1.

5.3.3.2 Method II

In this method, an irregularly-shaped area of decay can be converted into an equivalent circle as in Figure 5.14. The irregularly-shaped area of decay and its circular equivalent must share the same centroid and have the same area. The MCL of the section can be determined from Figures 5.6 or 5.8, as appropriate, using the equivalent circular decay area. For simple geometric shapes, like a rectangle, this method can be applied simply because to the equivalent area and its centroid can be found with ease. For

irregularly-shaped areas, determining the area and centroid requires more careful analysis, but could be done using image-analysis software. For practitioners, images can be gleaned from tomography (Gilbert and Smiley 2004, Wang and Allison 2008). The main drawback of this method is that it requires sophisticated tools and techniques, but the results are anticipated to be more precise.

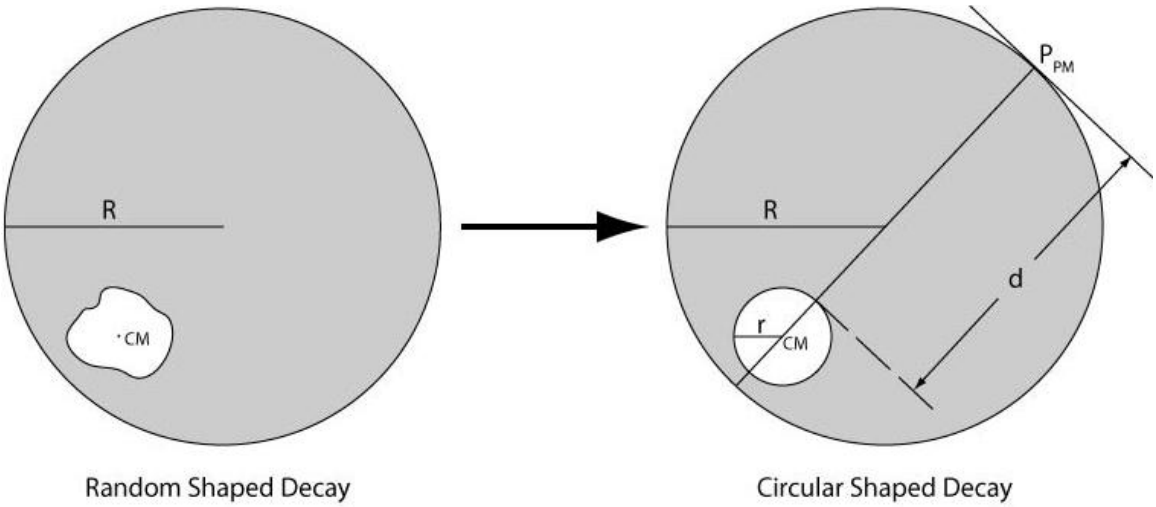

Figure 5.14: Approach for decays with irregular shape (Method II). The irregular decay is converted into an equivalent circular shaped decay. CM refers to the geometric center of the decays. R, r, d, and P_{PM} have already been described in Figure 5.1.

5.3.4 Comparison of the Results with the Experimental Results

To validate the method to calculate MCL, theoretically- and empirically-determined values of $LOSS_{SM}$ in tension side of tree cross-sections were compared for 10 trees tested by Kane (unpublished data). In each case the theoretical MCL was computed using two different values of n (1.10 and 2.00) considered to be within extreme practical limits. Theoretical predictions are not significantly different to empirical values for the values of n used in the theoretical approach (Table 5.3). MCL for each tree is predicted

with reasonable accuracy by using one of the two n values. In some cases both provide equally good estimates. There was no correlation between the magnitude of difference between empirically- and theoretically- determined values of $LOSS_{SM}$ for n = 2.00 (R^2 = -0.12 and p = 0.93 which could be calculated in SAS statistical software from SAS Institute Inc. at Cavy, NC) or n = 1.10 (R^2 = -0.04 and p = 0.43 by SAS statistical software from SAS Institute Inc. at Cavy, NC). Statistically, R^2 is the coefficient related to the goodness of fit of the regression analysis between the theoretical and empirical $LOSS_{SM}$, p is about how many chances the fitted relation between the empirical and theoretical $LOSS_{SM}$ values cannot be explained by all the empirical and theoretical data. Thus, R^2 and p for different n values, as well as the similar number and magnitude of positive and negative differences, suggests that differences were random rather than systematic. Differences were presumably due to assumptions used to derive the theoretical values of $LOSS_{SM}$ such as perfect circular areas for stem, values of n, and homogenous material properties within the compression and tension sides of the stem.

Measurement error may have also contributed to the observed differences. Diameter of trees was measured outside the bark, and it was assumed that a) bark thickness was 2 cm for all trees and b) bark was assigned a null value for E. From a practical standpoint, the highest difference is important because it reflects the degree to which an assessor might over- or under-estimate the loss in moment capacity of a tree. Using n = 1.10, the two greatest differences of 8.6% and 9.8% were nearly twice that of the two greatest differences obtained using n = 2.00 (Table 5.3). The standard deviation of the differences was also greater when using n = 1.10 compared to n = 2.00 (Table 5.3).

For large and open-grown red oaks, n is probably closer to 2.00 than 1.10, which explains the better results obtained when using n=2.00.

Table 5.3: Comparison of empirical and theoretical values of $LOSS_{SM}$; the difference was calculated by subtracting theoretical from empirical values of $LOSS_{SM}$.

n	NA	2.00		1.10	
Tree #	Empirical LOSSSM (%)	Theoretical LOSSSM (%)	Magnitude Difference (%)	Theoretical LOSSSM (%)	Magnitude Difference (%)
29	6.4	6.2	0.2	12.1	- 5.7
30	86.7	88.8	- 2.1	92.2	- 5.5
32	81.4	75.7	5.7	82.0	- 0.6
34	15.1	13.0	2.1	16.8	- 1.7
35	20.5	19.4	1.1	25.9	- 5.4
36	22.3	21.6	0.7	17.4	4.9
37	18.8	15.4	3.4	9.2	9.6
40	12.3	9.9	2.4	5.6	6.7
86	37.8	43.3	- 5.5	46.4	- 8.6
89	32.5	34.7	- 2.2	28.4	4.1
Mean	33.38	32.80	0.58	33.60	- 0.22
STD	28.24	28.52	3.20	30.57	6.20

5.4 Concluding Remarks

The critical MCL of any decayed cross-section can be approximately computed by using methods I and II and Figures 5.6 and 5.8. Similarity between a) theoretically- and empirically-determined values of $LOSS_{SM}$ and b) MCL values calculated for different values of n lends confidence that these methods can be reasonably applied under a variety of field conditions. Three limitations regarding applicability of the methods presented in this chapter are (1) neglecting axial stresses induced by dead load and the vertical component of the pulling tests; (2) altered E values of wood formed after wounding, and (3) neglecting wind-induced deflection of trees, which generates an additional moment due to the weight of the deflected crown (Peltola 2006). The third limitation has a greater effect on excurrent than decurrent trees (Kane and Ryan 2003). Another important limitation to the application of values of moment capacity loss in Figures 5.6 and 5.8 is that failure will not necessarily occur at the location of the critical MCL. Other defects (such as weak branch attachments or poor root anchorage) may fail prior to parts of the tree with decay.

While maximum moment capacity of trees has not been directly addressed in this chapter (MCL values are relative), the methods described can be used to estimate it. Following a storm, failed and intact branches and stems with decay could be measured to determine whether a threshold value of critical MCL existed. Previous attempts to find a threshold (Mattheck et al. 1993, Mattheck et al. 1994) have been problematic (Gruber 2008, Fink 2009), so care must be taken in sampling and analyzing such data. For instance, after using enough data in order to obtain a distribution related to tree failures and their critical MCL, the first and the second moments (mean and standard deviation)

of this distribution can show and give insight about the hazard of trees failing due to bending generated by wind forces.

Risk assessment of trees determined in Chapter 4 could be expanded to trees with decays. Fragility curves obtained by using the probability of exceedance theory were based on moment capacity of the cross-sections of the trees subjected to dynamic random wind loading. To obtain the fragility curve for a decayed tree, the critical moment capacity can be estimated by using the results of Chapter 5. Then, the methodology in Chapter 4 can be applied.

CHAPTER 6

EFFECTS OF CROWN ARCHITECTURE AND WOOD PROPERTIES ON TREE DYNAMICS

6.1 Introduction

A better understanding of the effect of crown architecture and wood properties on large, open-grown tree dynamics will help reduce the risk of failure of such trees, which can damage property and injure people. In the United States, from 1995-2007, 407 people died as a result of wind-related tree failures (Schmidlin 2009), and litigation often accompanies property damage and personal injury (Mortimer and Kane 2004).

Dynamic behavior of trees can be affected by geometric (e.g. mass distribution and cross-section along tree structures) and material (e.g. density, viscous damping and modulus of elasticity of species) properties of the trees. Thus, it is possible to find several studies focused on the effects of these properties on tree dynamics experimentally (Baker 1997, James et al. 2006, Kane and James 2011) or theoretically (Sellier and Fourcaud 2005, Moore and Maguire 2005, Sellier et al. 2006, Spatz et al. 2007, Rodriguez et al. 2008, Sellier and Fourcaud 2009).

Empirical studies (Baker 1997, Moore and Maguire 2004, Kane and James 2011) have demonstrated the effect of crown form on natural frequency of open-grown trees. Baker (1997) showed that the natural frequency of deciduous open-grown trees is inversely proportional to diameter at breast height (DBH). Then, Moore and Maguire (2004) state that the natural frequency of trees in forest has a linear relationship with the ratio of DBH to the square of tree height (DBH/H^2). In contrast to Moore and Maguire

(2004), predicting natural frequency of individual trees from the ratio, DBH/H^2 proved problematic Kane and James (2011).

Previous theoretical studies have investigated the effects of tree crown structure on only the natural frequency and damping ratio for trees. In multiple degree-of-freedom systems (MDOF), such as trees, higher frequencies may be as important as the fundamental frequency. The main difference between the research of Sellier and Fourcaud (2009) and other theoretical studies is their methodology. To describe the dynamic response of trees, Sellier and Fourcaud used the dynamic amplification factor for a specific harmonic wind frequency as a broader indicator of dynamic response instead of just natural frequency and damping ratio. A limitation of their research, however, is that a specific wind frequency was used in their analyses. The current research therefore employs a total of 38 different wind frequencies for application to different tree models (parametric models). These parametric models were developed by applying changes on selected several geometric and material properties (stem diameter, damping ratio, elastic modulus, and the number, slenderness, height, azimuth, and attachment angle of branches) of the base model, M100, which was described in Chapter 3. Then, by analyzing the dynamic amplification factor of each model varying with wind frequency, the relationship between branches and stem could be investigated to state some comments for, especially, arborists in order to reduce tree failures subjected to wind forces.

Additionally, the theory of the mass participation factor and its applications on branches will be addressed in Section 6.3, because this factor is important to examine

some of the model results. This factor has not been mentioned in detail by the authors studied on trees.

6.2 Parametric Models

All the parametric models were based on the prototype tree model, M100, as described in Chapter 3. To investigate the effect of tree morphometry on Rd, each of eight parameters (stem diameter; damping ratio; MOE; and the number, height, attachment angle, azimuth and slenderness ratio of branches) was varied independently, holding the other parameters constant. A nomenclature was created to represent all the parametric models, in which the second digit refers to the number of the parameter being varied and the third digit refers to the variation of the parameter. For example, models M111, M112, M113, and M114 are the four variations of the first parameter; M121 and M122 are two variations of the second parameter, and so on. Parameters were varied in accordance with reasonable expectations for open-grown sugar maples in the northeastern USA.

6.2.1 Parameter 1 – Stem Diameter

The effect of stem diameter was examined by multiplying the stem diameter of M100 by 1.25, 1.50, 1.75, and 2.00, which increased the stem diameter to 66, 79, 93, and 106 cm in models M111, M112, M113, and M114, respectively. Trees of smaller diameters were not modeled because it was intended to investigate large trees that posed a greater risk of damage if they failed. To maintain a realistic taper of the stem, the

diameter of the top branch (the axial extension of the stem) was also increased by the same factors in these models as can be seen in Figure 6.1.

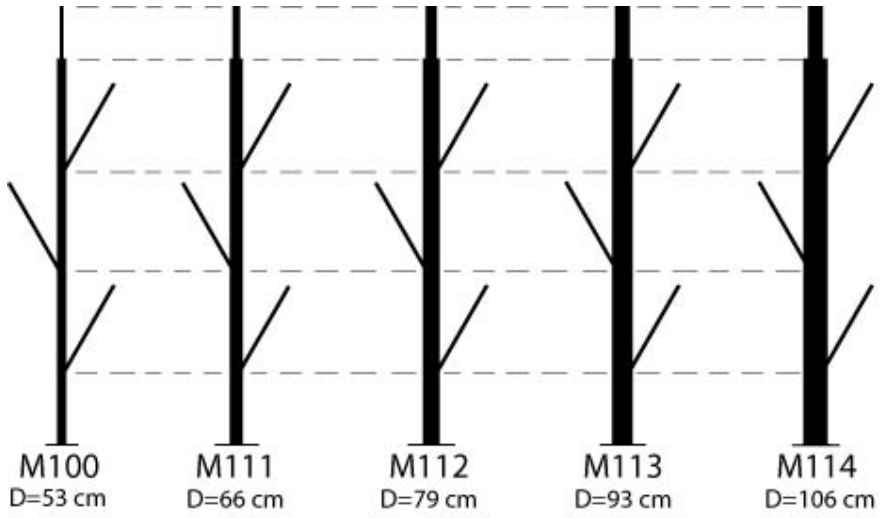

Figure 6.1: Illustration of models M100, M111, M112, M113, and M114, where the parameter varied is the stem diameter.

6.2.2 Parameter 2 – Slenderness Ratio of Branches

Branches on M100 were assumed to have a slenderness ratio of 50. This value was selected because it represented the mean slenderness (rounded to the nearest ten) of branches the diameter of which was at least 10% of stem diameter on M100. Only larger branches were considered because it was expected that more massive branches would exert a greater influence on Rd because of their larger mass participation in the overall dynamic response (Eq. 6.1). As shown in Figure 6.2, slenderness was changed to 60 and 40 in models M121 and M122, respectively. These values represented the mean slenderness (rounded to the nearest ten) of branches the diameter of which exceeded the

median and upper quartile diameters, respectively, on M100. Slenderness ratio was changed by altering branch length while keeping branch diameter constant.

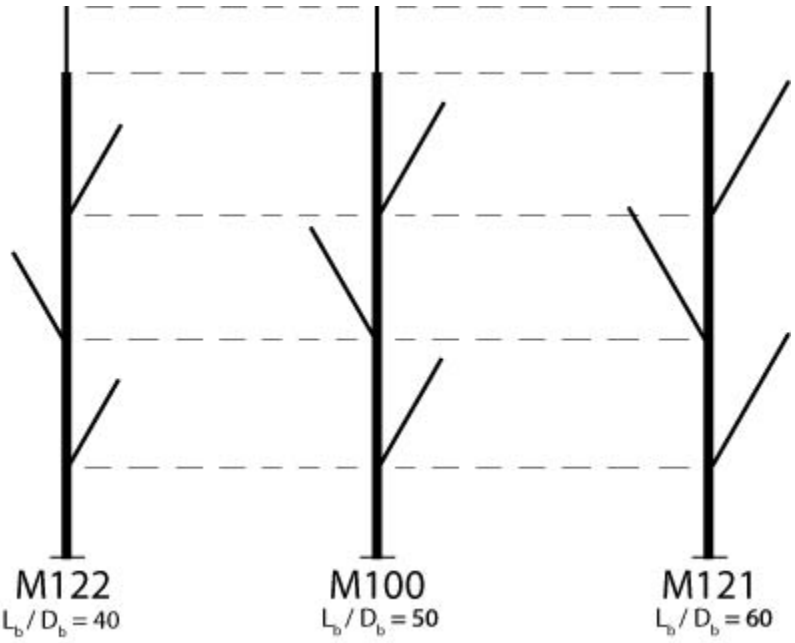

Figure 6.2: Illustration of models M122, M100, and M121, where the parameter varied is the slenderness ratio of the branches.

6.2.3 Parameter 3 – Number of Branches

The number of branches on the tree was varied as follows (Figure 6.3): model M130 included only the stem and the "top branch," the axial extension of the stem. Subsequent models added individual branches (see Table 3.1): models M131, M132, M133, and M134 added the first; first and second; first, second and third; and first, second, third and fourth branches of M100, respectively. Branches were added beginning with those closest to the ground because the first three branches had comparatively larger diameters while the fourth was of smaller diameter. This approach facilitated a

comparison of the effect of branch mass on Rd. In addition to these models, M131-7 included just the top and seventh branches. The seventh branch is the largest by diameter. The attachment height of the seventh branch was nearly twice as great as that of the first branch, so this model made it possible to investigate the effect of the spatial distribution of mass on Rd.

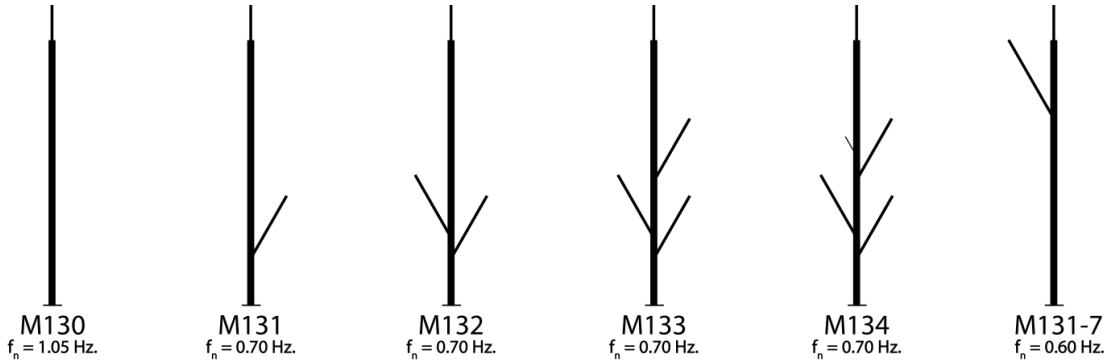

Figure 6.3: Illustration of models M130, M131, M132, M133, and M134, where the parameter varied is the number of the branches.

6.2.4 Parameter 4 – Damping Ratio

The effect of damping was examined by increasing the damping ratio from 0 to 0.15 with the following values: 0, 0.01, 0.05, 0.10, and 0.15. The range was chosen in accordance with the maximum measured value from pull and release test on M100 and values similar to those previously reported for deciduous trees (Roodbaraky et al. 1994, Kane and James 2011).

6.2.5 Parameter 5 – Branch Attachment Heights

To assess the effect of the branch attachment heights, branch attachment height was increased (M151) and decreased (M152) by 0.5 m simultaneously for all branches. These models were expected to serve as a comparison to models in which branches were added, because of the consistent change in the location of mass distribution along the stem.

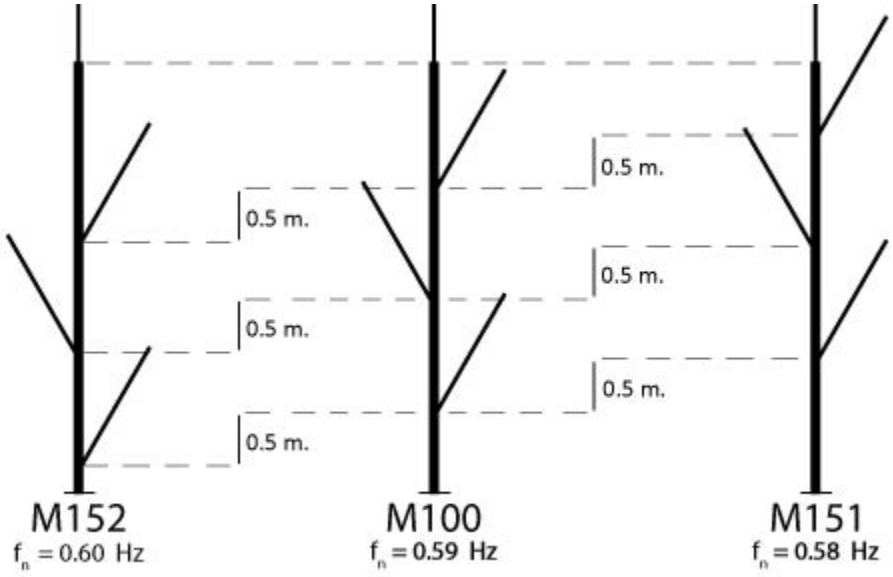

Figure 6.4: Illustration of models M152, M100, and M151, where the parameter varied is the branch attachment heights.

6.2.6 Parameter 6 – Branch Attachment Angles

In addition to a model using measured branch angles of the maple tree from which M100 was constructed, parametric models were also developed assuming constant branch angles of 70º, 60º and 50º for M161, M160, and M162, respectively, as illustrated in Figure 6.5. These attachment angles were selected because it was observed that many

branches on the prototype sugar maple curved upwards beyond their attachment to the stem. It means that these angles of the models, M100, M161, and M162 are approximately for the representation an average of where the branches on the actual tree pass through. It was not possible to measure the angle of the branch relative to its center of mass. Discussion of results shown in Figure 6.13, presented in section 6.3.6, demonstrate that a constant angle assumption was reasonable since results do not depart significantly from the response of M100.

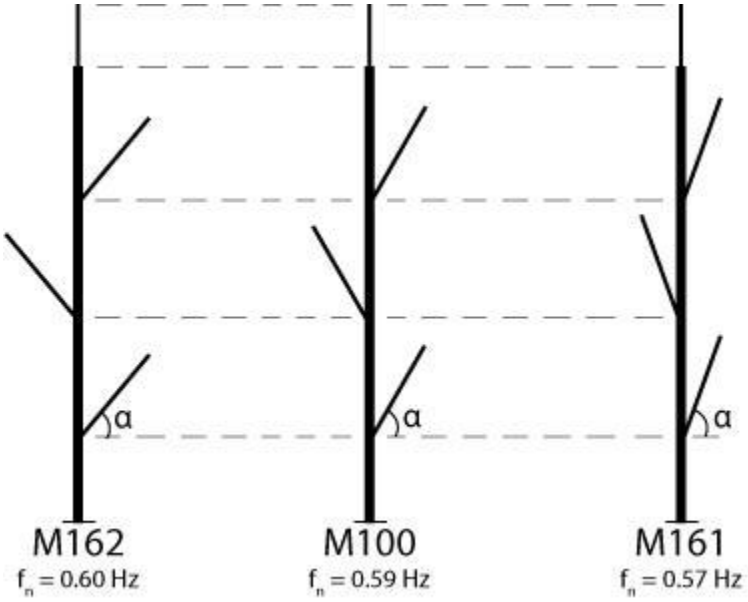

Figure 6.5: Illustration of models M162, M100, and M161, where the parameter varied is the branch attachment angles.

6.2.7 Parameter 7 – Branch Azimuth Angles

The effect of wind directionality was investigated by varying the branch azimuth angle (Figure 6.6) instead of changing the direction of wind forces. Models M171,

M172, and M173 increased the azimuth of each branch by 30, 60, and 90 degrees relative to their measured azimuth in M100.

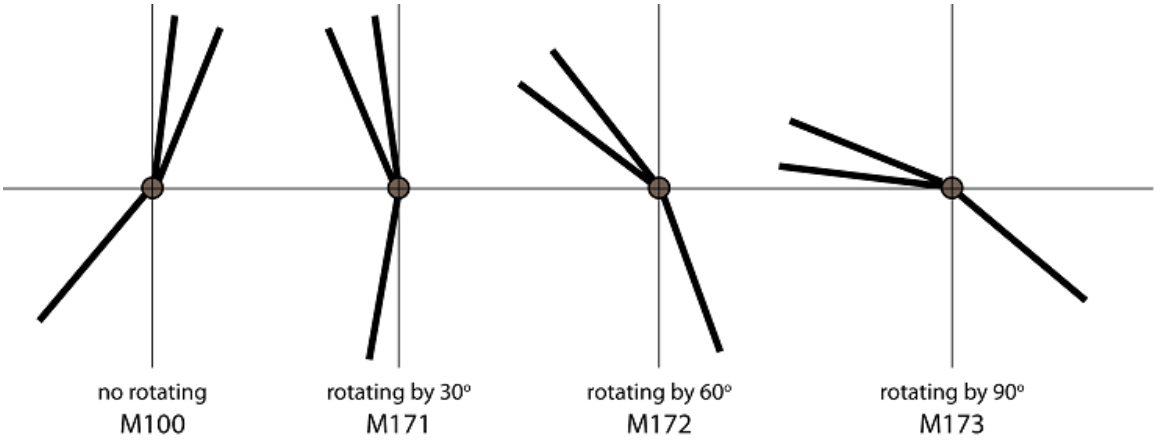

Figure 6.6: Illustration of models M100, M171, M172, and M173, where the parameter varied is the branch azimuth angles.

6.2.8 Parameter 8 – Modulus of Elasticity (MOE)

Two models were created to investigate the effect of varying MOE for the branches and the stem. In M181, MOE of the stem and branches was set to the constant value of 6.53 GPa, which was the mean MOE of all elements in M100, weighted by the mass of each element. In M182, MOE of each element of the stem was set to 9.0 GPa, the weighted mean of MOE of stem elements in M100; MOE of each branch element was set to 4.99 GPa, the weighted mean of MOE of all branch elements in M100.

6.3 Theory of Mass Participation and its Application on M100

In civil engineering (or earthquake engineering), Eq. 6.1 is a common formula to calculate the total static shear force on the basement of buildings. For simplification to

apply Eq. 6.1 and to see the effect of branch mass on tree trunk behaviors, it can be assumed that each branch mass is a lumped mass (m_j in Eq. 6.1) on trunks. According to this equation, the shear forces (s_{jn} in Eq. 6.1) on the attachment of branches depend on the mass of these branches, separately. Therefore the largest branches (7th, 1st, 3rd and 2nd branches, in descending order of diameter) in Table 3.1, which have the important portion of the total mass of the whole tree, cause great shear forces on the attachment points of these branches on the trunk. Those great forces cause greater displacement and greater Rd of the trunk.

$$V_{bn}^{st} = \sum_{1}^{N} s_{jn} = \sum_{1}^{N} \Gamma_n m_j \phi_{jn} \tag{6.1}$$

where Γ_n is the modal participation factor of the nth mode (Chopra 2007), m_j is the mass of the jth lumped mass and ϕ_{jn} is the nth-mode shape at the location of the jth lumped mass. Additionally, the modal participation factor (Γ_n) has the modal mass (M_n) of the total system at the denominator of its formula. Thus, the ratio of m_j in Eq. 6.1 to the modal mass (M_n) will be called mass participation of a branch or branches.

6.4 Results and Discussion

Again, as in Chapter 3, the parametric model results were evaluated through changes in the dynamic amplification factor, Rd, in order to characterize the dynamic response using a uniform approach. Effects of each parameter on the dynamic response of the base model (M100), which was described in Chapter 3, can be examined by comparisons and discussions on the Rd factors of each parametric study in the following sections (from 6.4.1 to 6.4.8).

6.4.1 Effects of Parameter 1 – Stem Diameter

Figure 6.7 shows Rd plotted with respect to wind frequency for M100 and models of trees with greater stem diameter. The plot can be divided into three regions, identified by ovals. The left-hand oval marks the region where the first peaks of the Rd curves occur. The first peaks reflect the first modal frequency of several large branches (see Table 3.1 for M100 values). Peaks in the center oval reflect the natural frequency of the top branch in the models. Peaks in the right-hand oval reflect the natural frequency of the stem in each model, although the peak that belongs to the stem natural frequency of M100 is not visible because of its small mass participation when using a 15% damping ratio. The first modal frequencies of the stem and top branch in each model are listed in Table 6.1.

Peaks in Figure 6.7 that coincide with natural frequencies of different branches (left-hand and center ovals) and the stem (right-hand ovals) are consistent with the mass participation of different elements in the tree. As the diameter of the stem and top branch increased, their mass participation increased, which explained why Rd of models of greater stem diameter decreased in the left-hand oval, but increased in the center and right-hand ovals. This finding is consistent with mass-induced damping (James et al. 2006) at selected frequencies. The frequency at which Rd was maximum increases in the center and right-hand ovals because of increased diameter and hence mass participation at these frequencies.

Table 6.1. Diameter and estimated first modal frequencies of the stem and top branch in models shown in Figure 6.7.

	Stem		Top Branch	
Model	Diameter (m)	Frequency (Hz)	Diameter (m)	Frequency (Hz)
M100	0.53	2.50	0.13	1.05
M111	0.66	3.00	0.16	1.20
M112	0.79	3.50	0.20	1.45
M113	0.93	4.00	0.23	1.70
M114	1.06	4.50	0.26	1.85

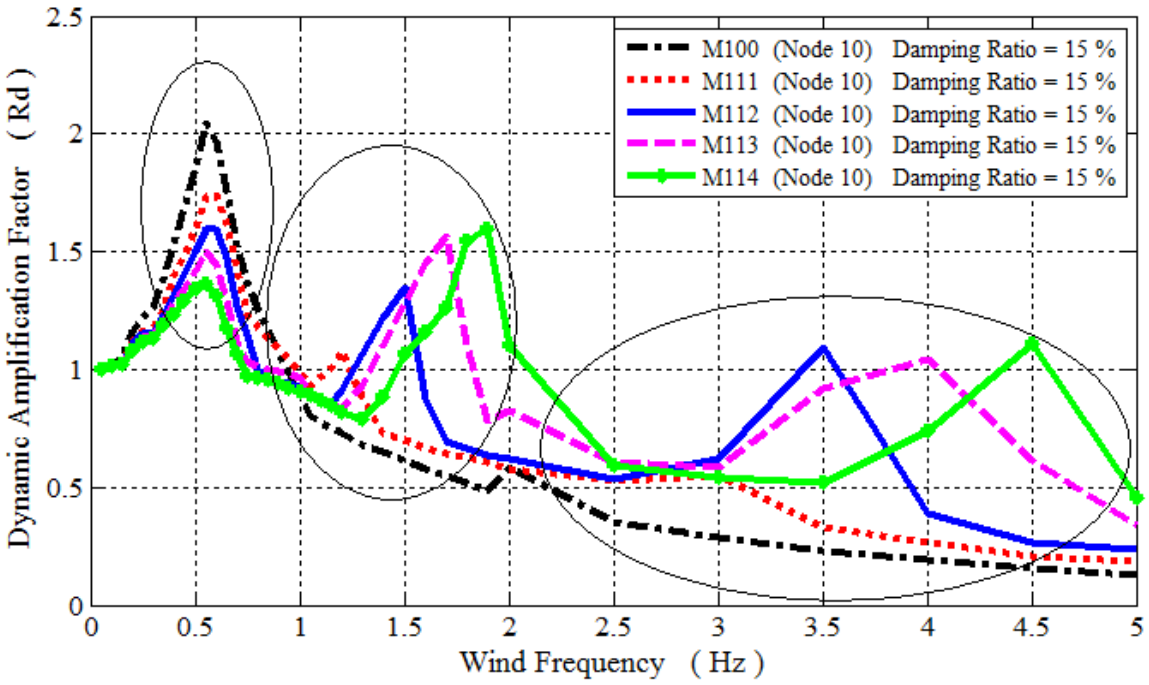

Figure 6.7: Dynamic amplification factors with respect to wind frequency for the selected models (M100 dashed and dotted line; M111 dotted line; M112 solid line; M113 dashed line; M114 solid line with the star (*) marker). Node 10 is one of the nodes on the main stems at the breast height (1.4 m).

The difference between decurrent (large branches with respect to stem) and excurrent (small branches with respect to stem) forms can be observed by changes in Rd induced by changes in stem diameter. Thus, it may be thought that the Rd factors of excurrent trees and decurrent trees must behave like M114 and M100, respectively. The decreasing of the Rd peaks in the left oval is consistent with findings from Sellier and Fourcaud (2009), who indicated that decreasing the diameters of primary branches in excurrent Maritime pine causes a decrease of Rd.

6.4.2 Effects of Parameter 2 – Slenderness Ratio of Branches

Changes in slenderness ratio were introduced by changing the length (and, consequently, the mass) of branches, which altered natural frequency of the branches as expected from the dynamics of a cantilever beam with uniformly distributed mass and elasticity:

$$f_n \propto \sqrt{\frac{\dot{E}I}{\dot{m}L^4}} \tag{6.2}$$

where Ė is the distributed elastic modulus, I is the moment of inertia, and ṁ and L are the distributed mass and length, respectively, of the cantilever beam. As branch slenderness decreased, Rd increased (Figure 6.8) because the natural frequency of larger branches became closer to the natural frequency of the stem and top branch of M100 (Table 3.1), which had slenderness ratios of 24 and 33, respectively.

Changing the length of primary and secondary branches by equal magnitudes altered Rd of a maritime pine (Sellier and Fourcaud 2009), but the magnitude of change of Rd was not as large as in the current study. This presumably reflects the effect of large

diameter branches in M100, as well as Sellier and Fourcaud's (2009) single excitation frequency not being near the natural frequency of the tree. Sellier and Fourcaud (2009) did predict reduced Rd for greater stem slenderness, however, which is consistent with the result for branches of M100. A more accurate accounting of slenderness of decurrent trees of different species would help improve predictions of Rd.

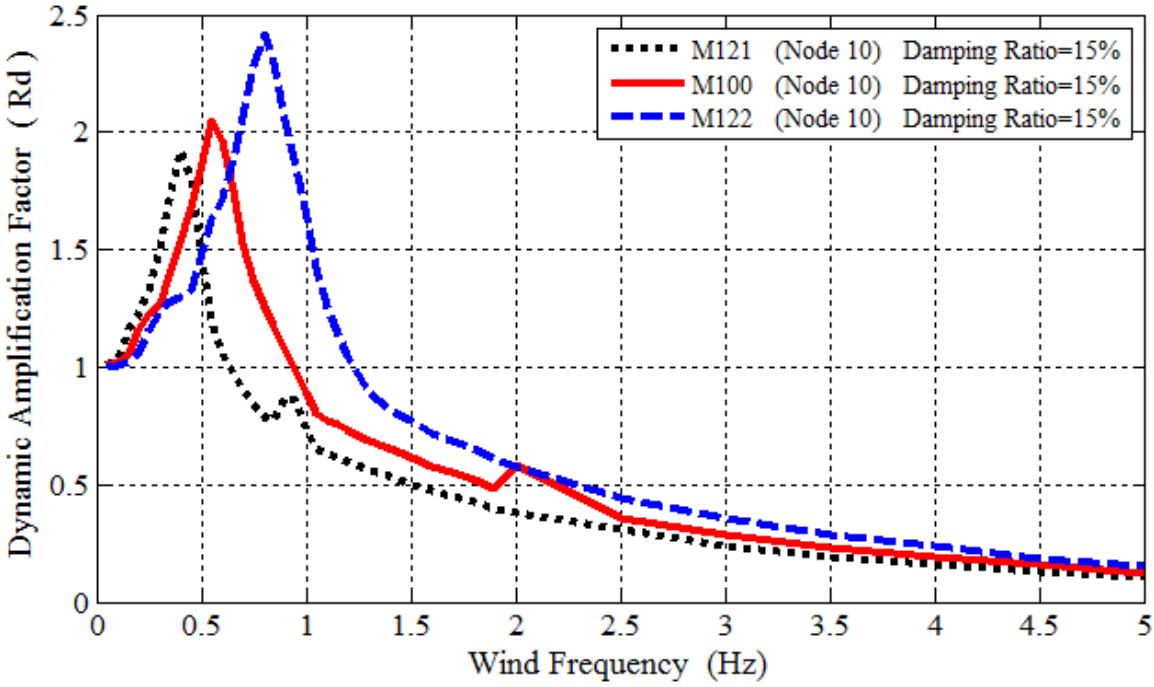

Figure 6.8: Dynamic amplification factors with respect to wind frequency for the selected models, M121, M100 and M122.

6.4.3 Effects of Parameter 3 – Number of Branches

Results from adding branches on Rd again can be explained by understanding mass participation of different elements in the system. The addition of branches of similar natural frequencies increased the magnitude of Rd at an excitation frequency close to the natural frequencies of the branches being added and decreased the magnitude of Rd at

excitation frequencies near the natural frequencies of the stem and top branch (Figure 6.9). Rd of M130 (just the stem and top branch) had maxima at 1.05 and 2.50 Hz, which corresponded to the natural frequencies of the top branch and stem, respectively (Table 3.1). Adding the first branch (M131) added another peak of Rd at 0.65 Hz, close to the natural frequency of the first branch (Table 3.1). Adding the first branch also reduced the magnitude of Rd at 1.05 and 2.50 Hz because (1) the natural frequency of the first branch was not similar to that of either the stem or top branch, and (2) the mass participations of the stem and top branch would decrease in the overall response of the system. This pattern recurred when the second (M132) and third (M133) branches were added. Adding the fourth branch did not meaningfully alter Rd because of the small diameter (thus small mass) of the fourth branch (Table 3.1). Adding the seventh branch to M130 (M131-7) shifted the left-hand peak of Rd to coincide with the natural frequency of the seventh branch. This suggests that the spatial location of mass is less important than mass magnitude because the height of the seventh branch was greater than that of the first branch (Table 3.1). Maxima of Rd associated with the natural frequencies of the top branch and stem are no longer visible when all branches have been added (M100), consistent with mass damping (James et al. 2006) or reduction of mass participations of the stem and top branch.

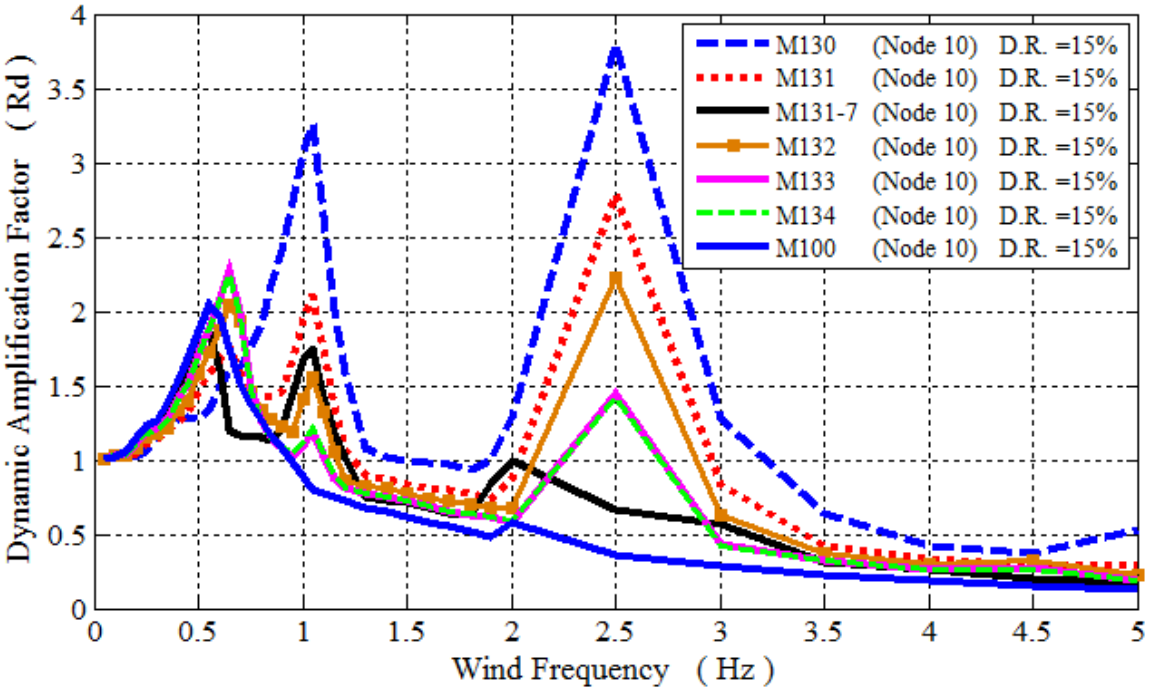

Figure 6.9: Dynamic amplification factors with respect to wind frequency for the selected models, M130, M131, M131-7, M132, M133, M134 and M100. Damping ratio, 15% is represented by DR for each model.

6.4.4 Effects of Parameter 4 – Damping Ratio

Damping in open-grown, deciduous trees derives primarily from aerodynamic drag on leaves (Kane and James 2011) and branch motion (James et al. 2006, Castro-García et al. 2008), but in a forest stand, collisions between branches of neighboring trees also play a role (Milne 1991, Rudnicki et al. 2008). This means that damping ratio can vary significantly among different trees. Thus several different magnitudes of damping ratios were plotted in Figure 6.10 to see the effect of these varying damping ratios on tree dynamics by only using the base model (M100).

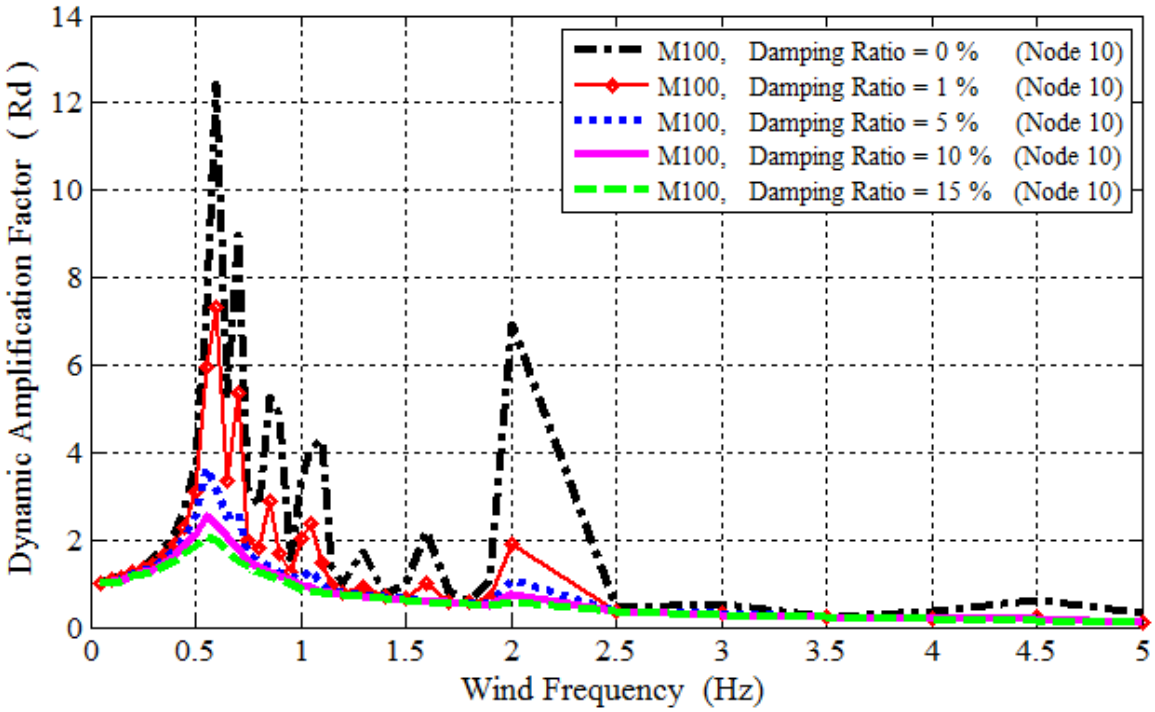

Figure 6.10: Dynamic amplification factors with respect to wind frequency for the base model (M100) with varying amounts of damping ranging from 0 to 15% of critical.

Figure 6.11 shows the variable effect that damping ratio has on dynamic amplification factor of the base model at several specific wind frequencies (0.60, 0.70, 0.85 and 1.05 Hz). These frequencies are the natural frequencies of the seventh branch, second branch, eighth branch and top branch as an example of the largest, large, medium and small sized branches. Although damping ratio affects Rd differently depending on wind frequency, the differences decrease as damping ratio increases. In fact all of the curves asymptotically approach a constant value at damping ratios close to 15%. Therefore damping ratios greater than 15% would not change Rd significantly from the values calculated at a damping ratio of 15%, so higher values were not considered in the parametric studies.

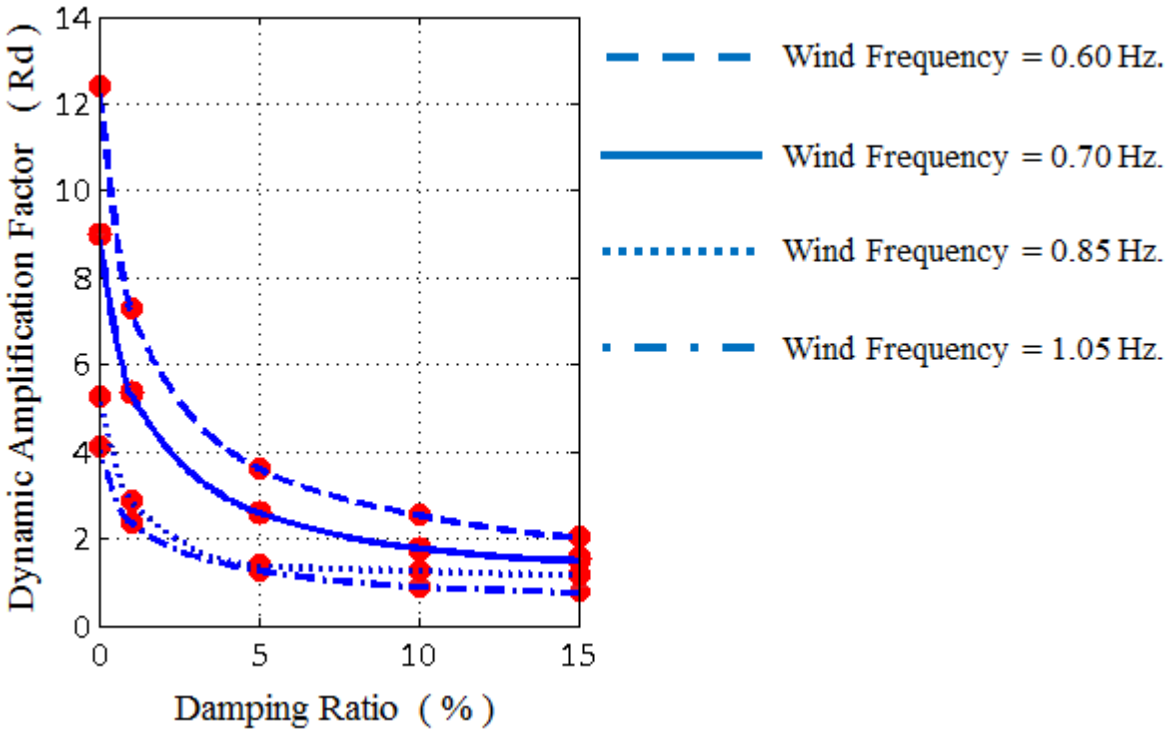

Figure 6.11: Interpolated Rd factors for varying damping ratio at the selected wind frequencies of the base model (M100). The selected wind frequencies are approximately seen in Table 3.1 as the natural frequencies of several branches.

6.4.5 Effects of Parameter 5 – Branch Attachment Heights

Altering branch attachment heights did not have a substantial effect on Rd (Figure 6.12), which was expected. Natural frequencies of the branches would remain the same since the geometry and material properties of branches were not changed, but the natural frequency of the tree would change due to changing the attachment points of branch masses on the main stem (see Eq. 6.1).

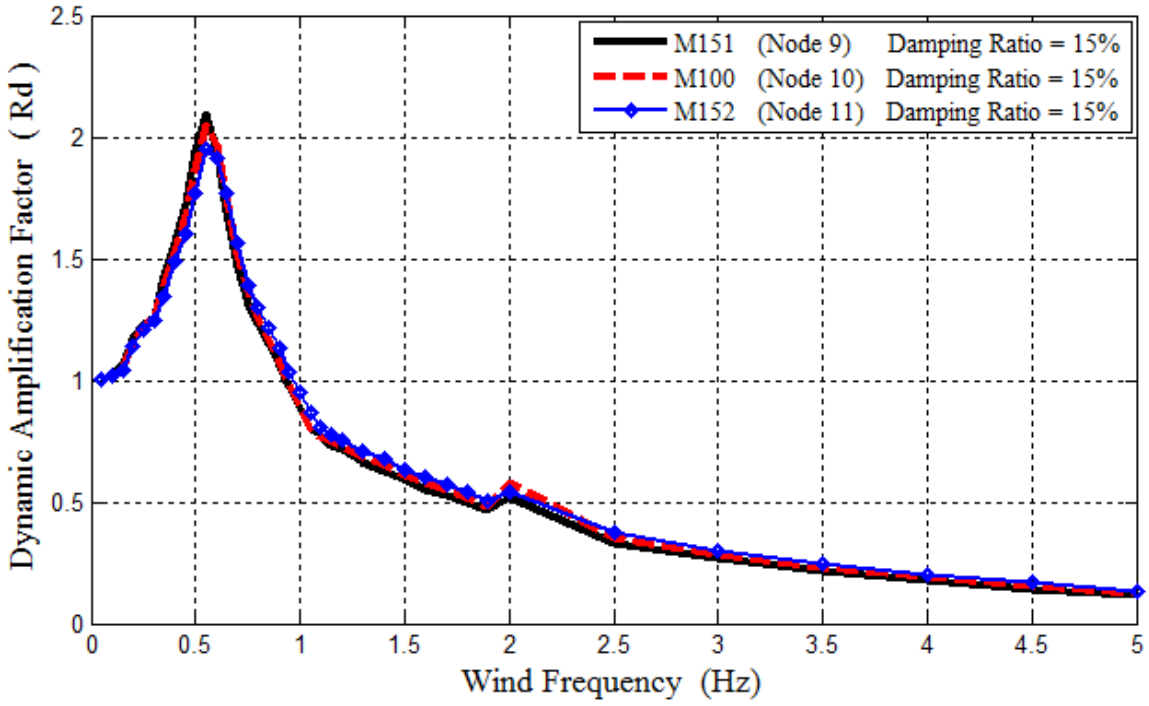

Figure 6.12: Dynamic amplification factors with respect to wind frequency for the selected models, M151, M100 and M152. All the nodes (Nodes 9, 10 and 11) are on the main stems of the models at the breast height (1.4 m).

6.4.6 Effects of Parameter 6 – Branch Attachment Angles

Attachment angle of branches did not have a substantial effect on Rd (Figure 6.13). The plot of Rd versus excitation frequency was similar regardless of whether models included actual angles or average angles. This result is consistent with the similarity between plots of M131 and M131-7, supporting the idea that mass magnitude, rather than its location influences Rd more significantly at a particular frequency. Sellier and Fourcaud (2009) showed a similar magnitude of change in Rd as attachment angles were altered.

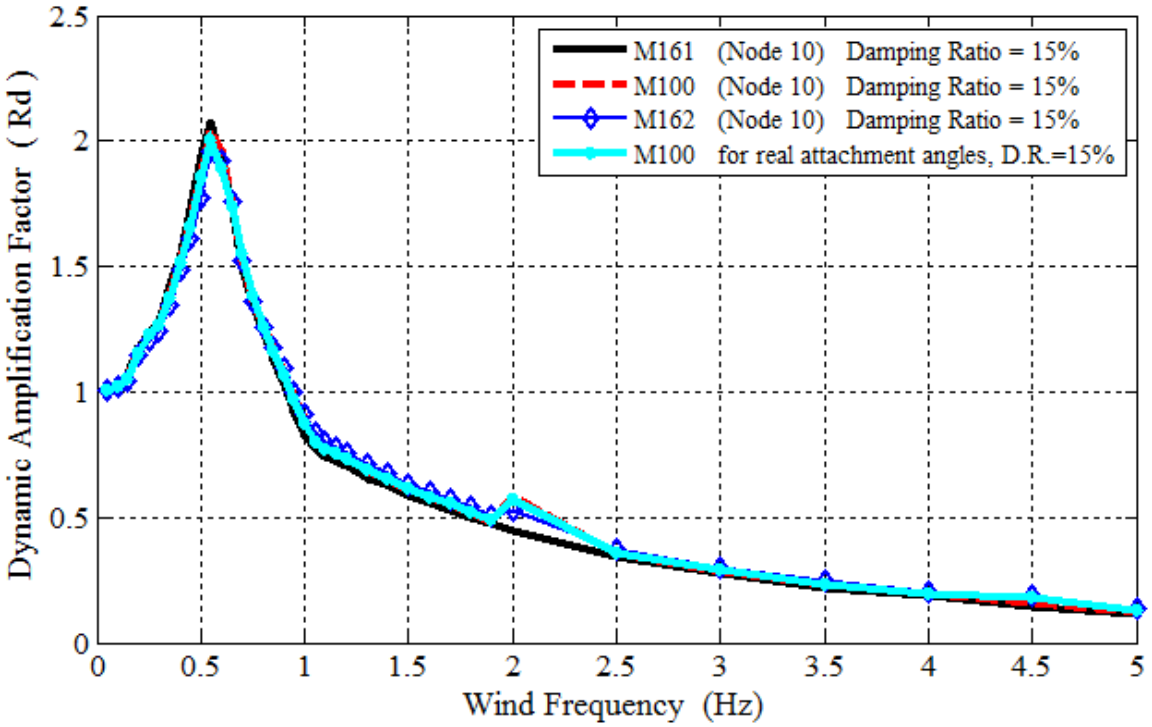

Figure 6.13: Dynamic amplification factors with respect to wind frequency for the selected models, M161, M100 and M162. M100 has been also obtained with the real branch attachment angles for the same damping ratio (DR).

6.4.7 Effects of Parameter 7 – Branch Azimuth Angles

Differences between models M100, M171, and M172 were very small, so Figure 6.14 has been plotted without damping to allow the influence of this parameter to be observed and discussed. This small disparity is consistent with the test results (Kane et al. in preparation).Since the values of the natural frequency from the tests were similar for both directions in which the tree was excited: 0.40 Hz in the north-south direction and 0.42 Hz in the east-west direction. Previous work on conifers has also demonstrated consistent sway frequency, independent of the direction of initial excitation (Milne 1991, Moore and Maguire 2005, Jönsson et al. 2007). The small disparity of the natural

frequencies depending on two orthogonal directions (north-south and east-west) was likely due to elliptical cross-sections of large branches, which would change the stiffness of those branches relative to the direction of sway. Modeling branches with circular cross-sections did not account for such differences, so changing the azimuth angle of branches in the model would not detect the resulting disparity in natural frequency. Future FE models of open-grown trees should account for elliptical cross-sections in branches, which have been observed on some species (Kane 2007).

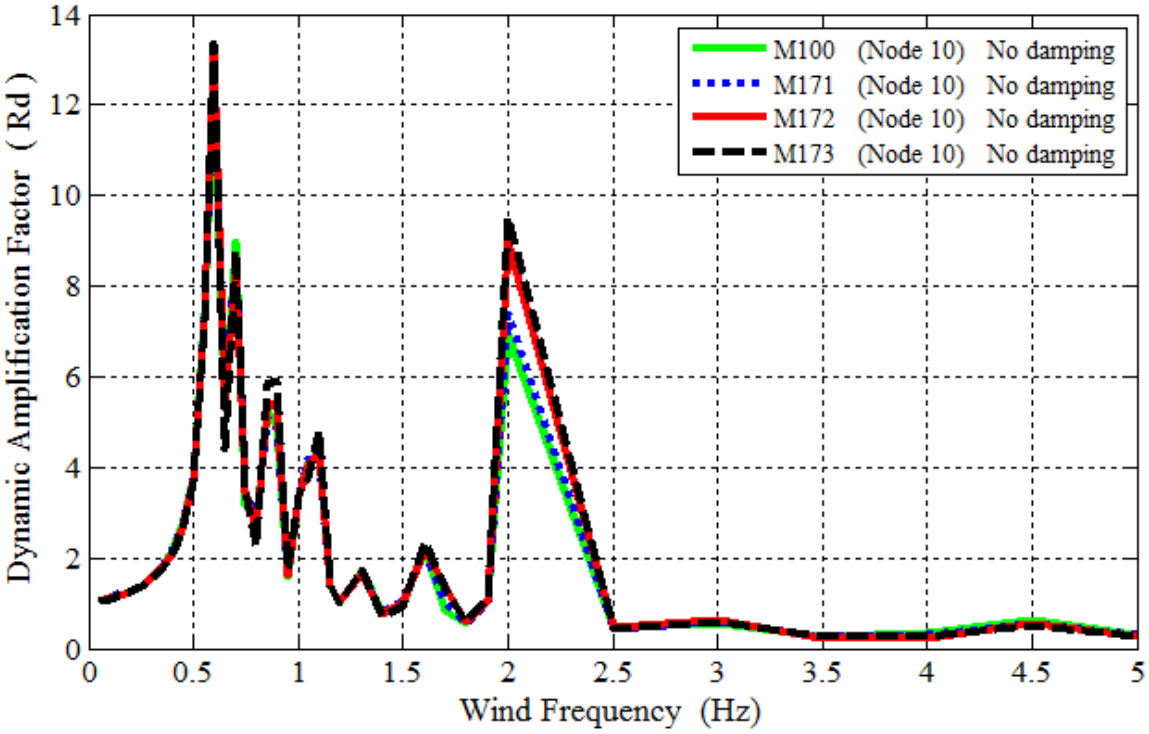

Figure 6.14: Dynamic amplification factors with respect to wind frequency for the selected models, M100, M171, M172 and M173.

6.4.8 Effects of Parameter 8 – Modulus of Elasticity

Assuming a constant MOE for the entire tree (M181) substantially increased Rd (Figure 6.15). This was expected because the fundamental frequency of each element in

the model would be more similar because each element had the same value of MOE (according to Eq. 3.7 and Eq. 3.12). The increase in the frequency at which the maximum Rd of M181 occurred was also expected because MOE of the seventh branch increased. The Rd peak in M100 corresponds primarily to the seventh branch, so with a change in MOE of branch 7, its natural frequency was expected to increase according to Eq. 3.7 and Eq. 3.12.

Assuming different, but constant values of MOE for stem and branches (M182) slightly reduced Rd relative to M100. This result was also expected because there was a greater disparity between natural frequency of the seventh branch and that of the stem and top branch. The excitation frequency at which maximum Rd occurred was slightly less for M182 because the natural frequency of the seventh branch would be slightly less assuming the slightly smaller value of MOE for that branch (see Eq. 3.7).

Previous work has shown that sway characteristics are influenced by MOE of the stem (Sellier and Fourcaud 2009) and branches (Moore and Maguire 2008). In both of these studies, MOE was held constant along the length of the stem and branches. Comparing Rd of M182 with M100 suggests that this was a reasonable assumption. Although there was a large disparity of Rd between M181 and M100, Sellier et al. (2006) assumed a constant value of MOE for the entire tree and their FE model reasonably predicted natural frequency of three small maritime pines. This inconsistency was likely related to the difference in tree size and relative proportion of crown and stem mass of M100 compared to the maritime pines. The results presented here do highlight, however, that trees with co-dominant branches with large mass and different MOE must be modeled with sufficient detail to capture relevant Rd peaks at appropriate frequencies.

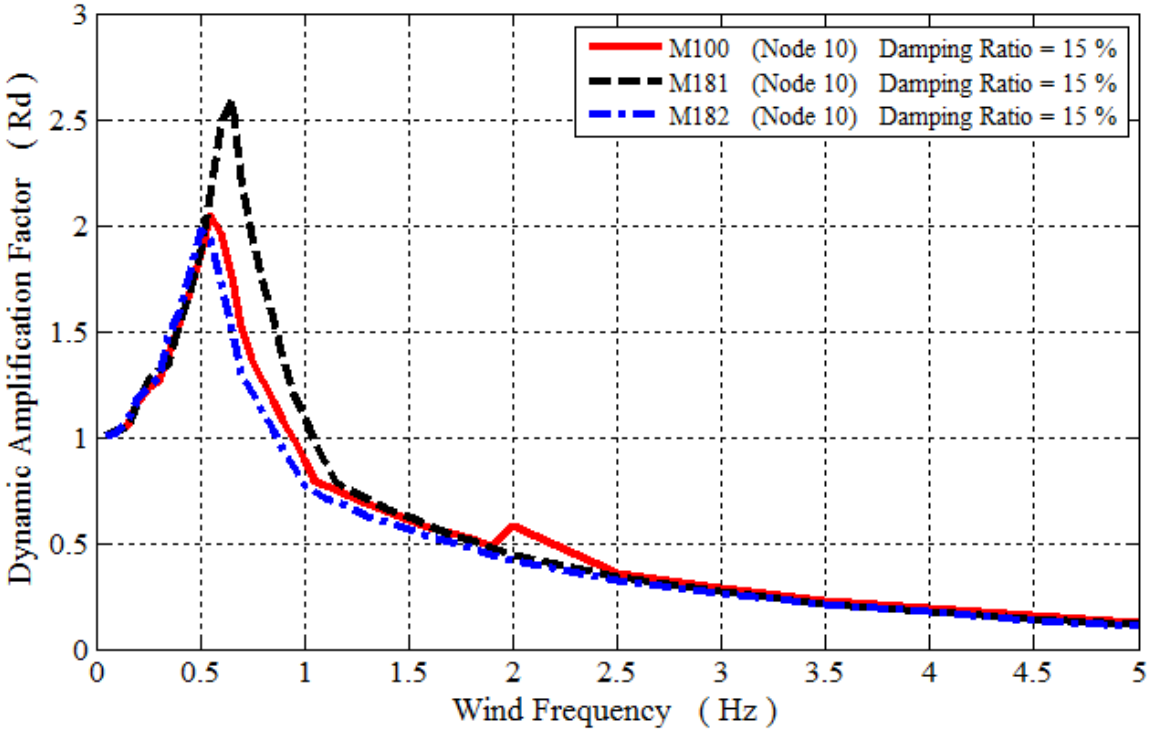

Figure 6.15: Dynamic amplification factors with respect to wind frequency for the selected models, M100, M181 and M182.

6.5 Conclusions for Parametric Analyses

The main parameters that affect the dynamic response of trees were found to be stem diameter, slenderness ratio of branches, number of branches, MOE, and damping ratio. Except damping ratio, each of these parameters changed Rd in accordance with the mass being contributed to the overall response of the models (mass participation, see Eq. 6.1). The effect of large branches on both the magnitude of Rd, and the frequency at which Rd is maximum is clearly important in decurrent trees. Pruning to remove lower branches in the crown of excurrent trees did not substantially alter natural frequency and damping until most of the branches had been removed (Mayhead et al. 1975, Moore and

Maguire 2005). Removing the seventh branch of M100, in contrast, would have removed 18% and 29% of the total tree mass and crown mass, respectively (see Table 3.1).

For decurrent amenity trees, predicting the natural frequency of large branches in the crown has important implications for pruning that warrant additional investigation. For example, removing one large branch from a crown that includes several branches of similar diameter may reduce Rd more effectively than pruning an equivalent amount of mass from several smaller branches. This approach ignores possible physiological and aesthetic constraints on pruning, but a better understanding of the mechanical effects of pruning may lead to alternative approaches to pruning that more effectively reduce the risk of branch or tree failure.

Several assumptions made in constructing the FE models limit the interpretation of the results. Assuming a uniform slenderness ratio for all branches may not be appropriate, and this parameter clearly influenced the magnitude of Rd and excitation frequency at which it was maximum. Assuming uniform attachment angles of branches did not alter Rd relative to using measured angles of individual branches, and the similar responses of models M131 and M131-7 suggest that the amount rather than the location of branch mass is a more important factor affecting Rd. However, future work should more carefully account for the curvature of branches on open-grown trees to better define the spatial distribution of branch mass.

Decay in trees was investigated in Chapter 5 to determine the moment capacity of the decayed trees and in Chapter 4 to show the fragility curves of these decayed trees subjected to wind forces. In addition to ignore the effect of decay in trees on tree dynamics by these chapters, Chapter 6 has not a parametric study on that topic, either. In

the absence of severe weather events, structurally-sound trees typically to do not fail. Trees with decay or poor branch attachments, however, are likely to fail in less severe weather, so including defects on future dynamic analysis to determine Rd would help advance the accuracy and reliability of methods to assess the likelihood of failure of such trees.

CHAPTER 7

CONCLUSION

7.1 Summary

This purpose of this research was organized to reach the answers of the questions mentioned in Section 1.2. Outcomes concluded from the dissertation will be addressed in Section 7.2, after a brief overview of chapter contents. The outcomes of this research are intended to be useful for arborists and urban foresters. Limitations of the research and several suggestions for future works are presented in Section 7.3.

Chapter 2 presents relevant studies and conclusions from existing literature that has been used in this dissertation. In Chapter 3, to the techniques used to model trees have been addressed by using a tree prototype located in Belchertown, MA. Following the modeling techniques presented in Chapter 3, models of two different trees are subjected to varying wind effects in Chapter 4 to obtain fragility curves for the probability of failure of these trees. In Chapter 5, decay effects on these fragility curves have been investigated by considering decreasing the moment capacity of cross-sections of trees due to decays. The effects of different parameters in the dynamic response of trees subjected to wind forces were studied in Chapter 6 to identify those elements that are critical for tree failure reduction that may control.

7.2 Practical Outcomes

The word conducted in this dissertation will serve to provide tools for arborists, urban foresters, and insurance companies that will assist in quantifying risk of tree failure

as a consequence of wind loading. The fragility curves presented in Section 4.5 provide a concise way with which one can evaluate the risk of failure of trees subjected to wind forces. But these fragility curves are not sufficient by themselves to base a decision on whether a tree is hazardous or safe. Other parameters must be considered such as the possibility of decay since fragility curves are dependent on the amount of decay considered as mentioned in Section 4.5. Thus, for arborists, urban foresters or consultants work with insurance companies, one of the most important problems is to find or estimate how much moment capacity loss occurs due to such decays in tree cross-sections. To estimate this moment capacity loss, two methods in Sections 5.3.3.1 and 5.3.3.2 can be utilized with respect to decay shapes. The first method is easiest and practical way for arborists, because they commonly drill tree cross-sections, and they can approximately construct the decay shapes in the cross-sections. For arborists, the second method can be better and more accurate, but requires use of expensive methodologies such as tomography and radar in order to perfectly determine the shapes of the decays. Additionally, the methodology addressed by Sections 4.3 and 4.4 can be extended to the fragility curves with or without decay of different tree species by researchers if needed.

Another important outcome of this Thesis is about pruning trees. For this outcome, the question is to decide how much amount of which branches or maybe stem should be pruned. Thus, firstly, the natural frequencies of all the branches and stem in a tree should be estimated. The most efficient and easiest option is to use Mabie and Rogers' formula mentioned in Section 3.6 instead of doing expensive and time consuming tree models to estimate the fundamental frequencies of the tapered branch and stem in trees. Secondly, by considering the results of the parametric studies addressed by

Section 6.4, when arborists and urban foresters do several changes on crown architecture, tree dynamics will have been changed. For example, they can prune some of the branches in order to obtain a variety for the natural frequency of the members (branches and stem), because this variety can cause reducing Rd factor due to the tuned mass damping and mass participation effects of branches on tree dynamics.

7.3 Limitation and Suggestions

The research results presented in this dissertation are dependent on assumptions that have been described in detail in each of the chapters. For convenience to the reader, some of the most important limitations are again repeated here.

Chapter 3 presented the assumptions used to model a prototype tree using the finite element (FE) method. One of the assumptions used pertained to branch slenderness ratio, assumed equal to 50 for the tree in Belchertown, MA, after which the model was constructed. When slenderness ratio was changed to 60 as was done in Chapter 6 (for model M121), the tree response was more accurately captured as seen by the closer agreement of M121 results to the empirical test results. This assumed parameter plays an important role in the response of trees and should, therefore, be measured carefully in the field in the future.

A second limitation of the FE models was the assumption of support fixity at the base of the trunk, and neglecting to consider the effects of soil-root system deformations. These deformations or, in other words, support flexibility would vary if the ground is saturated or unsaturated. If the connection between the trunk and ground could be represented more accurately, the result of M100 would have been probably closer to the

empirical test results, because the model would have been more flexible. Ground flexibility is difficult to model and as pointed out may vary with soil conditions. It might be more sensible to conduct several analyses by setting upper and lower bounds to the support condition to bracket the response of the model.

Throughout the research, bark thickness was neglected in the FE modeling, another limitation of the models. If the bark thickness could be subtracted from the measured diameters for each element in tree modeling, the model, M100 would have been, again, more flexible and closer to the results of the empirical tests. This requires, however, that bark thickness be measured in the field to allow an accurate representation of tree elements.

The fourth important limitation is that geometric nonlinearity was ignored in the modeling and its effect on stiffness reduction caused by P-Delta effects was considered negligible given the relatively small mass near the top of the trees. Although for the work presented in this dissertation this assumption seemed reasonable, second-order effects may increase with higher gravity loads on trees such as those caused by ice and snow accretions on branches, especially, on which leaves exist. Thus, for a future work related to trees subjected to the combination of wind load and ice or snow accretions, the effect of geometric nonlinearity on fragility curves for tree failures may be investigated.

Finally, the assumed values of the MOE and density values for each segment in the tree models present an important limitation of this work. Even if several research studies are based to define the MOE and density of each segment, these values can vary because of inherent randomness in trees. For example, decay can change the density and MOE value of the segments, and so the stiffness and mass matrices of trees can be

different. These differences in stiffness and mass generate differences in tree dynamic response under wind excitation forces. Thus, for future work, the effect of cylindrical decays on tree dynamics can be investigated as a parametric study like in Chapter 6, or perhaps more importantly the variation of MOE and density should be considered as a random variable in the models.

The most significant limitation of the work presented in Chapter 4 is that random wind loading has been applied on two different trees that are considered deterministic. Thus, for future work, the fragility curves in this chapter may change after considering the effect of random tree models in Monte Carlo (MC) simulations. The other important limitation relates to the generation of random wind loading based on experimental wind speed data. These experimental data consist of small values of wind speeds, but the random wind loading in this chapter has been generated for higher wind speeds. In other words, the characteristics of the wind speed spectrum may change for different mean values of wind speed data when experimental data for higher wind speeds are included. The modified Ochi-Shin equation developed in this chapter can be tested for greater wind speed data such as hurricanes. MC simulation techniques in this chapter can be applied to obtain the fragility curves of the tree failures under these higher intensity wind events. The other future work can be that all the methodologies in this chapter can be applied for the uprooting and branch failures, because in this chapter only stem breakage at breast height has been investigated.

Chapter 5 included several assumptions used to calculate the moment capacity loss of tree cross-sections. One of these assumptions is that shear and axial stresses or combination of shear, axial, and bending stresses are neglected. The other assumption is

that trees have homogenous material property along the cross-section of the trees, although they are heterogeneous orthotropic materials. Thus, for future work, it can be recommended that these heterogeneous orthotropic material properties can be applied in FE models for different decay size and location in tree cross-sections by considering the combination of shear, axial, and bending stresses. Then, by using the results of these FE models, the moment capacity of tree decayed cross-sections can be compared with the moment capacity of the non-decayed sections in order to obtain moment capacity loss diagrams like in Chapter 5.

The parametric models presented in Chapter 6 provide a first step in identifying those parameters that importantly affect the dynamic response of trees. Additional analyses could be conducted following a similar philosophy as that used in Chapter 6 to compute the risk of failure given variations in tree models. . For example, the effects of common pruning types (crown reduction, crown thinning, and crown raising), and vertical decay in trees on tree dynamics can be investigated as a first step in hazard reduction of tree failure. Furthermore, all the parametric studies were related to the Rd factor of the tree in Belchertown, MA at approximately breast height (1.4 m), so this Rd factor diagrams can be examined for several other points on the tree such as every 1.0 m above the breast height and the points at lower and higher levels of the large branches of trees. The Rd factor provides a convenient way to synthesize the dynamic response of trees using a single parameter, but this should not be viewed as the only way one can represent the dynamic response.

BIBLIOGRAPHY

Albers, J., & Hayes, E. (1993). How to Detect, Assess and Correct Hazard Trees in Recreational Areas: Department of Natural Resources.

Alméras, Tancrède, Thibaut, Anne, & Gril, Joseph. (2005). Effect of circumferential heterogeneity of wood maturation strain, modulus of elasticity and radial growth on the regulation of stem orientation in trees. *Trees - Structure and Function, 19*(4), 457-467. doi: 10.1007/s00468-005-0407-6

Ancelin, Philippe, Courbaud, Benoît, & Fourcaud, Thierry. (2004). Development of an individual tree-based mechanical model to predict wind damage within forest stands. *Forest Ecology and Management, 203*(1–3), 101-121. doi: 10.1016/j.foreco.2004.07.067

Arwade, Sanjay R., & Deodatis, George. (2011). Variability response functions for effective material properties. *Probabilistic Engineering Mechanics, 26*(2), 174-181. doi: 10.1016/j.probengmech.2010.11.005

Baker, C. J. (1995). The development of a theoretical model for the windthrow of plants. *Journal of Theoretical Biology, 175*(3), 355-372. doi: 10.1006/jtbi.1995.0147

Baker, C.J. (1997). Measurements of the natural frequencies of trees. *Journal of Experimental Botany, 48*(5), 1125-1132. doi: 10.1093/jxb/48.5.1125

Blackburn, P., Petty, J. A., & Miller, K. F. (1988). An Assessment of the Static and Dynamic Factors Involved in Windthrow. *Forestry, 61*(1), 29-43. doi: 10.1093/forestry/61.1.29

Bodig, J., & Jayne, B.A. (1993). *Mechanics of wood and wood composites*: Van Nostrand Reinhold.

Bruchert, F., Becker, G., & Speck, T. (2000). The mechanics of Norway spruce [Picea abies (L.) Karst]: mechanical properties of standing trees from different thinning regimes. *Forest ecology and management, 135*(1/3), 45-62.

Brüchert, Franka, & Gardiner, Barry. (2006). The effect of wind exposure on the tree aerial architecture and biomechanics of Sitka spruce (Picea sitchensis, Pinaceae). *American journal of botany, 93*(10), 1512-1521. doi: 10.3732/ajb.93.10.1512

Bucher, C. (2009). *Computational Analysis of Randomness in Structural Mechanics*: Taylor and Francis.

Butnor, J.R. , Pruyn, M.L. , Shaw, D.C. , Harmon, M.E. , Mucciardi, A.N., & Ryan, M.G. . (2009). Detecting defects in conifers with ground penetrating radar: Applications and challenges. *Forest Pathology, 39*, 309-322.

Carta, J. A., Ramírez, P., & Velázquez, S. (2009). A review of wind speed probability distributions used in wind energy analysis: Case studies in the Canary Islands. *Renewable and Sustainable Energy Reviews, 13*(5), 933-955. doi: 10.1016/j.rser.2008.05.005

Castro-García, Sergio, Blanco-Roldán, Gregorio, Gil-Ribes, Jesús, & Agüera-Vega, Juan. (2008). Dynamic analysis of olive trees in intensive orchards under forced vibration. *Trees - Structure and Function, 22*(6), 795-802. doi: 10.1007/s00468-008-0240-9

Chauhan, S. S., & Walker, J. C. F. (2006). Variations in acoustic velocity and density with age, and their interrelationships in radiata pine. *Forest Ecology and Management, 229*(1–3), 388-394. doi: 10.1016/j.foreco.2006.04.019

Chopra, A.K. (2007). *Dynamics of Structures: Theory and Applications to Earthquake Engineering*: Pearson/Prentice Hall.

Chowdhury, I., & Dasgupta, S. (2003). *Computation of Rayleigh Damping Coefficients for Large Systems*.

Cionco, Ronald M. (1978). Analysis of canopy index values for various canopy densities. *Boundary-Layer Meteorology, 15*(1), 81-93. doi: 10.1007/BF00165507

Coder, K. D. (1989). Should you or shouldn't you fill tree hollows? *Grounds maintenance, 24*(9), 68-70.

Cullen, S. (2005). Trees and wind: a practical consideration of the drag equation velocity exponent for urban tree risk management. *Journal of arboriculture., 31*(3), 101-113.

Cutler, D. F., Gasson, P. E., & Farmer, M. C. . (1990). The wind blown tree survey: analysis of results. *Arboricultural Journal, 14*(3), 265-286.

Dahle, Gregory A., & Grabosky, Jason C. (2010). Variation in modulus of elasticity (E) along Acer platanoides L. (Aceraceae) branches. *Urban Forestry & Urban Greening, 9*(3), 227-233. doi: 10.1016/j.ufug.2010.01.004

Davenport, A. G. (1961). The spectrum of horizontal gustiness near the ground in high winds. *Quarterly Journal of the Royal Meteorological Society, 87*(372), 194-211. doi: 10.1002/qj.49708737208

Deflorio, Giuliana, Johnson, Craig, Fink, Siegfried, & Schwarze, Francis Willis Mathew Robert. (2008). Decay development in living sapwood of coniferous and deciduous trees inoculated with six wood decay fungi. *Forest Ecology and Management, 255*(7), 2373-2383. doi: 10.1016/j.foreco.2007.12.040

Duryea, M.L., Blakeslee, G.M., Hubbard, W.G., & Vasquez, R.A. (1996). Wind and trees: A survey of homeowners after Hurricane Andrew. *Journal of Arboriculture, 22*, 44-50.

Duryea, Mary L., Kampf, Eliana, & Ramon, C. Littell. (2007). Hurricanes and the urban forest II: effects on tropical and subtropical tree species. *Arboriculture & Urban Forestry, 33*, 98-112.

England, A.H., Baker, C.J., & Saunderson, S.E.T. (2000). A dynamic analysis of windthrow of trees. *Forestry, 73*(3), 225-238. doi: 10.1093/forestry/73.3.225

Ennos, A. R. (1999). The aerodynamics and hydrodynamics of plants. *J Exp Biol, 202*(Pt 23), 3281-3284.

Fink, Siegfried. (2009). Hazard tree identification by visual tree assessment (VTA): Scientifically solid and practically approved. *Arboricultural Journal, 32*(3), 139-155. doi: 10.1080/03071375.2009.9747570

Flesch, Thomas K., & Wilson, John D. (1999). Wind and remnant tree sway in forest cutblocks. II. Relating measured tree sway to wind statistics. *Agricultural and Forest Meteorology, 93*(4), 243-258. doi: 10.1016/S0168-1923(98)00113-0

Fournier, Meriem, Moulia, Bruno, Stokes, Alexia, Coutand, Catherine, & Fourcaud, Thierry. (2006). Tree Biomechanics and Growth Strategies in the Context of Forest Functional Ecology. In A. Herrel, T. Speck & N. Rowe (Eds.), *Ecology and Biomechanics* (pp. 1-33): CRC Press.

Fransic, J. K. (2000). Comparison of hurricane damage to several species of urban trees in San Juan, Puerto Rico. *Journal of Arboriculture, 26*, 189-197.

Fransic, J. K., & Gillespie, A. J. R. (1993). Relating gust speed to tree damage in hurricane Hugo, 1989. *Journal of Arboriculture, 19*(6), 369-373.

Gardiner, B. A. (1995). Wind-tree interactions. In M. P. Coutts & J. Grace (Eds.), *Wind and Trees* (pp. 41-59). Cambridge: Cambridge University Press.

Gardiner, B. A., Stacey, G. R., Belcher, R. E., & Wood, C. J. (1997). Field and wind tunnel assessments of the implications of respacing and thinning for tree stability. *Forestry, 70*(3), 233-252. doi: 10.1093/forestry/70.3.233

Gardiner, Barry, Byrne, Ken, Hale, Sophie, Kamimura, Kana, Mitchell, Stephen J., Peltola, Heli, & Ruel, Jean-Claude. (2008). A review of mechanistic modelling of wind damage risk to forests. *Forestry, 81*(3), 447-463.

Gardiner, Barry, & Quine, C. P. (2000). *The mechanical adaptation of tree to environmental influences.* Paper presented at the Proceeding of third Plant Biomechanics Conference, Freiberg.

Gibbs, J.N., & Greig, B.J.W. (1990). Survey of parkland trees after the great storm of 16 October 1987. *Arboricultural Journal, 14*, 321-347.

Gilbert, Elizabeth A. , & Smiley, E. Thomas (2004). Picus sonic tomography for the quantification of decay in white oak (Quercus alba) and hickory (Carya spp.). *Journal of Arboriculture, 30*, 277–281.

Gilman, E. F. (2003). Branch to stem ratio affects strength of attachment. *Branch to stem ratio affects strength of attachment, 29*, 291-294.

Glaberson, William, & Foderado, Lisa W. (2012). Neglected, Rotting Trees Turn Deadly. *The New York Times*.

Green, David. W. (2001). Wood: Strength and stiffness *Science and Technology* (pp. 9732-9736): Elsevier Science.

Gruber, Franz. (2008). Reply To The Response Of Claus Mattheck And Klaus Bethge To My Criticisms On Untenable Vta-Failure Criteria, Who Is Right And Who Is Wrong? *Arboricultural Journal, 31*(4), 277-296.

Hankinson, R. L. (1921). *Investigation of crushing strength of spruce at varying angles of grain*. Washington: U.S. GPO.

Harris, R. I. (1971). The Nature of the Wind, the Modern Design of Wind Sensitive Structures. *Construction Industry Research and Information Association*, 29-55.

Hoadly, R. Bruce. (1980). *Undestanding Wood*. Newton, CT: Taunton Press.

Hsu, S.A., Meindl, Eric A., & Gilhousen, David B. (1994). Determining the Power-Law Wind-Profile Exponent under Near-Neutral Stability Conditions at Sea. *Journal of Applied Meteorology, 33*(6), 757-765.

Humar, J.L. (1990). *Dynamics of Structures*: Prentice Hall.

James, Ken. (2003). Dynamic Loadig of Trees. *Journal of Arboriculture, 29*(3), 165-171.

James, Kenneth R., Haritos, Nicholas, & Ades, Peter K. (2006). Mechanical stability of trees under dynamic loads. *American journal of botany, 93*(10), 1522-1530. doi: 10.3732/ajb.93.10.1522

James, Kenneth R., & Kane, Brian. (2008). Precision digital instruments to measure dynamic wind loads on trees during storms. *Journal of Arboriculture, 148*(6–7), 1055-1061. doi: 10.1016/j.agrformet.2008.02.003

Jim, C. Y., & Liu, H. H. T. (1997). Storm damage on urban trees in Guangzhou, China. *Landscape and urban planning, 38*(1-2), 45-60.

Jönsson, Mari T., Fraver, Shawn, Jonsson, Bengt Gunnar, Dynesius, Mats, Rydgård, Mats, & Esseen, Per-Anders. (2007). Eighteen years of tree mortality and structural change in an experimentally fragmented Norway spruce forest. *Forest Ecology and Management, 242*(2–3), 306-313. doi: 10.1016/j.foreco.2007.01.048

Kane, B. (2008). Tree failure following a windstorm in Brewster, Massachusetts, USA. *Urban Forestry & Urban Greening, 7*(1), 15-23.

Kane, Brian. (2007). Branch Strength of Bradford Pear (Pyrus calleryana var. 'Bradford'). *Arboriculture & Urban Forestry, 33*(4), 283-291.

Kane, Brian, Farrell, Robert, Zedaker, Shepard M., Loferski, J.R., & Smith, D.W. (2008). Failure Mode and Prediction of the Strength of Branch Attachments. *Arboriculture & Urban Forestry, 34*(5), 308-316.

Kane, Brian, & Clouston, Peggi L. (2008). Tree Pulling Tests of Large Shade Trees in the Genus Acer. *Arboriculture and Urban Forestry, 34*(2), 101-109.

Kane, Brian, & James, Kenneth R. (2011). Dynamic properties of open-grown deciduous trees. *Canadian Journal of Forest Research, 41*(2), 321-330. doi: 10.1139/x10-211

Kane, Brian, & Ryan, Dennis. (2003). Examining formulas that assess strength loss due to decay in trees: woundwood toughness improvement in red maple (Acer rubrum). *Journal of Arboriculture, 29*(4), 207-217.

Kane, Brian, & Ryan, Dennis. (2004). The accuracy of formulas used to assess strength loss due to decay in trees. *Journal of Arboriculture, 30*(6), 347-356.

Kane, Brian, Ryan, Dennis, & Bloniarz, David V. (2001). Comparing formulae that assess strength loss due to decay in trees. *Journal of Arboriculture, 27*(2), 78-87.

Kane, Brian, & Smiley, E. Thomas. (2006). Drag coefficients and crown area estimation of red maple. *Canadian Journal of Forest Research, 36*(8), 1951-1958. doi: 10.1139/x06-086

Kane, B, Modarres-Sadeghi, Y., James, K.R., & Reiland, M. (In preparation). Branches affect sway characteristics of large sugar maples.

Kastner-Klein, P., Berkowicz, R., & Britter, R. (2004). The influence of street architecture on flow and dispersion in street canyons. *Meteorology and Atmospheric Physics, 87*(1), 121-131. doi: 10.1007/s00703-003-0065-4

Kennard, D.K., Putz, F.E., & Niederhofer, M. (1996). The predictability of tree decay based on visual assessments. *Journal of Arboriculture, 22*(6), 249-254.

Kerzenmacher, Tobias, & Gardiner, Barry. (1998). A mathematical model to describe the dynamic response of a spruce tree to the wind. *Trees - Structure and Function, 12*(6), 385-394. doi: 10.1007/s004680050165

Kiss, Péter, & Jánosi, Imre M. (2008). Comprehensive empirical analysis of ERA-40 surface wind speed distribution over Europe. *Energy Conversion and Management, 49*(8), 2142-2151. doi: 10.1016/j.enconman.2008.02.003

Kretschmann, David E. (2010). Mechanical Properties of Wood *Wood Handbook, Wood as an Engineering Material* (Vol. 5, pp. 1-46). Madison, WI, U.S. : Department of Agriculture, Forest Service, Forest Products Laboratory.

Langum, Christopher E. , Yadama, Vikram , & Lowell, Eini C. (2009). Physical and mechanical properties of young-growth Douglas-fir and western hemlock from western Washington. *Forest Products Journal, 59*, 37-47.

Lanquaye-Opoku, Naa, & Mitchell, Stephen J. (2005). Portability of stand-level empirical windthrow risk models. *Forest ecology and management, 216*(1-3), 134-148.

Lichtenegger, H., Reiterer, A., Stanzl-Tschegg, S. E., & Fratzl, P. (1999). Variation of cellulose microfibril angles in softwoods and hardwoods-a possible strategy of mechanical optimization. *J Struct Biol, 128*(3), 257-269. doi: 10.1006/jsbi.1999.4194

Lindström, H., Evans, J. W., & Verrill, S. P. (1998). Influence of Cambial Age and Growth Conditions on Microfibril Angle in Young Norway Spruce (Picea abies [L.] Karst.). *Holzforschung, 52*, 573-581.

Lucas, R. C., Bacon, W. R., Beardsley, W., Brown, P. J., Christensen, H. H., Clark, R. N., Weingart, P. D. (1984). Outdoor Recreation Management. In K. F. Wenger (Ed.), *Forestry Handbook* (pp. 801-886). New York: John Wiley & Sons.

Luley, C., Sisinni, S., & Pleninger, A. (2002). *The effect of wind gust on branch failures.* Paper presented at the Tree Structure and Mechanics Conference Proceedings, Champaign, IL.

Luna, R. E., & Church, H. W. (1974). Estimation of long-term concentrations using a "universal" wind speed distribution. *journal of applied meteorology, 10*, 910-916.

Mabie, E. E., & Rogers, C. B. (1972). Transverse Vibrations of Double-Tapered Cantilever Beams. *J. Acoust. Soc. Am, 51*(5), 1771-1774.

Matheny, N.P., & Clark, J.R. (1991). *A photographic guide to the evaluation of hazard trees in urban areas*: International Society of Arboriculture.

Mattheck, C., & Bethge, K. . (2004). Simple mathematical approaches to tree biomechanics. *Arboricultural Journal, 24*(4), 307-326.

Mattheck, C., Bethge, K., & Erb, D. (1993). Failure Criteria for Trees. *Arboricultural Journal, 17*, 201-209.

Mattheck, C., Lonsdale, D., & Breloer, H. (1994). *The body language of trees: a handbook for failure analysis*: HMSO.

Mayer, H. (1987). Wind-induced tree sways. *Trees - Structure and Function, 1*(4), 195-206. doi: 10.1007/BF01816816

Mayhead, G. J. (1973). Swaying periods of forest trees. *Scottish Forestry, 27*, 19-23.

Mayhead, G.J., Gardiner, J.B.H., & Durrant, D.W. (1975). *A Report on the Physical Properties of Conifers in Relation to Plantation Stability*. Great Britain: Forestry Commission Research and Development Division.

Mencuccini, M., Grace, J., & Fioravanti, M. (1997). Biomechanical and hydraulic determinants of tree structure in Scots pine: anatomical characteristics. *Tree Physiol, 17*(2), 105-113.

Mergen, F. (1954). Mechanical aspects of windbreakage and windfirmness. *Journal of Forestry, 52*, 119-125.

Miller, K.F. (1985). *Windthrow Hazard Classification*: H.M. Stationery Office.

Miller, V. J. (1959). Crotch influence on strength and breaking point of apple tree branches. *Journal of the American Society for Horticultural Science, 73*, 27-32.

Mills, L.J. , & Russel, K. (1984). *Detection and Correction of Hazard Trees in Washington's Recreation Areas*: State of Washington Department of Natural Resources.

Milne, R. (1991). Dynamics of swaying of Picea sitchensis. *Tree Physiology, 9*(3), 383-399. doi: 10.1093/treephys/9.3.383

Mitchell, S. J. (1998). A diagnostic framework for windthrow risk estimation. *The Forestry Chronicle, 74*(1), 100-105. doi: 10.5558/tfc74100-1

Moore, John R., & Maguire, Douglas A. (2004). Natural sway frequencies and damping ratios of trees: concepts, review and synthesis of previous studies. *Trees - Structure and Function, 18*(2), 195-203. doi: 10.1007/s00468-003-0295-6

Moore, John R., & Maguire, Douglas A. (2005). Natural sway frequencies and damping ratios of trees: influence of crown structure. *Trees - Structure and Function, 19*(4), 363-373. doi: 10.1007/s00468-004-0387-y

Moore, John R., & Maguire, Douglas A. (2008). Simulating the dynamic behavior of Douglas-fir trees under applied loads by the finite element method. *Tree Physiology, 28*(1), 75-83. doi: 10.1093/treephys/28.1.75

Morgan, Eugene C., Lackner, Matthew, Vogel, Richard M., & Baise, Laurie G. (2011). Probability distributions for offshore wind speeds. *Energy Conversion and Management, 52*(1), 15-26. doi: 10.1016/j.enconman.2010.06.015

Mortimer, Michael J., & Kane, Brian. (2004). Hazard tree liability in the United States: Uncertain risks for owners and professionals. *Urban Forestry & Urban Greening, 2*(3), 159-165. doi: 10.1078/1618-8667-00032

Moulia, B., Coutand, C., & Lenne, C. (2006). Posture control and skeletal mechanical acclimation in terrestrial plants: implications for mechanical modeling of plant architecture. *Am J Bot, 93*(10), 1477-1489. doi: 10.3732/ajb.93.10.1477

Nataf, A. (1962). D´etermination des distributions de probabilit´es dont les marges sont donn´ees *Comptes Rendus de l'Academie des Sciences* (Vol. 225, pp. 42-43).

Nicolotti, G., Socco, L.V., Martinis, R., Godio, A., & Sambuelli, L. (2003). Application and comparison of three tomographic techniques for detection of decay in trees. *Journal of Arboriculture, 29*(2), 66-78.

Niklas, Karl J. (1997). Size- and Age-dependent Variation in the Properties of Sap- and Heartwood in Black Locust (Robinia pseudoacacia L.). *Annals of Botany, 79*(5), 473-478. doi: 10.1006/anbo/79.5.473

Nowak, David J., & Dwyer, John F. (2000). Understanding the Benefits and Costs of Urban Forest Ecosystems. In J. E. Kuser (Ed.), *Handbook of Urban and Community Forestry in the Northeast* (pp. 11-25). New York City, NY: Plenum Publishers.

Ochi, M.K. , & Shin, V.S. (1988). *Wind Turbulent Spectra For Design Consideration Of Offshore Structures*. Paper presented at the Offshore Technology Conference.

Oliver, H. R., & Mayhead, G. J. (1974). Wind Measurements in a Pine Forest During a Destructive Gale. *Forestry, 47*(2), 185-194. doi: 10.1093/forestry/47.2.185

Panofsky, H.A., & Dutton, J.A. (1984). *Atmospheric turbulence: models and methods for engineering applications*: Wiley.

Panshin, A.J., De Zeeuw, C., & Brown, H.P. (1980). *Structure, Identification, Uses, and Properties of the Commercial Woods of the United States*: Mac Graw-Hill.

Peltola, H. , & Kellomäki, S. (1993). A mechanistic model for calculating windthrow and stem breakage at stand edge. *Silva Fennica, 27*, 99-111.

Peltola, H., Kellomäki, S., Väisänen, H., & Ikonen, V. P. (1999). A mechanistic model for assessing the risk of wind and snow damage to single trees and stands of Scots pine, Norway spruce, and birch. *Canadian Journal of Forest Research, 29*(6), 647-661. doi: 10.1139/x99-029

Peltola, Heli. (1996). Swaying of trees in response to wind and thinning in a stand of Scots pine. *Boundary-Layer Meteorology, 77*(3), 285-304. doi: 10.1007/BF00123529

Peltola, Heli M. (2006). Mechanical stability of trees under static loads. *American Journal of Botany, 93*(10), 1501-1511.

Plomion, Christophe, Leprovost, Grégoire, & Stokes, Alexia. (2001). Wood Formation in Trees. *Plant Physiology, 127*(4), 1513-1523. doi: 10.1104/pp.010816

Potter, M.C., Wiggert, D.C., & Ramadan, B.H. (2011). *Mechanics of Fluids*: Cengage Learning.

Putz, F.E., & Sharitz, R.R. (1996). Hurricane damage to old growth forest in Congaree Swamp National Monument, South Carolina, USA *USDA Forest Service General Technical Report SR3-5* (pp. 92-100).

Read, J., & Stokes, A. (2006). Plant biomechanics in an ecological context. *Am J Bot, 93*(10), 1546-1565. doi: 10.3732/ajb.93.10.1546

Reiterer, A., Lichtenegger, H. , Tschegg, S. , & Fratzl, P. . (1999). Experimental evidence for a mechanical function of the cellulose microfibril angle in wood cell walls. *Philosophical Magazine, 79*(A), 2173-2184.

Robbins, K. (1986). *How to recognize and reduce tree hazards in recreation sites*: U.S. Dept. of Agriculture, Forest Service.

Rodriguez, Mathieu, Langre, Emmanuel de, & Moulia, Bruno. (2008). A scaling law for the effects of architecture and allometry on tree vibration modes suggests a biological tuning to modal compartmentalization. *American journal of botany, 95*(12), 1523-1537. doi: 10.3732/ajb.0800161

Roodbaraky, H. J., Baker, C. J., Dawson, A. R., & Wright, C. J. (1994). Experimental observations of the aerodynamic characteristics of urban trees. *Journal of Wind Engineering and Industrial Aerodynamics, 52*(0), 171-184. doi: 10.1016/0167-6105(94)90046-9

Rowe, Nick, & Speck, Thomas. (2005). Plant growth forms: an ecological and evolutionary perspective. *New Phytologist, 166*(1), 61-72. doi: 10.1111/j.1469-8137.2004.01309

Rudnicki, Mark, Meyer, Thomas, Lieffers, Victor, Silins, Uldis, & Webb, Vincent. (2008). The periodic motion of lodgepole pine trees as affected by collisions with neighbors. *Trees - Structure and Function, 22*(4), 475-482. doi: 10.1007/s00468-007-0207-2

Rudnicki, Mark, Mitchell, Stephen J., & Novak, Michael D. (2004). Wind tunnel measurements of crown streamlining and drag relationships for three conifer species. *Canadian Journal of Forest Research, 34*(3), 666-676. doi: 10.1139/x03-233

Saunderson, S. E. T., England, A. H., & Baker, C. J. (1999). A Dynamic Model of the Behaviour of Sitka Spruce in High Winds. *Journal of Theoretical Biology, 200*(3), 249-259. doi: 10.1006/jtbi.1999.0983

Schelhaas, Mart-Jan , Eggers, Jeannette , Lindner, Marcus , Nabuurs, Gert-Jan , Pussinen, Ari , Päivinen, Risto , . . . Zudin, Sergey (2007). Model documentation for the European Forest Information Scenario model (EFISCEN 3.1.3) (Vol. 26, pp. 118).

Schmidlin, Thomas. (2009). Human fatalities from wind-related tree failures in the United States, 1995–2007. *Natural Hazards, 50*(1), 13-25. doi: 10.1007/s11069-008-9314-7

Sellier, Damien, Brunet, Yves, & Fourcaud, Thierry. (2008). A numerical model of tree aerodynamic response to a turbulent airflow. *Forestry, 81*(3), 279-297. doi: 10.1093/forestry/cpn024

Sellier, Damien, & Fourcaud, Thierry. (2005). A mechanical analysis of the relationship between free oscillations of Pinus pinaster Ait. saplings and their aerial architecture. *Journal of Experimental Botany, 56*(416), 1563-1573. doi: 10.1093/jxb/eri151

Sellier, Damien, & Fourcaud, Thierry. (2009). Crown structure and wood properties: Influence on tree sway and response to high winds. *American journal of botany, 96*(5), 885-896. doi: 10.3732/ajb.0800226

Sellier, Damien, Fourcaud, Thierry, & Lac, Patrick. (2006). A finite element model for investigating effects of aerial architecture on tree oscillations. *Tree Physiology, 26*(6), 799-806. doi: 10.1093/treephys/26.6.799

Shigo, Alex L. (1984). How to Assess the Defect Status of a Stand. *Northern Journal of Applied Forestry, 1*(3), 41-49.

Sinn, G. , & Wessolly, L. (1989). A Contribution to the Proper Assessment of the Strength and Stability of Trees. *Arboricultural Journal, 13*, 45-65.

Smiley, E. T., & Fraedrich, B. R. (1992). Determining strength loss from decay. *Journal of Arboriculture, 18*(4), 201-204.

Smiley, E.T., & Fraedrich, B.R. (1993). Hazardous Tree Evaluation and Management.

Smith, Marra Ann. (2009). *A Monte Carlo based method for the dynamic performance analysis of tall buildings under turbulent wind loading.* (Master), North eastern University. Retrieved from http://hdl.handle.net/2047/d20000048 (9)

Spatz, H.-CH., Emanns, A., & Speck, O. (2004). The structural basis of oscillation damping in plant stems—biomechanics and biomimetics. *Journal of Bionics Engineering, 1*, 149-158.

Spatz, Hanns-Christof, Brüchert, Franka, & Pfisterer, Jochen. (2007). Multiple resonance damping or how do trees escape dangerously large oscillations? *American journal of botany, 94*(10), 1603-1611. doi: 10.3732/ajb.94.10.1603

Spatz, Hanns-Christof, & Bruechert, Franka. (2000). Basic biomechanics of self-supporting plants: wind loads and gravitational loads on a Norway spruce tree. *Forest Ecology and Management, 135*(1–3), 33-44. doi: 10.1016/S0378-1127(00)00296-6

Speck, O., & Spatz, H. C. (2004). Damped oscillations of the giant reed Arundo donax (Poaceae). *Am J Bot, 91*(6), 789-796. doi: 10.3732/ajb.91.6.789

Telewski, F. W. (2006). A unified hypothesis of mechanoperception in plants. *Am J Bot, 93*(10), 1466-1476. doi: 10.3732/ajb.93.10.1466

Thomson, W.T. (1993). *Theory of Vibration with Applications*: Chapman & Hall.

Tiren, L. (1929). Einige Untersuchungen Über Die Schaft Form. *Med Statens Skogsforsoks Anstalt 24*, 4.

Valinger, Erik, & Fridman, Jonas. (1997). Modelling probability of snow and wind damage in Scots pine stands using tree characteristics. *Forest Ecology and Management, 97*(3), 215-222. doi: 10.1016/S0378-1127(97)00062-5

Vollsinger, Stephan, Mitchell, Stephen J., Byrne, Kenneth E., Novak, Michael D., & Rudnicki, Mark. (2005). Wind tunnel measurements of crown streamlining and drag relationships for several hardwood species. *Canadian Journal of Forest Research, 35*(5), 1238-1249. doi: 10.1139/x05-051

Wagener, Willis W. (1963). *Judging hazard from native trees in California recreational areas: a guide for professional foresters*. Berkeley, Calif.: Pacific Southwest Forest and Range Experiment Station, Forest Service, U.S. Dept. of Agriculture.

Wang, Xiping, & Allison, R. Bruce (2008). Decay Detection in Red Oak Trees Using a Combination of Visual Inspection, Acoustic Testing, and Resistance Microdrilling. *Arboriculture & Urban Forestry, 34*(1), 1-4.

White, R.G. , White, M.F. , & Mayhead, G.J. (1976). Measurement of the motion of trees in two dimensions (I. o. S. a. Vibration, Trans.). Southampton: University of Southampton.

Woodrum, C. L., Ewers, F. W., & Telewski, F. W. (2003). Hydraulic, biomechanical, and anatomical interactions of xylem from five species of Acer (Aceraceae). *Am J Bot, 90*(5), 693-699. doi: 10.3732/ajb.90.5.693

Yoshida, M. , Okuyama, T., Yamamoto, H., & Sugiyama, K. (1992). Tree forms and internal stresses, 2: Stresses around the base of a branch. *Journal of the Japan Wood Research Society, 38*(7), 657-662.

Yue, L. I., & Ellingwood, Bruce R. (2006). Hurricane damage to residential construction in the US : Importance of uncertainty modeling in risk assessment. *Engineering structures, 28*(7), 1009-1018.

Zhu, Jiaojun, Matsuzaki, Takeshi, & Sakioka, Kenji. (2000). Wind speeds within a single crown of Japanese black pine (Pinus thunbergii Parl.). *Forest Ecology and Management, 135*(1–3), 19-31. doi: 10.1016/s0378-1127(00)00295-4